

Université du Québec

INRS-EMT

Synthesis and Characterization of High-quality Near Infrared-emitting Quantum
Dots in an Organic Phase or in Water

By

Zhao Haiguang

A thesis submitted to the Department of Energy, Materials and Communications in conformity
with the requirements for the degree of Doctor of Philosophy

Committee

External examiner

Fabio Variola
Université d'Ottawa

Hua-Zhong Yu
Simon Fraser University

Internal examiner

Ana Tavares
INRS-EMT, Université du Québec

Supervisor

Dongling Ma
INRS-EMT, Université du Québec

Co-supervisor

Mohamed Chaker
INRS-EMT, Université du Québec

Copyright@Zhao Haiguang, 2011

Abstract

Near infrared (NIR) emitting PbS quantum dots (QDs) have attracted much attention due to their unique size-dependent photophysical properties that are distinctly different from the corresponding bulk material. They are currently exploited for various applications, such as optoelectronics and biological sensors. To have significant impact in practical applications, they are required to show high quantum efficiency and good stability, such as photostability and colloidal stability, depending on targeted applications. It is still a big challenge to synthesize high-quality NIR-emitting QDs stable in an organic phase or in aqueous environments.

I firstly developed a simple and greener approach to synthesize high-quality PbS QDs in the organic phase. I investigated the effects of the reaction time, molar ratios of reactants, reaction temperature, capping ligands and purity of ligands and precursors on the growth of PbS QDs and how these synthetic conditions influence their structure and optical properties. Finally, the optimal synthesis conditions for high-quality PbS QDs emitting at varying NIR wavelengths were identified. Such synthesized PbS QDs show a quantum yield (QY) as high as 40% in the organic phase.

Aiming to enhance the QY of PbS QDs, the cation exchange approach was used to form PbS/CdS core/shell QDs. With this strategy, I was able to obtain a QY of 67% at optimal shell thickness of 0.7 nm. The shell composition was investigated in detail. As the experimental

identification of the shell composition of thin-shell QDs is difficult, experimental data and calculations were combined to give clues. Based on the comparison of band gap versus core size plots of different compositional models, it was found that the thin shell is primarily made of CdS. Furthermore, by developing a two-step cation exchange approach, the previous synthesis barrier was overcome and I achieved PbS/CdS QDs with various shell thickness. Owing to the preparation of a relatively thick shell, not only can the core/shell structure be easily observed by transmission electron microscopy (TEM), the characteristic absorption and emission of CdS can also be observed when shell thickness reaches 1.8 nm. Furthermore, X-ray diffraction (XRD) shows the overall diffraction pattern is basically the same as that of the CdS standard when the thickness of shell reaches 3.6 nm. The thick-shell QDs were further analyzed by performing energy dispersive X-ray spectrometry (EDX) in core and shell regions, respectively. It was found that Pb is absent in the shell region. All of these results consistently suggest that, in thick-shell PbS/CdS QDs, the shell is also made of CdS, instead of ternary $\text{Pb}_x\text{Cd}_{1-x}\text{S}$ alloy. In addition to exhibiting significantly improved QY, importantly, these core/shell structured PbS/CdS QDs also show better photo- and thermal stability than the shell-free PbS QDs.

As-synthesized PbS QDs are insoluble in water. In order to disperse them into water, amphiphilic polymers of poly(maleic anhydride-alt-1-octadecene-co-poly(ethylene glycol)) (PMAO-PEG) were used as phase transferring agents. I firstly transferred the PbS QDs capped by oleylamine (OLA) ligands from chloroform into water via PMAO-PEG. The PbS QDs lose their photoluminescence (PL) in 5 minutes and change the size distribution from mono to double, attributed to ligand etching together with Ostwald ripening. These QDs further show self-selected size-dependent recovery of the PL with time, which was not reported before. After

thorough investigations, it was found that the decrease in the percentage of unpassivated surface atoms during aging explains the PL recovery behavior of the subset of smaller QDs stored in water, which is distinctly different from that of the subset of larger QDs. Realizing a significant role of ligands in the water transfer process, I further investigated the effect of different types of surface ligands on the structure and optical property of water-soluble PbS QDs encapsulated by amphiphilic polymers. Among all the samples, PbS QDs capped with oleic acid (OA)/trioctylphosphine show the highest QY (20% in water) and those capped by OA show the least spectral shift.

Overcoating PbS with a robust inorganic shell before water transfer may further improve the properties of PbS nanocrystals in aqueous solutions and minimize their dependence on the original capping ligands. I therefore applied a two-step strategy to synthesize water soluble PbS/CdS QDs. In the first step, I overcoated PbS QDs with CdS in an organic phase as aforementioned and in the second step, I transferred them into water via amphiphilic polymers. The CdS shell around the PbS core maintains the structural integrity of PbS nanocrystals and leads to a significantly higher QY in buffer as compared to that can be achieved with “bare” (without an inorganic shell) PbS QDs. Further improvement may be made by optimizing core/shell structures. By carefully varying the initial size of PbS QDs and finely tuning cation exchange experimental conditions, I am able to synthesize PbS/CdS core/shell QDs with a similar PbS core size of 4.4 ~ 4.5 nm yet different CdS shell thickness from 0.2 to 2.3 nm via a cation exchange approach. This enables me to study the effect of the shell thickness on the optical properties of these NIR emitting PbS/CdS core/shell QDs after their transfer from an organic solvent into water via PMAO–PEG. It was found that the QY of PbS core QDs (~4.5 nm

in diameter) dispersed in water firstly increases with the increase of the shell thickness up to ~0.7 nm, reaching the maximum of 33%, due to better surface passivation and then decreases to 1.7% when the shell thickness reaches 2.3 nm. The decline in the QY is due to the formation of new defects with shell deposition. In contrast, as the CdS shell thickness increases, the amplitude of variation of QY, due to water transfer, decreases monotonically from 58% to 42%, because a thicker shell can endow the PbS core better protection from their environments. For the same reason, the photostability of PbS core QDs is steadily enhanced with increasing CdS shell thickness. It is clear that although the defects introduced during relatively thick shell deposition play a fundamental role in the absolute QY, they do not show any overwhelmingly negative effects on the variation of QY with environments and QD photostability. On the other hand, the colloidal stability of QDs in buffers containing different salt concentrations seems not affected by the shell thickness, quite possibly due to the same steric stabilization effect of the amphiphilic polymer in all the samples. Further investigation on a series of core/shell samples with different core size and different shell thickness confirms that ~ 0.7 nm is an optimal shell thickness for the various core sizes investigated herein, consistently yielding the maximum QY and reasonably good photostability.

Acknowledgements

I would like to thank Prof. Dongling Ma and Prof. Mohamed Chaker for providing advice and direction throughout my research. They have created an exciting environment of discovery and learning that has allowed me explore a complex and fascinating field of research. Thanks to them for their kindness and support during my PhD path. I learned lots from them.

I want to acknowledge the contributions to this work made by Dr. Teng Zhang and Dr. Defa Wang, who collaborated closely with me on many aspects of this research. Thanks to all the group members for their help throughout the work. I am grateful to have been part of such a supportive, hardworking, and inspiring group of graduate students and post doctoral fellows. Over the course of my research I have been fortunate enough to work with a truly outstanding group. These people include: Ibrahima Ka, Dr. Teng Zhang, Jianming Zhang, Dr. Guozhu Chen, Hongyan Liang, Dr. Defa Wang, Dr. Stephano Desian and Belete Atomsa Gonfa.

I have to pay special thanks to Dr. Hui Meng, Dr. Shuhui Sun, Dr. Gaixia Zhang, Dr. Guiping Dai, Dr. Fangxin Li, and Dr. Juan Tian. They always cheered me up.

I thank to the departmental and technical staff at INRS-EMT. They are very helpful, particularly Pierre-Paul Mercier, Georges Lamoureux, Louise Hudon and Christophe Chabanier.

I would like to thank Jean Philippe Masse for TEM measurements and Lin Chandler for

the training of fluorescence spectrometer. Thanks to Dr. Daria Riabinina for analyzing the data of XPS and also discussion of work. Thanks to Ibrahima Ka for the correction of the resume. Thanks to Prof. Nianqiang Wu for the discussion of work.

I thank my family and my friends for their continuing love and support. I am eternally grateful to my wife, Hongmin, who has been a constant source of love, encouragement, and sound advice.

Finally, I wish to acknowledge the following organizations for their financial support: the Natural Sciences and Engineering Research Council of Canada and Fonds de la recherche sur la nature et les technologies.

Contents

Chapter 1 Introduction	1
1.1 What quantum dots are and their properties.....	1
1.2 Why are NIR emitting quantum dots attractive?.....	4
1.3 PbS synthesis.....	6
1.4 Synthesis of core/shell quantum dots.....	8
1.5 Thesis objectives and contributions of this work.....	10
1.6 Thesis organization.....	11
Chapter 2 Experimental	14
2.1 Materials.....	14
2.2 Reaction setup.....	15
2.3 Synthesis.....	15
2.3.1 Synthesis of PbS and PbS/CdS quantum dots in the organic phase.....	15
2.3.1.1 Synthesis of PbS quantum dots.....	15
2.3.1.2 Synthesis of PbS/CdS quantum dots.....	18
2.3.2 Synthesis of PbS and PbS/CdS quantum dots in water.....	20
2.3.2.1 Synthesis of amphiphilic polymer.....	20
2.3.2.2 Transfer of PbS and PbS/CdS quantum dots into water.....	21
2.4 Characterization.....	22
2.4.1 Structure characterization.....	22
2.4.2 Property characterization.....	23
Chapter 3 Synthesis and characterization of PbS quantum dots	26
3.1 Quantum dots synthesis.....	26
3.2 Effect of reaction parameters.....	29

3.2.1 Effect of reaction time.....	29
3.2.2 Effect of the molar ratio of precursors.....	32
3.2.3 Effect of reaction temperature.....	34
3.3 Effect of capping ligands.....	37
3.4 Purity effect of ligands and precursors.....	39
3.4.1 Ligands purity effect.....	40
3.4.2 Precursor purity effect.....	44
3.5 Summary.....	46
Chapter 4 Synthesis and characterization of PbS/CdS quantum dots.....	47
4.1 Core/shell structure.....	48
4.2 Synthesis and characterization of PbS/CdS quantum dots.....	49
4.2.1 Structure of thin-shell PbS/CdS quantum dots.....	49
4.2.2 Structure of thick-shell PbS/CdS quantum dots.....	57
4.3 Optical property of PbS/CdS quantum dots.....	63
4.3.1 Quantum yield.....	63
4.3.2 Photostability.....	64
4.3.3 Thermal-stability.....	65
4.4 Summary.....	66
Chapter 5 Synthesis and characterization of water-soluble PbS quantum dots.....	67
5.1 Synthesis approach of water-soluble quantum dots.....	68
5.1.1 Synthesis of water-soluble PbS quantum dots in an aqueous system.....	68
5.1.2 Water transfer approach.....	68
5.2 Synthesis of amphiphilic-polymer encapsulated PbS quantum dots.....	69
5.3 Self PL recovery of water-soluble PbS quantum dots.....	70
5.3.1 Structure variation.....	70
5.3.2 Fast PL decay.....	73
5.3.3 PL recovery.....	76
5.4 Ligands effect.....	83
5.4.1 Synthesis of PbS quantum dots capped with different surface ligands.....	83

5.4.2 Ligand-dependent optical properties.....	87
5.4.3 XPS characterization of PbS quantum dots.....	90
5.4.4 Photostability of PbS quantum dots.....	91
5.5 Summary.....	94
Chapter 6 Synthesis and characterization of water-soluble PbS/CdS quantum dots.....	96
6.1 Synthesis of water-soluble PbS/CdS quantum dots.....	97
6.2 CdS shell thickness effect.....	102
6.2.1 PbS/CdS core/shell quantum dots in an organic phase.....	102
6.2.2 PbS/CdS core/shell quantum dots transferred into water.....	107
6.2.2.1 Variation of optical properties with water transfer.....	108
6.2.2.2 Colloidal stability.....	112
6.2.2.3 Photostability.....	114
6.2.2.4 Identifying optimal shell thickness.....	115
6.3 Summary.....	116
Chapter 7 Conclusions and perspectives.....	118
7.1 Conclusions.....	118
7.2 Perspectives.....	122
Bibliography.....	125
Appendix.....	141
A List of acronyms.....	141
B List of chemical formula.....	142
C Résumé de la thèse.....	143

List of Figures

Figure 1.1 Electronic energy states of a semiconductor in the transition from nanosized crystals to bulk crystals. Blue shading denotes ground state electron occupation. Figures 1.1 is from [18].....	2
Figure 1.2 (a) Size tunable photoluminescence (PL) spectra of CdSe QDs. (b) Emission maxima and sizes of QDs of different composition [4, 6, 7, 8, 9, 10, 11]. Inset: representative emission spectra for some materials. (c) Absorption (upper curves) and emission (lower curves) spectra of four CdSe/ZnS QDs samples. The blue vertical line indicates the 488-nm line of an argon-ion laser, which can be used to efficiently excite all QDs simultaneously [3, 5]. Figure 1.2a is our unpublished data. Figures 1.2b and c are from [3].....	3
Figure 1.3 NIR luminescence imaging of BALB/c mouse treated with lysine cross-linked mercaptoundecanoic acid core/shell CdSe _{0.25} Te _{0.75} /CdS QDs as NIR optical probes [26]. The background autofluorescence (from the mouse) is colored green and NIR QD signal is pseudocolored red.....	5
Figure 1.4 Ligand exchange and amphiphilic polymer encapsulation approaches for transferring QDs from an organic phase into water.....	8
Figure 1.5 A guide relating the chapters of this thesis to the synthesis of high-quality PbS and PbS/CdS QDs in an organic phase and in water in this work.....	13
Figure 2.1 Schematic illustration of the air-free reaction setup for synthesizing PbS QDs.....	15
Figure 2.2 Synthesis of thin-shell PbS/CdS QDs by cation exchange.....	18
Figure 2.3 A flow chart displaying the process for achieving water-soluble QDs.....	21
Figure 3.1 The XRD pattern of PbS QDs. Inset: a high resolution TEM image of a PbS QD.....	28
Figure 3.2 Absorption (a) and PL (b) spectra of PbS QDs prepared at 90 °C with the PbCl ₂ /S ratio of 3:1.....	30

Figure 3.3 TEM images of PbS QDs synthesized at 90 °C with the PbCl ₂ /S ratio of 3:1. The growth time is 1 minute (a) and 150 minutes (b). Inset: a TEM image of small-sized QDs in (b).....	31
Figure 3.4 PL (a) and absorption (b) of QDs after 1-minute growth at 90 °C with the Pb/S ratio ranging from 2:1 to 10:1.....	33
Figure 3.5 PL (a) and absorption (b) spectra of PbS QDs after 1-minute growth at different temperatures. The PbCl ₂ /S ratio is 3:1.....	36
Figure 3.6 Absorption spectra of PbS QDs prepared at 120 °C with the PbCl ₂ /S ratio of 3:1.....	37
Figure 3.7 PL (a) and absorption (b) spectra of PbS QDs after the injection of 200 μL of TOP ligands. The reaction temperature is 90 °C and the PbCl ₂ /S ratio is 10:1.....	39
Figure 3.8 Absorption spectra of PbS QDs synthesized with the PbCl ₂ /S ratio of 3:1 and the reaction time of 1 minute at different temperatures by using OLA#1 (a) and OLA#2 (b) as ligands. The ratio of the integrated absorption A at different synthesis temperatures to that at 80 °C (A/A_{180}) as function of temperature (c). The integrated absorption is calculated herein by integrating the absorbance over the long-wavelength side of the first exciton absorption peak. Absorption HWHM obtained at different synthesis temperatures as function of temperature (d). The solid line is drawn to guide the eye. PbCl ₂ #1 was used as a precursor in both cases.....	42
Figure 3.9 PL (a) and lifetime (b) of PbS QDs in toluene. The PbS QDs were synthesized at 90 °C with the PbCl ₂ /S ratio of 3:1 for 1 minute. Inset: integrated PL intensity versus absorbance at 670 nm for the QDs prepared using either OLA#1 or OLA#2 as a ligand. The linear fit of the data is also shown. PbCl ₂ #1 was used as a precursor in both cases.....	43
Figure 3.10 Absorption and PL of PbS QDs prepared at 90 °C with the PbCl ₂ /S ratio of 10:1 by using PbCl ₂ #1 (a) or PbCl ₂ #2 (b) as a precursor.....	44
Figure 3.11 Absorption (a) and PL (b) of PbS QDs prepared at different conditions. From left to right, emission curves correspond to absorption curves. OLA#2 was used as ligands. PbCl ₂ #1 was used as a precursor.....	45
Figure 3.12 TEM images of PbS QDs synthesized at 90 °C with the PbCl ₂ /S ratio of 3:1 and the reaction time of (a) 1 minute and (b) 2 hours using OLA#2 and PbCl ₂ #2. Scale bar is 50 nm.....	45
Figure 4.1 PL spectra (a) and typical TEM image (b) of PbS/CdS QDs.....	49
Figure 4.2 (a) XPS spectra PbS and PbS/CdS QDs with different shell thickness. Insets of (a): high resolution XPS spectra of Pb 4f of PbS and Cd 3d of CdS for PbS/CdS QDs.....	50

Figure 4.3 EDX spectra of PbS and PbS/CdS QDs, indicating the presence of Pb, S and Cd.....	51
Figure 4.4 Size distribution of PbS QDs in chloroform (5.2 ± 0.2 nm) and PbS/CdS QDs after cation exchange in chloroform (5.0 ± 0.3 nm).....	51
Figure 4.5 Absorption spectra of PbS during cation exchange process.....	52
Figure 4.6 HRTEM image of an individual PbS/CdS QD. Scale bar is 5 nm.....	53
Figure 4.7 TEM image of PbS/CdS QDs. The size of parent PbS QDs is ~ 12 nm.....	53
Figure 4.8 Schematic presentation of pure-CdS-shell (a) and alloy-shell structures (b) of PbS/CdS QDs. (c) Bandgap of PbS and PbS/CdS QDs as a function of PbS diameter. The black solid curve represents the data from ref 24. The blue, cyan and pink solid lines are guides to the eye.....	54
Figure 4.9 Tunable absorption spectra of (a) PbS and (b) PbS/CdS QDs.....	55
Figure 4.10 TEM images of PbS QDs with the first exciton peak at 1460 nm (a) and 1900 nm (b), respectively.....	56
Figure 4.11 TEM images of PbS/CdS QDs with the first exciton peak at 1250 nm (a) and 1800 nm (b), respectively.....	56
Figure 4.12 TEM images of PbS/CdS QDs (a) synthesized by cation exchange at 200 °C for 5 minutes and (b) synthesized via a two-step cation exchange (100 °C for 1 hour, following at 200 °C for 20 hours). The size of parent PbS is ~ 5.2 nm.....	58
Figure 4.13 Schematic presentation of two step cation exchange to synthesize thick-shell PbS/CdS QDs.....	58
Figure 4.14 Representative TEM images of parent PbS (~ 10 nm in diameter) (a) and (b) PbS/CdS QDs synthesized at 100 °C for 1 hour (b), 4 hours (c) and PbS/CdS QDs following growth at 200 °C for another 20 hours (d). Inset of (c) and (d) are HRTEM images of (c) and (d), respectively, indicating clearly the core shell structure. Scale bar for inset images of (c) and (d) is 5 nm.....	59
Figure 4.15 (a) HRTEM image of a thick-shell PbS/CdS QD clearly displaying the core and shell. (b) Absorption spectra of PbS and thick-shell PbS/CdS QDs in toluene. Inset of (b) is the PL spectra of PbS/CdS QDs manifesting characteristic emission from CdS and PbS.....	60
Figure 4.16 PL spectra of PbS (initial) and PbS/CdS QDs with tunable CdS shell thickness. Excitation wavelength was set at 345 nm.....	61

Figure 4.17 PL decay curve for thick-shell PbS/CdS QDs, measured at emission peak of ~ 510 nm in toluene, and shown on a logarithmic scale.....	61
Figure 4.18 XRD patterns of PbS and PbS/CdS QDs with different shell thickness. The JCPDS card files for PbS (05-0592, cyan line) and for CdS (01 089 0440, magenta line) are shown below the spectra for identification.....	62
Figure 4.19 (a) TEM image of a PbS/CdS QD. (b) EDX spectra from the core (yellow circle) and shell (red circle) of the PbS/CdS QD.....	63
Figure 4.20 PL lifetime of parent PbS measured at ~ 1460 nm and PbS/CdS QDs measured at ~ 1320 nm in toluene.....	64
Figure 4.21 (a) The variation in the PL intensity of PbS and PbS/CdS QDs in ODE after four hours of continuous illumination. (b) The PL spectra of PbS and PbS/CdS QDs before and after heat treatment (PbS: 100 °C for 5 minutes in ODE; PbS/CdS: 150 °C for 30 minutes in ODE).....	65
Figure 5.1 FT-IR characterizations of (a) PEG-OH, (b) PMAO and (c) PMAO-PEG.....	70
Figure 5.2 TEM images of as prepared PbS QDs in chloroform (a), and PbS/PMAO-PEG QDs in chloroform (b), immediately after transfer into water (c) and ethanol (d). Scale bar is 20 nm.....	72
Figure 5.3 Schematic representation of the process leading to the double size distribution of PbS QDs after transfer into water.....	74
Figure 5.4 (a) PL of PbS QDs in chloroform prior to polymer encapsulation, after PMAO-PEG encapsulation in chloroform, following transfer into water and after being stored in water at 4 °C for 1 minute and 5 minutes. (b) PL of PbS/PMAO-PEG QDs in chloroform and following transfer into ethanol.....	75
Figure 5.5 (a) PL of PbS QDs being stored at 4 °C for 3 months in water and following transfer back into chloroform. Two resolved PL peaks from the Gauss fitting for the PL curve of PbS QDs in chloroform are also shown. (b) PL of PbS solid films dried from PbS/PMAO-PEG QDs dispersed in chloroform or stored in water for 3 months.....	78
Figure 5.6 (a) Representative TEM photographs of PbS QDs stored at 4 °C for 3 months in water. (b) XRD of PbS QDs prior to water transfer and after being stored in water for 3 months. Inset of (a): enlarged TEM images of the larger and smaller QDs.....	81
Figure 5.7 High resolution Pb 4f XPS spectra of smaller (a) and larger (b) PbS/PMAO-PEG QDs following transfer into water and after being stored in water at 4 °C for 3 months. The dots represent experimental data. The red and blue lines are fitting curves and the gray line is the sum of them. The light blue line is a background curve.....	82

Figure 5.8 XRD (a) and XPS (b) spectra of PbS-OLA, PbS-OA and PbS-OA/TOP QDs. Data of the JCPDS card (05-0592) for PbS are also included for identification.....	84
Figure 5.9 TEM images of (a,d) PbS-OLA, (b,e) PbS-OA and (c,f) PbS-OA/TOP QDs in chloroform (a, b, c) and after polymer encapsulation and transfer into water (d, e, f) via PMAO-PEG. Scale bar is 20 nm.....	86
Figure 5.10 Hydrodynamic diameter of PbS-OLA QDs in chloroform (a), PMAO-PEG encapsulated PbS-OLA QDs before transfer in chloroform (b) and after transfer into water (c), measured by dynamic light scattering.....	86
Figure 5.11 Absorption and PL spectra of PMAO-PEG encapsulated PbS QDs capped by different ligands (OLA, OA and OA/TOP) in chloroform prior to water transfer and PL spectra of QDs following transfer into water.....	88
Figure 5.12 High resolution XPS spectra of Pb 4f in PbS capped by OLA (a), OA (b) and OA/TOP (c) ligands before and after transfer into water via PMAO-PEG. The dots represent experimental data. The thin lines are fitting curves and the thick line is the sum of them. The dash line is a background curve. S_{Pb} represents surface Pb atoms bonded with OA ligands and V_{Pb} the Pb atoms in the interior of QDs.....	91
Figure 5.13 PL spectra of freshly prepared PMAO-PEG encapsulated PbS-OA QDs in water (a) and integrated PL intensity of freshly prepared PMAO-PEG encapsulated PbS QDs capped by different types of capping ligands (b) subject to UV illumination for different time. The quickly drop in PL intensity of PbS-OLA in water occurs within 1 minute.....	92
Figure 6.1 Dynamic light scattering measurement of the hydrodynamic radius of PbS/CdS QDs in water (average hydrodynamic size is ~22 nm).....	98
Figure 6.2 Representative TEM images of (a) PbS/CdS QDs before transfer, and (b) PbS/CdS QDs following transfer into water. Inset of (a) is a high resolution TEM image of an individual QD and scale bar is 5 nm.....	98
Figure 6.3 Size distribution of PbS/CdS QDs in chloroform (5.0 ± 0.3 nm) and in water (5.0 ± 0.3 nm).....	99
Figure 6.4 PL (a) and absorption (b) spectra of PbS, and PbS covered by a CdS shell before and after transfer into water using PMAO-PEG. Absorption curves correspond to emission curves of the same color.....	99
Figure 6.5 High resolution XPS spectra of Pb 4f of PbS/CdS QDs before and after transfer into water via PMAO-PEG.....	101
Figure 6.6 High resolution XPS spectra of Cd 3d in PbS/CdS before and after transfer into water via PMAO-PEG, indicating the CdS shell is stable during the transfer	

process.....	101
Figure 6.7 Absorption (a) and PL (b) spectra of initial PbS QDs (dot) and PbS/CdS QDs (line) dispersed in chloroform.....	105
Figure 6.8 (a) Typical TEM image of PbS/CdS QDs synthesized at 100 °C for 4 hours with initial PbS size of 5.2 nm. (b) High resolution TEM image of (a).....	107
Figure 6.9 TEM images of PbS/CdS#1 (a, d), PbS/CdS#2 (b,e) and PbS/CdS#3 (c,f) before polymer encapsulation in chloroform (a, b, c) and after transfer into water (d, e, f) via PMAO-PEG. Scale bar is 20 nm.....	108
Figure 6.10 PL and absorption spectra of PbS/CdS QDs after transfer into water via PMAO-PEG.	109
Figure 6.11 The QY of PbS/CdS QDs before and after water transfer as a function of CdS shell thickness. The solid lines are guides to the eye.....	110
Figure 6.12 Absorption peak shifts and QY variation of PbS/CdS QDs before and after transfer into water as a function of CdS shell thickness. The solid lines are guides to the eye.....	111
Figure 6.13 (a) PL spectra of PbS/CdS QDs in PBS buffers containing different NaCl concentrations and (b) PL intensity of PbS/CdS QDs in PBS buffer as a function of NaCl concentration.....	113
Figure 6.14 TEM image of PbS/CdS#3. PbS/CdS QDs were dispersed in PBS buffer containing 300 mM NaCl.....	113
Figure 6.15 (a) PL spectra of PbS/CdS QDs in PBS buffer under continuous illumination and (b) PL intensity of PbS/CdS QDs in PBS buffer as a function of illumination time. Inset of (b) is the PL variation of PbS/CdS QDs after 2-hour of illumination as a function of CdS shell thickness.....	115
Figure 6.16 (a) PL spectra of water-soluble PbS/CdS QDs with varying core size and constant CdS shell thickness of 0.7 nm. (b) Typical TEM image of water-soluble, 0.7-nm-thick-shell PbS/CdS QDs.....	116

List of Tables

Table 4.1 Experimental parameters for synthesizing PbS/CdS QDs presented in Figure 4.1a...51

Table 5.1 PL maxima (λ_{em}), FWHM, lifetime (τ) and intensity variation (reflected by: PL intensity ratio = PL intensity after transfer into water/PL intensity before transfer) of PMAO-PEG encapsulated PbS QDs capped by different ligands before and after transfer into water. The fluorescence lifetime of PbS-OLA QDs in water cannot be measured due to the fast decay of PL.....88

Table 6.1 Initial PbS size based on TEM observations, PbS size estimated from absorption peak positions [86], Absorption maxima (λ_{abs}), and PL maxima (λ_{em}) of PbS QDs in chloroform. PL peak positions of PbS/CdS#6-7 cannot be measured due to the limitation of our NIR detector.....104

Table 6.2 The overall size of PbS/CdS QDs based on TEM observations, estimated core size and shell thickness from methods #1 and #2, absorption maxima (λ_{abs}), PL maxima (λ_{em}), PL FWHM and QY for PbS/CdS QDs in chloroform. Method#1: core size estimated from absorption peak positions and shell thickness calculated by: overall size – core size; Method#2: core size and shell thickness estimated from Cd/Pb ratios determined by ICP-OES measurements and overall sizes by TEM [70].....104

Chapter 1

Introduction

1.1 What quantum dots (QDs) are and their properties

Semiconductor QDs are fluorescent nanocrystals normally smaller than 20 nanometers in diameter [1]. Bulk semiconductors are characterized by composition-dependent band gap, which is the minimum energy required to excite an electron from the valence band into the conduction band. With the absorption of a photon of energy greater than band gap energy, the excitation of an electron leaves an orbital *hole* in the valence band to form an electron-hole pair (exciton). Relaxation of the excited electron back to the valence band may be accompanied by the emission of a photon, a process known as *radiative recombination* (Figure 1.1). The exciton has a finite size defined by the exciton Bohr radius. When the size of a semiconductor nanocrystal is smaller than the Bohr radius, the charge carriers become spatially confined and energy levels are quantized (Figure 1.1), with values directly related to the QD size [1, 2]. In the case of quantum confinement, QDs show size-dependent band gap, as described in Equation 1.1 [2],

$$E = E_g + (\hbar^2 \pi^2 / 2R^2) (1/m_e + 1/m_h) - 1.8e^2 / \epsilon R \quad (1.1)$$

where E_g is the band gap energy of corresponding bulk material, \hbar is Plank constant, m_e and m_h are the effective mass of electron and hole, respectively, e is the charge of electron, and R and ϵ are the

radius and dielectric constant of QDs, respectively. It is to say that semiconductor nanocrystals with dimensions smaller than the exciton Bohr radius show size-dependent absorption and emission [3, 4, 5, 6, 7, 8, 9, 10, 11]. For example, as shown in Figure 1.2a, the emission wavelength of CdSe QDs (E_g , 1.76 eV) can be tuned throughout the visible range by adjusting the QD size. Together with the composition control, the emission of QDs can span essentially the entire visible and near infrared (NIR) spectral range (Figure 1.2b).

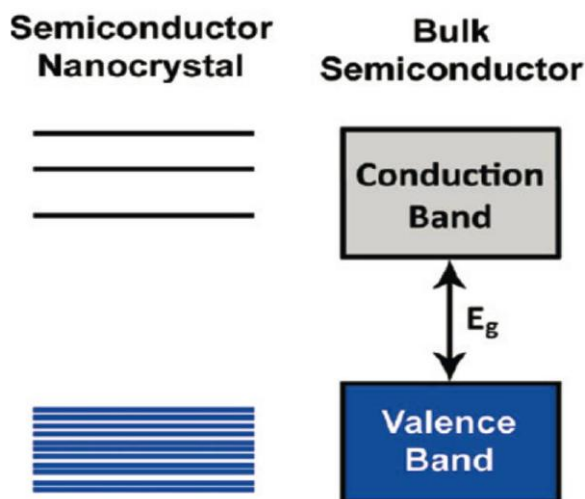


Figure 1.1 Electronic energy states of a semiconductor in the transition from nanosized crystals to bulk crystals. Blue shading denotes ground state electron occupation. Figures 1.1 is from [18].

It is worthwhile to make comparison between QDs and conventional fluorophores. As mentioned above, the emission of QDs can well cover the NIR range, which is difficult to achieve with conventional organic fluorophores. In addition, in marked contrast to most of conventional fluorophores, QDs have broadband absorption and narrow emission, which promises their use in multiplex detection (Figure 1.2c). Another advantage of QDs is that they are several tens of times brighter than organic dyes, which enables more sensitive detection of analytes in low concentration solutions [3]. QDs also show much higher photostability, which is advantageous for the long-term,

real-time monitoring and tracking of biospecies and bioactivities [3]. Last but not least, the long fluorescence lifetime of QDs, typically on the order of several tens of nanoseconds, allows us to distinguish the emission of QDs from background autofluorescence in cells which leads to a high signal-to-noise ratio, important for the use of QDs as efficient bio-labels [12, 13, 14, 15, 16, 17]. To summarize, QDs have great potential to become a new generation of biomarkers for highly demanding applications. Tailored synthesis of water soluble QDs is the key to realize their high potential.

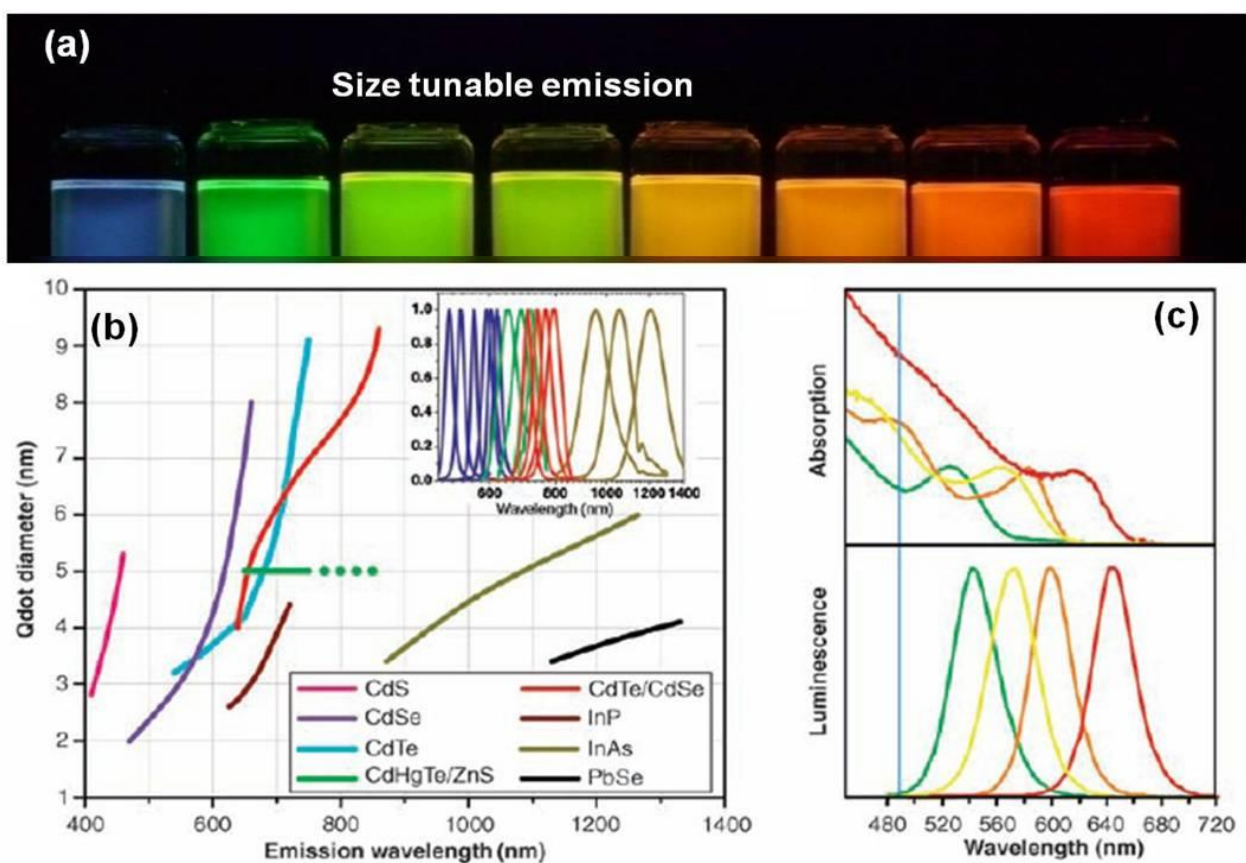


Figure 1.2 (a) Size tunable photoluminescence (PL) spectra of CdSe QDs. (b) Emission maxima and sizes of QDs of different composition [4, 6, 7, 8, 9, 10, 11]. Inset: representative emission spectra for some materials. (c) Absorption (upper curves) and emission (lower curves) spectra of four CdSe/ZnS QDs samples. The blue vertical line indicates the 488-nm line of an argon-ion laser, which can be used to efficiently excite all QDs simultaneously [3, 5]. Figure 1.2a is our unpublished data. Figures 1.2b and c are from [3].

1.2 Why are NIR emitting QDs attractive?

In vivo optical bioimaging prefers the use of fluorophores whose excitation and emission lights are least absorbed and scattered by biological fluids and tissues (water, hemoglobin, and lipids) [19, 20]. Based on this consideration, the NIR ranges of 700–900 nm and 1200–1600 nm have been theoretically predicted and partially experimentally confirmed as two best spectral windows for bioimaging [19, 20]. Although organic NIR dyes are being employed for in vivo optical imaging [21, 22], their emission wavelengths are limited to below 950 nm [23, 24]. Not to mention most of them have the susceptibility to photobleaching [23, 24]. It is thus highly desirable to develop more flexible and robust NIR labeling agents.

Over the last ten years, research interest in NIR-emitting QDs has grown rapidly all over the world. NIR-emitting QDs show broader absorption, greater tunability in the emission wavelength, higher quantum yield (QY, defined as the ratio of the photons emitted to the photons absorbed) and better photostability compared to organic dyes. Owing to these beneficial properties, they hold great potential for live cell imaging, for tracking the movement of molecules within a single cell, for single-particle detection and for deep tissue imaging [19, 24, 25]. As an example, Figure 1.3 shows NIR-emitting lysine cross-linked mercaptoundecanoic acid core/shell CdSe_{0.25}Te_{0.75}/CdS QDs can potentially be used for long-term targeted imaging in vivo [26]. However, most of QDs contain toxic elements, such as Cd, Pb, Hg and As. To alleviate the toxicity of QDs, a variety of synthesis and surface modification techniques have been proposed and realized, and some of them were shown to be able to reduce the cytotoxicity [12, 13, 14, 15, 16, 17, 26].

Various kinds of NIR-emitting QDs have been reported. These include HgSe, HgTe, InAs, InSb, PbX (X=S, Se, Te), CdHgTe and CdTe/CdSe QDs [18, 27, 28, 29, 30, 31, 32, 33, 34, 35, 36,

37]. Among them, lead chalcogenide QDs have large exciton Bohr radii sharing almost equally between the electron and hole. For instance, PbS QDs have the equal hole and electron radii of 9 nm [31]. This permits similarly strong confinement of both electrons and holes in relatively large sized QDs. In contrast, although InSb QDs have a large exciton Bohr radius of 54 nm, the Bohr radius of its hole is only 2 nm [18]. This prevents strong confinement of the hole in InSb nanocrystals even if their diameter is only a few nm. Meanwhile, the lead chalcogenide QDs have small bulk band gaps (0.41, 0.28 and 0.31 eV at 300 K for PbS, PbSe and PbTe, respectively) [14], and can be tuned to emit over a quite large spectral range of 850 to 2200 nm with a very broad absorption spectrum and a narrow PL spectrum [31, 32]. These features make lead chalcogenide QDs especially attractive for in vivo bioimaging and among them, PbS QDs are of particular interest because they can be produced with inexpensive and relatively less hazardous precursors [31].

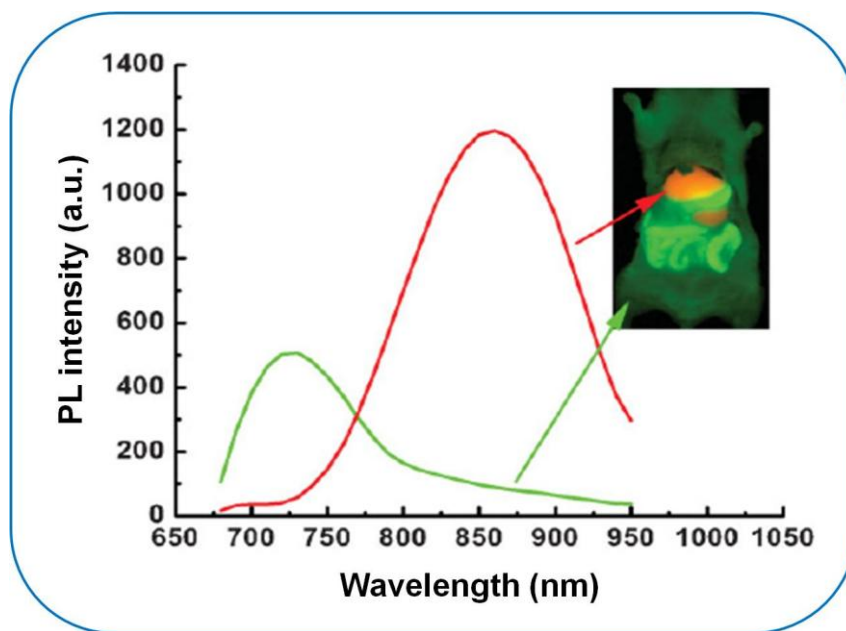


Figure 1.3 NIR luminescence imaging of BALB/c mouse treated with lysine cross-linked mercaptoundecanoic acid core/shell $\text{CdSe}_{0.25}\text{Te}_{0.75}/\text{CdS}$ QDs as NIR optical probes [26]. The background autofluorescence (from the mouse) is colored green and NIR QD signal is pseudocolored red.

1.3 PbS synthesis

PbS QDs have been synthesized in diverse media: glasses [38, 39, 40], polymer matrices [41, 42], aqueous solution [43, 44], organics [45], zeolites [46], liquid crystals [47], and on self-assembled monolayers using different approaches such as electrochemical [48] and sonochemical techniques [49]. Those with the high QY are almost exclusively synthesized by a high temperature organometallic route using a popular hot-injection method [31, 32]. For example, Hines and Scholes for the first time reported the organometallic synthesis of PbS QDs with size-tunable emission in NIR using oleic acid (OA) as a ligand, and lead oxide and bis(trimethylsilyl) sulfide ((TMS)₂S) as precursors [31]. Typical details of synthesis are shown in the following. First, certain amount of PbO dissolved in OA was purged with nitrogen gas flow and heated in a reaction flask to 150 °C. Stock solutions of (TMS)₂S and octadecene (ODE) were then added to the flask and mixed with vigorous stirring, where the PbS nanocrystals nucleated quickly. The temperature was maintained at 100 °C for the growth of nanocrystals. Aliquots of the reaction solution were removed from the flask at regular time intervals to obtain different sizes of QDs. This synthetic approach is able to produce PbS nanocrystals with an absorption edge ranging from about 800 to 2000 nm [31]. Currently, most of the synthesis of PbS QDs follows this or slightly modified recipe and involves the use of (TMS)₂S, which is toxic, odorous and chemically unstable [31, 50, 51]. A greener approach, in which (TMS)₂S is replaced with S, has been explored recently by Ozin's group [32]. In their synthesis, high-quality PbS nanocrystals could be produced in multigram-scale quantities. However, the reaction is required to undergo in a viscous system with a very high concentration of lead precursors and a high molar ratio of Pb-to-S [32]. A greener yet simpler synthesis method is thus needed.

On the other hand, to be used in biological systems, QDs are required to have good water solubility, colloidal stability, photostability and biocompatibility as well as exhibit high QYs [17]. Nowadays, several methods have been employed to synthesize water-soluble NIR-emitting PbS QDs [44, 52, 53, 54, 55, 56, 57, 58, 59]. One approach is based on the direct synthesis of PbS QDs in water, which however, in general leads to a low QY with broad absorption and emission spectra [44, 52, 53, 54, 55]. Moreover, as-synthesized water-soluble PbS QDs show very poor stability due to the QD surface sensitivity to oxygen. Zhao *et al.* have reported that PbS QDs in water aggregated due to the oxidation of thiol capping groups [52].

Ligand exchange, based on the concept of transferring high-quality PbS QDs originally prepared in an organic phase into water via changing surface capping agents from hydrophobic to hydrophilic ones, appears to be a better approach [56, 57] (Figure 1.4). Over the past decade, this approach has been widely used as an efficient way to move nanoparticles around in different phases in addition to modifying the surfaces of various nanoparticles. However, in the case of QDs, this approach has been found to lead to a significant decrease of the QY after water transfer because of stripping of original surface ligands from QD surfaces and the sensitivity of this property to the surface chemistry of QDs [56, 57]. As for PbS QDs, the maximum QY that can be achieved by this method is 26% in a buffer solution [57].

To avoid ligand stripping and thereby keep the high QY of organometallically prepared QDs, the method of amphiphilic polymer encapsulation has recently been investigated [58, 59]. It is believed that this approach will not disturb the original capping ligands from QD surfaces (Figure 1.4). Instead, multiple hydrophobic chains of the amphiphilic polymer can have numerous interactions with the native hydrophobic ligands on the QD surface, and thus helping “fix” the ligands on the surface [58]. On the other hand, the hydrophilic end groups of the amphiphilic

polymer endow the QDs with good water solubility and even biocompatibility. This approach has indeed been successfully applied to ultraviolet (UV)-visible (Vis) QDs [58, 59].

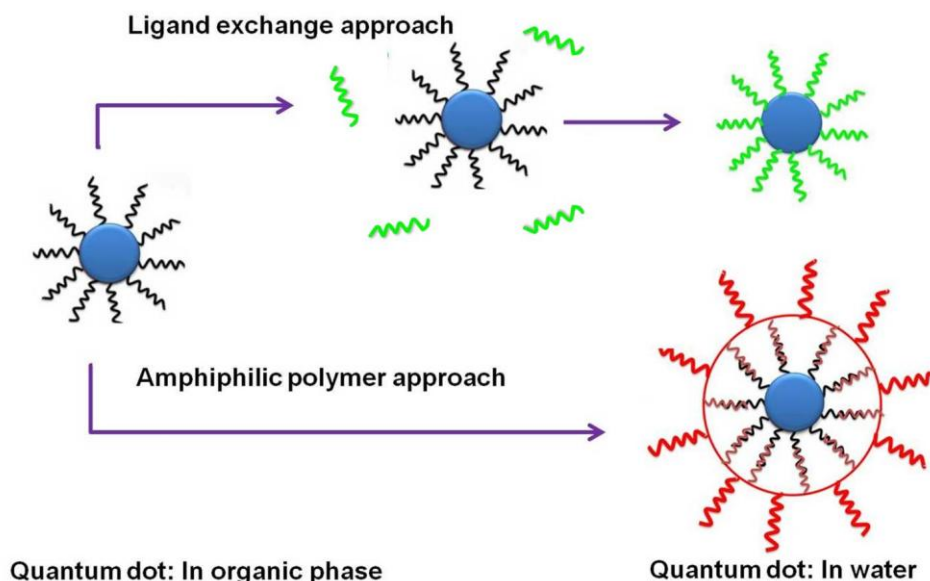


Figure 1.4 Ligand exchange and amphiphilic polymer encapsulation approaches for transferring QDs from an organic phase into water.

1.4 Synthesis of core/shell QDs

Normally, QDs capped only by organic surface ligands are very sensitive to the surface status due to their high surface-to-volume ratio. The introduction of trap states can lead to the considerable decrease of fluorescence QY. Recent studies have revealed that a core/shell structure can stabilize and maximize the fluorescence of core QDs [60, 61, 62, 63]. A robust, larger band gap inorganic shell not only passivates surface atoms, but also buries the core semiconductor in a potential energy well, and thus concentrating the charge carriers in the nanocrystal core and keeping them away from the surface and surrounding environment [61, 62, 63]. As a result, surface defect states, trap sites and environmental factors will have diminished impact on the fluorescence efficiency and stability [61, 62, 63, 64, 65]. For example, in the core/shell structured CdSe/ZnS QDs, the wider band gap

ZnS shell not only largely enhances the QY (from around 15% to 50%) of CdSe nanocrystals, but also improves their stability [65].

The growth of the shell has most commonly been achieved by exposing core nanocrystals to all the precursors of shell elements. A representative example is the use of diethylzinc (Zn precursor) and hexamethyldisilathiane (S precursor) for the synthesis of ZnS overcoated CdSe QDs [65]. In that case, the core size remains essentially constant during the overcoating process. Similar approach has also been explored for synthesizing NIR core/shell QDs, such as PbSe/PbS [67]. Recently, a relatively less used approach, cation exchange, has been reported for the growth of a wider band gap material onto lead chalcogenide QDs [60]. In contrast to the above-mentioned common approach, only the precursor of cationic constituent of a shell material was introduced in this approach and the shell growth proceeds through the gradual replacement of Pb cations by newly introduced cations in solution and anion sublattice remains basically un-disturbed [60]. As a result, the shell grows at the expense of core nanocrystals, *i.e.*, the shell growth is accompanied by the decrease of the lead chalcogenide core size.

The formation of PbSe/CdSe core/shell QDs by cation exchange has been demonstrated for the first time by Pietryga *et al.* and it is found that the core/shell structure large enhances the QY of PbSe QDs [60] due to the effective “inorganic passivation” of the PbSe core by the CdSe shell, in a manner similar to the well-known CdSe/ZnS core/shell system [65]. Moreover, the CdSe shell exhibits relatively higher stability under ambient conditions, resulting in dramatic improvement in the stability of PbSe/CdSe QDs compared to “bare” PbSe QDs [60]. Although the visible-emitting core/shell QDs have been widely studied, relevant reports on NIR-emitting QDs, especially PbS-based core/shell QDs, are still quite limited.

1.5 Thesis objectives and contributions of this work

Synthesis of high-quality PbS QDs in the organic phase has been reported [31, 32]. However, in their synthesis, the toxic $(\text{TMS})_2\text{S}$ is used as S precursor [31] or the reaction is required to undergo in a viscous system formed by using a very high concentration of PbCl_2 in oleylamine (OLA) [32]. It is highly desirable to develop a simple and greener approach with good reproducibility and easy manipulation. In addition, although overcoating QDs with large bandgap semiconducting materials is expected to enhance their QY, the QY of recently developed, CdS overcoated PbS QDs is still quite low (typically 20-30%) [60]. In addition, the cation exchange approach seems to have its limitation on the maximum shell thickness that can be achieved [60]. The core/shell structure has not been thoroughly investigated either. It is challenging while important to develop a more feasible method to synthesize PbS/CdS core/shell QDs, to carefully characterize their structure and properties, and to further optimize experimental conditions for the best possible properties.

Meanwhile, as mentioned above, the amphiphilic polymer approach is a very promising method to synthesize water-soluble QDs. Although this approach has been applied to Vis-emitting QDs [59], relevant reports on NIR-emitting PbS QDs are still lacking. It is highly desirable but also challenging to develop a feasible approach to synthesize high-quality water-soluble NIR-emitting PbS-based QDs.

To address all these issues and gain more understanding on PbS-based QDs, I plan to synthesize and characterize high-quality PbS QDs and CdS overcoated PbS QDs (i.e., PbS/CdS core/shell QDs) in an organic phase and in water. Therefore, the objectives of my projects are:

1. to find a greener yet simple approach to synthesize high-quality PbS QDs in the organic phase and to characterize their structure and properties.

2. to develop a new, flexible approach to synthesize PbS/CdS core/shell QDs with varying shell thickness and to perform detailed structural and property investigations.
3. to secure a new route to synthesize high-quality water-soluble NIR emitting PbS and PbS/CdS QDs via amphiphilic polymers.

1.6 Thesis organization

This thesis is divided into seven parts and organized as follows:

Chapter 1 introduces the topic of this thesis and outlines the motivation for this work.

Chapter 2 describes experimental details of synthesis process for PbS and PbS/CdS QDs in the organic phase and in water. Characterization details of PbS and PbS/CdS QDs are also given in Chapter 2.

Chapter 3 presents and discusses a greener and simple route to synthesize colloidal PbS QDs in the organic phase. To be more specific, the synthesis was done in a “non-viscous”, solventless OLA organic phase by using relatively low concentrations of PbCl₂ and S. The publications related to this chapter are:

[68] **H. Zhao**, M. Chaker, and D. Ma. Bimodal Photoluminescence during the Growth of PbS Quantum Dots. *Journal of Physical Chemistry C*, 113:6497–6504, 2009.

[69] **H. Zhao**, T. Zhang, M. Chaker, and D. Ma. Ligand and Precursor Effects on the Synthesis and Optical Properties of PbS Quantum Dots. *Journal of Nanoscience and Nanotechnology*, 10:4897–4905, 2010.

Chapter 4 presents a new two-step cation exchange approach to synthesize PbS/CdS core/shell QDs with varying shell thickness in the organic phase and discusses the core/shell structure and

chemical composition of the shell in PbS/CdS QDs. In Chapter 4 I also discuss the properties of PbS/CdS QDs including QY and photo- and thermal- stability. The publication related to this chapter is:

[70] **H. Zhao**, M. Chaker, N. Wu, D. Ma. Towards Controlled Synthesis and Better Understanding of Highly Luminescent PbS/CdS Core/shell Quantum Dots. *Journal of Materials Chemistry*, 21:8898–8904, 2011.

Chapter 5 explores the structure and optical properties of PbS QDs capped by OLA ligands after being transferred into water via amphiphilic polymers. Furthermore, I study the mechanism for the PL disappearance and automatic, size-selected PL recovery of PbS QDs in water. Finally, I investigate the effect of different types of surface capping ligands on the final optical properties of PbS QDs after water transfer. The publications related to this chapter are:

[71] **H. Zhao**, M. Chaker, and D. Ma. Self-selective Recovery of Photoluminescence in Amphiphilic Polymer Encapsulated PbS Quantum Dots. *Physical Chemistry Chemical Physics*, 12:14754–14761, 2010.

[72] **H. Zhao**, D. Wang, M. Chaker, and D. Ma. Photoluminescence Effect of Different Types of Surface Ligands on the Structure and Optical Property of Water-soluble PbS Quantum Dots Encapsulated by Amphiphilic Polymers. *Journal of Physical Chemistry C*, 115:1620–1626, 2011.

Chapter 6 describes a novel two-step approach (synthesis of core/shell QDs followed by water transfer via amphiphilic polymers) to prepare high-quality PbS QDs in water. In this chapter, I also investigate the effect of CdS shell thickness on the optical properties of water-soluble PbS/CdS QDs and identify optimal experimental conditions. The publications related to this chapter are:

[73] H. Zhao, D. Wang, T. Zhang, M. Chaker, and D. Ma. Two-step Synthesis of High-quality Water-soluble Near-infrared Emitting Quantum Dots via Amphiphilic Polymers. *Chemical Communications*, 46:5301–5303, 2010.

[74] H. Zhao, M. Chaker, and D. Ma. Effect of CdS Shell Thickness on the Optical Properties of Water-soluble Amphiphilic Polymer Encapsulated PbS/CdS Quantum Dots. *Journal of Materials Chemistry*, 21:17483–17491, 2011.

Chapter 7 briefly summarizes important contributions of this work and states future challenges in this field.

Following the main body of thesis is an appendix providing a summary of this thesis in French as per INRS requirements.

I show in Figure 1.5 a visual guide relating the chapters of this thesis to the synthesis and characterization of high-quality PbS and PbS/CdS QDs in an organic phase and in water in this project.

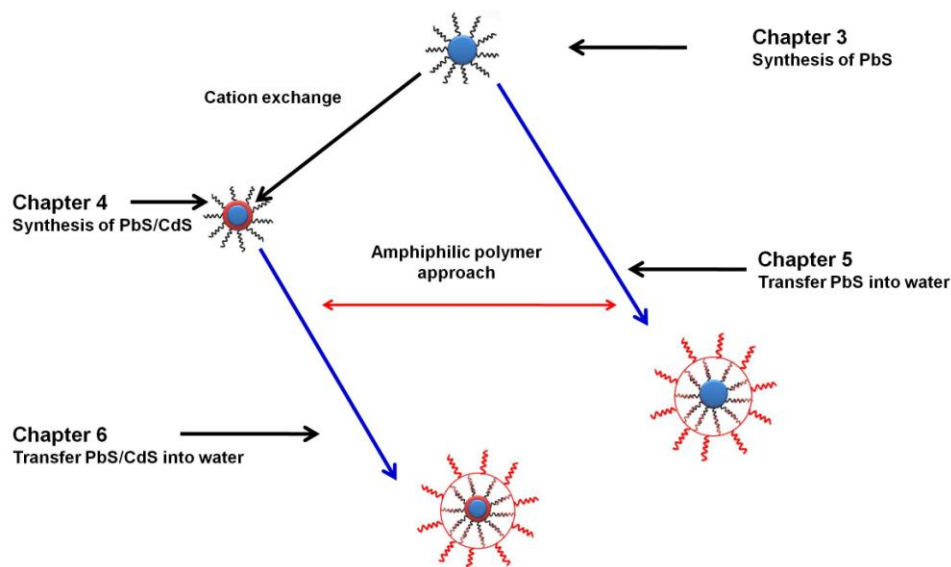


Figure 1.5 A guide relating the chapters of this thesis to the synthesis of high-quality PbS and PbS/CdS QDs in an organic phase and in water in this work.

Chapter 2

Experimental

In this chapter I introduce the synthesis and characterization details for colloidal PbS and PbS/CdS QDs related to the results to be presented and discussed in Chapter 3–6. Firstly, PbS QDs were synthesized in a “non-viscous”, solventless, mild-constant-temperature system with PbCl₂ and S as precursors and characterized. Then I turned to synthesize PbS/CdS QDs, via cation exchange in the organic phase, which show largely enhanced QY of PbS core QDs. Furthermore, I focused on the development of high-quality water-soluble PbS and PbS/CdS QDs by transferring high-quality QDs synthesized in an organic phase into water via amphiphilic polymers.

2.1 Materials

PbCl₂ (100 wt%), sulfur (100%), OA, OLA (amine content, 97 wt%; C₁₈-amine content, 80-90 wt%), hexane, ethanol, tetrahydrofuran (THF), chloroform and toluene were purchased from Fisher Scientific Company. PbCl₂ (98 wt%), OLA (amine content, >98 wt%; C₁₈-amine content, 70 wt%), lead acetate trihydrate, sulfur (100%), trioctylphosphine (TOP, 90%), cadmium oxide (99%), (TMS)₂S, phenyl ether, poly(maleic anhydride-alt-1-octadecene) (PMAO, number average molecular weight, 30000-50000), cardiogreen (IR 125), rhodamine 6G, poly(ethylene glycol) methyl ethers (PEG–OH, molecular weight 2000), dimethyl sulfoxide, ODE, phosphate buffered saline buffer (PBS) and concentrated H₂SO₄ (98%) were obtained from Sigma-Aldrich Inc. All

chemicals were used as purchased. All air and water-sensitive chemicals are kept in the glove box under the protection of N_2 .

2.2 Reaction setup

QDs are very sensitive to oxygen during the nucleation and growth processes. With the presence of oxygen (or air), the QDs will oxidize, leading to the low QY and bad photostability. Therefore, I set up the reaction in an air-free system, as schematically shown in Figure 2.1. The oxygen can be removed by vacuum pumping and nitrogen purging, and nitrogen flux can further protect the entire chemical reaction from the air. In the following, all the QDs were synthesized by using this reaction setup.

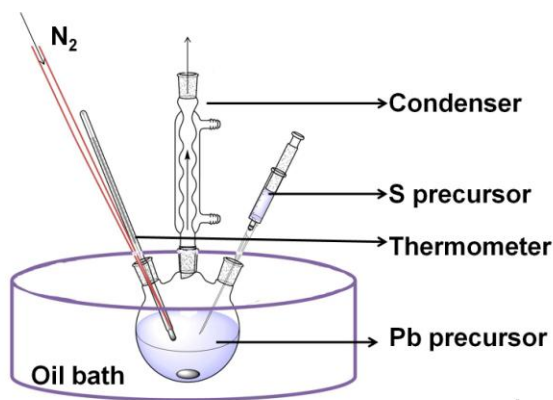


Figure 2.1 Schematic illustration of the air-free reaction setup for synthesizing PbS QDs.

2.3 Synthesis

2.3.1 Synthesis of PbS and PbS/CdS QDs in the organic phase

2.3.1.1 Synthesis of PbS QDs

PbS QDs were synthesized by using OLA as ligands in a simple, “non-viscous”, solventless,

constant-temperature reaction system using a relatively safe precursor S. The typical procedure is as follows:

1. PbCl_2 (1 mmol) and 5 mL of OLA were loaded into a 50 mL three-neck flask at room temperature. The mixture was first vacuumed and purged by N_2 for 45 minutes to remove oxygen and then heated to $90\text{ }^\circ\text{C}$ to form the homogeneous PbCl_2 -OLA suspension under magnetic stirring.
2. Two and half milliliters of a solution of sulfur (0.33 mmol) in OLA was purged by N_2 for 30 minutes to remove oxygen and then heated to $90\text{ }^\circ\text{C}$.
3. The S-OLA mixture was quickly injected into the PbCl_2 -OLA suspension under vigorous stirring and the reaction was allowed to continue at the same temperature for 1 minute to 540 minutes.
4. The reaction mixture was taken from the reaction setup and quenched by cold hexane.
5. Excess PbCl_2 precursors were precipitated by centrifugation at $4\text{ }^\circ\text{C}$. Further purification of PbS QDs can be done with ethanol to completely remove un-reacted precursors by repeated centrifugation and decantation.

In order to understand the growth mechanism for PbS QDs and also choose the optimal reaction conditions for achieving the high-quality PbS QDs, the synthesis was also carried out by varying the reaction parameters (reaction time, reaction temperature and PbCl_2/S ratios) and capping ligands. In addition, the synthesis of PbS QDs using chemicals (OLA and PbCl_2) of different purity status was also carried out following the same procedure. The synthesis process can produce the PbS QDs with excitonic absorption wavelength covering from 1180 to 1600 nm by varying the reaction conditions.

I also synthesized PbS QDs capped by OA or OA/TOP ligands with similar size according to literatures [31, 35] which were used for investigating the surface capping ligand effect on the optical property of PbS QDs during the water transfer process via the amphiphilic polymer approach. The synthesis of PbS QDs capped by OA ligands was conducted as follows.

1. A mixture of lead acetate trihydrate (1 mmol), OA (1.2 mL) and ODE (15 mL) was heated at 150 °C for 1 hour under N₂.
2. Then the system was cooled down to 100 °C under vacuum to drive off two intermediate products (water and acetic acid) and afterwards re-stabilized at 130 °C.
3. Subsequently, the mixture containing (TMS)₂S (0.5 mmol) and 5 mL of ODE was quickly injected into the reaction flask.
4. The reaction was quenched by cold water.

A slightly modified method was used to synthesize PbS QDs capped by OA/TOP double-type ligands [50]. A typical synthesis procedure is shown in the following:

1. A mixture of lead acetate trihydrate (1 mmol), OA (1.2 mL), TOP (1 mL) and ODE (15 mL) was heated at 150 °C for 1 hour under N₂.
2. Then the temperature was lowered to 100 °C under vacuum to drive off two intermediate products (water and acetic acid) and afterwards re-stabilized at 150 °C.
3. Subsequently, the reaction mixture containing (TMS)₂S (0.5 mmol), 0.2 mL of TOP and 4.8 mL of ODE was quickly injected into the reaction flask.
4. The reaction was allowed to last for 10 minutes at 130 °C.

5. The reaction was quenched by cold water.

The PbS QDs capped by OA or OA/TOP were precipitated by adding alcohol and then re-dispersed in hexane. Un-reacted precursors were completely removed by repeated centrifugation and re-dispersion at least three times. The purified PbS QDs were dispersed in toluene or chloroform for characterizations or subsequent preparations.

2.3.1.2 Synthesis of PbS/CdS QDs

Recent studies have revealed that the core/shell structure can stabilize and maximize the fluorescence of core QDs. And cation exchange approach is an efficient way to produce the core/shell structure of QDs. Herein, the thin-shell PbS/CdS QDs were achieved by cation exchange method [60], as shown in Figure 2.2.

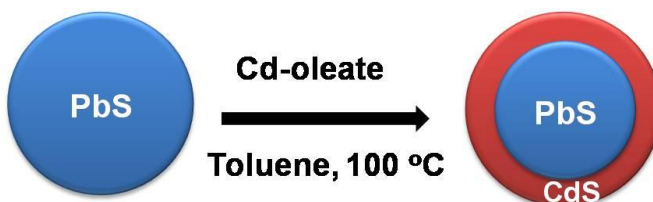


Figure 2.2 Synthesis of thin-shell PbS/CdS QDs by cation exchange.

The cation exchange procedure was carried out under N₂ atmosphere. All solvents used in the procedure are anhydrous and oxygen free. The procedure is as follows:

1. PbS QDs were synthesized by using OLA as ligands [32, 68, 69].

2. PbS QDs dispersed in toluene (10 mL, with an absorbance of 0.3 at the first exciton peak) were purged by N₂ for 30 minutes to remove oxygen and then quickly heated to 100 °C.
3. CdO (2.3 mmol), OA (2 mL) and phenyl ether (10 mL) were heated to 255 °C under N₂ for 20 minutes.
4. The clear solution was cooled to 155 °C under vacuum for 15 minutes. The flask was then reopened and the N₂ flux was restored.
5. The Cd/OA mixture was injected into PbS QDs suspension in toluene.
6. The reaction cell was quenched with cold water after the growth reaction was conducted at 90 or 100 °C for different time.
7. Alcohol was added (QD solution: alcohol = 1:1 in volume), and then the suspension was centrifuged and supernatant was removed. QDs were re-dispersed in hexane. This process was repeated for at least two times. The final QDs were re-dispersed in toluene or chloroform.

The general synthesis process can produce the PbS/CdS QDs with excitonic absorption wavelength spanning from 800 to 1960 nm by choosing different, initial PbS sizes and varying the reaction time and molar ratio of PbS QD to Cd-oleate. The CdS shell thickness that can be achieved with the above procedure is around 0.1 to 1.5 nm. In order to achieve the PbS/CdS QDs with a thicker shell, I developed a two-step approach. The procedure is as follows:

1. CdO (11 mmol), OA (10 mL) and phenyl ether (15 mL) were heated to 255 °C under N₂ for 2 hours.
2. The Cd precursor solution (155 °C) was injected to PbS QDs suspension in toluene at 100 °C (10 mL, with an absorbance of 0.3 at the first exciton peak).
3. Growth reaction was conducted at 100 °C for 240 minutes.
4. The reaction temperature was increased to 200 °C ~ 240 °C and the reaction was allowed to proceed for 0.5 to 48 hours.
5. Alcohol was added and then the suspension was centrifuged and supernatant was removed. QDs were dispersed in hexane. This process was repeated for two times. The final QDs were dispersed in toluene or chloroform.

PbS/CdS QDs with similar core size and tunable shell thickness were synthesized by choosing the tunable PbS dimension and varying the reaction time and temperature.

2.3.2 Synthesis of PbS and PbS/CdS QDs in water

2.3.2.1 Synthesis of amphiphilic polymer

Amphiphilic polymers were synthesized according to a published method [59], as described below:

1. One gram of PMAO and 1.5 g of PEG–OH were mixed with 50 µL of concentrated H₂SO₄.
2. The mixture was refluxed in chloroform (10 mL) for 12 hours.
3. As synthesized amphiphilic polymers of poly(maleic anhydride-alt-1-octadecene-co-poly(ethylene glycol) (PMAO–PEG) were neutralized by 1 M NaOH and then centrifuged to remove Na₂SO₄ and water.
4. The PMAO–PEG was dried under the fume hood for 1 week.

2.3.2.2 Transfer of PbS and PbS/CdS QDs into water

The PbS and PbS/CdS QDs were further transferred from an organic phase into water via amphiphilic polymers. As shown in Figure 2.3, the PbS or PbS/CdS QDs were firstly dispersed in chloroform and then mixed with PMAO–PEG. After stirring for 6 hours under dark, chloroform was then gradually removed by evaporation after adding air-free water. The water transfer procedure is as follows:

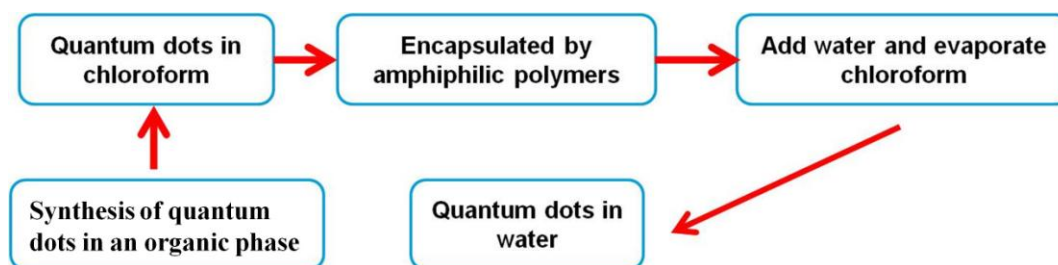


Figure 2.3 A flow chart displaying the process for achieving water-soluble QDs.

1. The amphiphilic polymer PMAO–PEG was dispersed into the chloroform and sonicated for 10 minutes.
2. QDs in toluene were precipitated by adding alcohol and then re-dispersed in hexane. The additional ligands were completely removed by repeated centrifugation and re-dispersion at least three times. Finally the QDs were dispersed in chloroform.
3. Monodispersed QDs (1 mL, with an absorbance of 1 at the first exciton peak) were mixed with PMAO–PEG (1.6 mL, 30 mM) in chloroform and stirred for 6 hours.
4. Nitrogen bubbled water (2.6 mL) was added to the mixture. Chloroform was then gradually removed by evaporation.

5. The water-soluble QDs were purified by centrifugation at 8000 revolutions per minute for 30 minutes. The purified QDs were then dispersed in water or buffer and kept under dark for future characterizations.

By following the transfer process mentioned above, the PbS QD capped by different types of capping ligands (OLA, OA or OA/TOP) and the PbS/CdS QDs with varying core size and shell thickness were transferred into water via amphiphilic polymers.

All reactions were repeated at least five times and all of them showed good reproducibility.

2.4 Characterization

2.4.1 Structure characterization

Samples for transmission electron microscopy (TEM) measurements were deposited onto copper TEM grids coated with thin (5-50 nm thickness) carbon films. One drop of PbS or PbS/CdS QDs dispersed in chloroform or water was placed on the grid. The grid was allowed to dry in air. The grid was examined by TEM. Low- and high-resolution TEM images were obtained using a JEOL 2100F microscope.

The X-ray diffraction (XRD) study of PbS or PbS/CdS QDs after extensive purification was carried out with a Philips X'pert diffractometer using Cu K_{α} radiation source ($\lambda = 0.15418$ nm). Nanocrystals were placed on glass for measurements. Diffraction patterns were collected in the 2θ range 20–80°, by using the step of 0.1 ° and counting time of 10 seconds.

X-ray photoelectron spectrometry (XPS) was performed on a VG Escalab 220i-XL equipped with an Al K_{α} source. Thin cast films of QDs were placed on silicon substrate for measurements.

The Pb/Cd ratio was measured by using inductively coupled plasma optical emission spectrometry (ICP-OES, Perkin Elmer Model Optima 7300 DV). These experiments were performed at the University of Toronto. A known mass of QDs was digested with a HNO₃/HCl (volume ratio: 1:3) mixture on a hotplate. The obtained clear solution was diluted with Millipore water for further measurements.

Dynamic light scattering technique (Malvern, Zetasizer Nano S90) was used to determine the hydrodynamic radius of QDs. All samples were purified by using 200-nm filters for at least three times.

Amphiphilic polymers were characterized by Fourier Transform Infrared (FT-IR) spectroscopy (Nicolet 6700 spectrometer, Thermo Scientific) in the transmission mode by using undoped and double-side polished silicon as substrates.

The size of QDs was measured by TEM with good precision. About 200 QDs were analyzed for each sample; the size distribution was analyzed with a Gaussian distribution.

The band gap energy was calculated from the absorption peak following the equation:

$$E = hc/\lambda \quad (2.1)$$

where E is band gap energy, h is Planck constant and λ is the first excitation absorption peak position.

2.4.2 Property characterization

Absorption spectra were acquired with a Cary 5000 UV-visible-NIR spectrophotometer (Varian) with a scan speed of 600 nm/minute. Samples were dispersed in toluene, chloroform, or water for measurements.

Fluorescence spectra were taken with a Fluorolog®-3 system (Horiba Jobin Yvon) using an excitation wavelength of 674 nm. For the PbS/CdS QDs, the excitation wavelength of the CdS shell was set at 345 nm. The concentration of samples was adjusted so as to their optical densities were below 0.2 at the chosen excitation wavelength.

QY measurements of PbS QDs were performed at HORIBA Jobin Yvon, NJ, USA. The dye IR 125 dissolved in dimethyl sulfoxide was used as a reference. The QY of the CdS shell was measured by using rhodamine 6G dissolved in water as a reference. The general process is shown in the following:

1. Record the UV-visible-NIR absorption spectrum of the QD solution.
2. Record the fluorescence spectrum of the same solution in a 10 mm fluorescence cuvette.
3. Repeat steps 1 and 2 for five solutions with decreasing concentrations of QDs.
4. Plot a graph of integrated fluorescence intensity *versus* absorbance.
5. Repeat steps 1 to 4 for the standard reference.

All the fluorescence spectra were recorded with a constant slit width. The gradients of the graphs obtained in the step 4 are proportional to the QY of samples. The absolute QY value can be obtained using a standard sample which has a known fluorescence QY value as a reference, according to the following equation:

$$\Phi_x / \Phi_{st} = (Grad_x / Grad_{st}) * (\eta_x^2 / \eta_{st}^2) \quad (2.2)$$

where the subscripts ST and X denote standard and unknown respectively, Φ is the fluorescence QY, *Grad* is the gradient from the plot of integrated fluorescence intensity *versus* absorbance, and η is

the refractive index of the solvents used for the measurements. The QY of IR 125 in dimethyl sulfoxide is 13% [75]. The excitation wavelength for IR 125 is set at 765 nm and for PbS QDs 670 nm. The excitation wavelength for rhodamine 6G is set at 526 nm and for CdS shell of PbS/CdS core/shell QDs 345 nm.

Fluorescence lifetimes of PbS QDs and PbS cores in PbS/CdS nanocrystals in different solvents (toluene, chloroform or water) were measured using a pulsed laser diode of 636 nm and the fast multichannel scaler mode in the Fluorolog®-3 system. The decay signals were found to be best fitted to a single-exponential function, shown in the following:

$$I(t) = I_0 \exp(-t/\tau) \quad (2.3)$$

where τ is lifetime, I is PL, t is time and I_0 is the initial PL at $t = 0$.

The fluorescence lifetime of the CdS shell was measured in time-correlated single-photon counting (TCSPC) mode with a 374 nm laser. The decay signals were found to be best fitted to a two-exponential function, according to the following equation:

$$I(t) = I_0 \exp(-t/\tau_1) + I_0 \exp(-t/\tau_2) \quad (2.4)$$

where τ_1 and τ_2 is lifetime of the first and second process, respectively. I is PL, t is time and I_0 is the initial PL at $t = 0$.

The photostability of PbS and PbS/CdS QDs dispersed in different solvents were tested using a 4 W UV lamp (115 V, 60 HZ, Model 22-UV, Optical Engineering, UV light Inc.).

The thermal stability of PbS and PbS/CdS QDs were tested by dispersing QDs in air-free ODE held at certain temperature and monitoring the variation in their PL spectra with time.

Chapter 3

Synthesis and characterization of PbS QDs

In this chapter I discuss the synthesis of colloidal PbS QDs in the organic phase in a “non-viscous”, solventless OLA system by using relatively low concentrations of PbCl₂ and S [68, 69]. I investigated the effects of the reaction time, molar ratios of reactants, reaction temperature, capping ligands and purity of ligands and precursors on the growth of PbS QDs. Finally, the optimal synthesis conditions for PbS QDs with high quality were fixed.

3.1 QDs synthesis

Organometallic synthesis was first used in 1983 to produce CdS nanocrystals and the technique has been further employed to synthesize PbS QDs in an organic solution [76, 31, 32]. Hines and Scholes for the first time reported the organometallic synthesis of PbS QDs, which exhibit size-tunable emission in the NIR [31]. They obtained PL peaks with full width at half-maximum (FWHM) of about 100 meV. Recently, a breakthrough in the PbS synthesis was achieved by Ozin’s group [32]. The group used a high concentration of PbCl₂ in OLA to form a quite “viscous” suspension and a less toxic precursor of S to synthesize high-quality PbS QDs. By applying the hot injection method to such a viscous system, they produced PbS QDs with PL FWHM as low as 52 meV. In comparison, they also synthesized PbS QDs in a “non-viscous” system by decreasing the concentration of PbCl₂. However, the PL FWHM of such synthesized PbS QDs was found to

remain high, at about 100 meV. Very recently, in a relatively “non-viscous” system, Abel *et al.* reported the synthesis of very photostable and highly photoluminescent PbS QDs with a narrow size distribution [50]. However, their synthesis method involved the same, dangerous chemical of (TMS)₂S as Hines’s and Scholes’s method. It is highly desirable to develop a simple and greener approach with good producibility and easy manipulation.

Understanding crystal growth kinetics of QDs is of great benefit to fundamental research and also contributes to securing greener synthetic schemes yet leading to excellent properties [77]. Studies have shown that, in most of the cases, the growth of nanocrystals involves one of the two mechanisms namely, crystallographically specific oriented attachment mechanism [78, 79] and Ostwald ripening mechanism [80, 81, 82]. The oriented attachment growth is related to the direct self-organization of two particles into a single crystal by sharing a common crystallographic orientation [83, 84]. In contrast, Ostwald ripening mechanism involves the dissolution of smaller particles, which feeds the growth of larger particles [80, 81, 82]. Ostwald ripening only begins to play a role when monomers are depleted due to the nucleation and growth of small crystals, causing the critical size becomes larger than the average size of particles present in the synthesis system [80, 81, 82]. The occurrence of Ostwald ripening results in the broadening of particle size distribution (*i.e.*, size defocusing). When it eventually ends, the size distribution becomes narrow again (*i.e.*, size re-focusing). Generally, the size distribution after Ostwald ripening is still broader than before [77]. Knowing that, QDs with a narrow size distribution have been prepared by postponing Ostwald ripening and quenching the reaction before it starts [77].

Growth of QDs is affected by many factors (such as temperature) whose effects could differ from system to system [16]. For example, a higher initial concentration of precursors may yield a narrow size distribution of spherical QDs in one system, while QDs of different shapes in another

system [16]. To the best of my knowledge, the growth of PbS QDs under different reaction conditions (such as in a “non-viscous”, constant-temperature system developed herein) is still lacking. In addition, precursors themselves also play a key role in controlling the size and shape of PbS nanocrystals. It is not clear how the purity status of ligands and precursors influence the synthesis and photophysical properties of PbS QDs. I expect this unknown factor is at least partially responsible for the irreproducibility problem commonly encountered in QD synthesis.

I have developed a simple, greener, solventless, mild-constant-temperature approach to synthesize PbS QDs, in which PbCl_2 is used as lead precursor and sulfur is used as S precursor. OLA serves as ligands and controls the growth of PbS QDs. In contrast to a popular hot-injection method, this synthesis was performed at a constant reaction temperature. In addition, the “non-viscous” condition was applied.

The crystalline nature of such synthesized PbS QDs is confirmed by XRD studies (Figure 3.1). High resolution TEM suggests that the nanoparticles from my synthesis are highly crystalline and free of any major defects (Figure 3.1 inset).

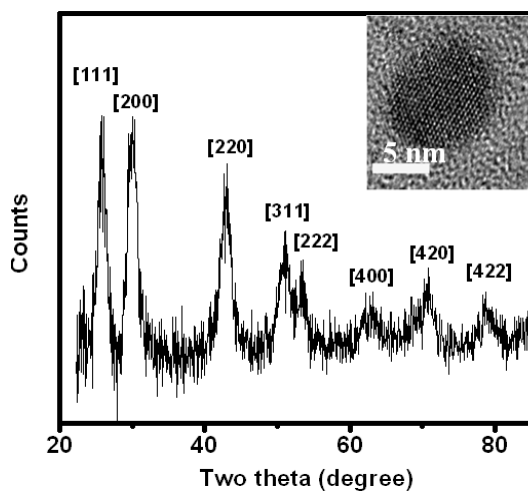


Figure 3.1 The XRD pattern of PbS QDs. Inset: a high resolution TEM image of a PbS QD.

In the following, I present the effects of several reaction parameters on the growth and photophysical properties of PbS QDs (Section 3.2). In addition, I also investigated the effects of ligands (Section 3.3) and chemical purity status (Section 3.4) on the synthesis and photophysical properties of PbS QDs.

3.2 Effect of reaction parameters

3.2.1 Effect of reaction time

The growth of QDs was investigated in detail by means of absorption and fluorescence spectroscopy. Especially, the absorption and PL spectra can be used to imply the average size and size distribution of QDs [85, 86]. In the case of PbS QDs, their average size can be estimated from the following empirical equation [86]:

$$E = 0.41 + 0.96/r^2 + 0.85/r \quad (3.1)$$

where E is the band gap energy, which can be calculated from the absorption peak using equation 2.1 ($E = hc/\lambda$), and r is *the average* radius of QDs. In addition, Thessing et al, have used the absorption and PL peak width to evaluate the size distribution of QDs [86]. Following their work, we will use the absorption and PL spectra to assess the size and size distribution of PbS QDs synthesized in our work. In order not to lose any synthesized PbS QDs and thus ensure the observed absorption and emission spectra representing faithfully (or as close as possible) the as-prepared samples, both absorption and fluorescence spectra in the following study were taken immediately after synthesis and one-time low-temperature centrifugation to precipitate excess PbCl_2 , while without any further purification. The evolution of absorption and PL spectra with respect to time during the growth of PbS QDs at 90 °C with an initial PbCl_2/S ratio of 3:1 is illustrated in Figure 3.2a and Figure 3.2b, respectively.

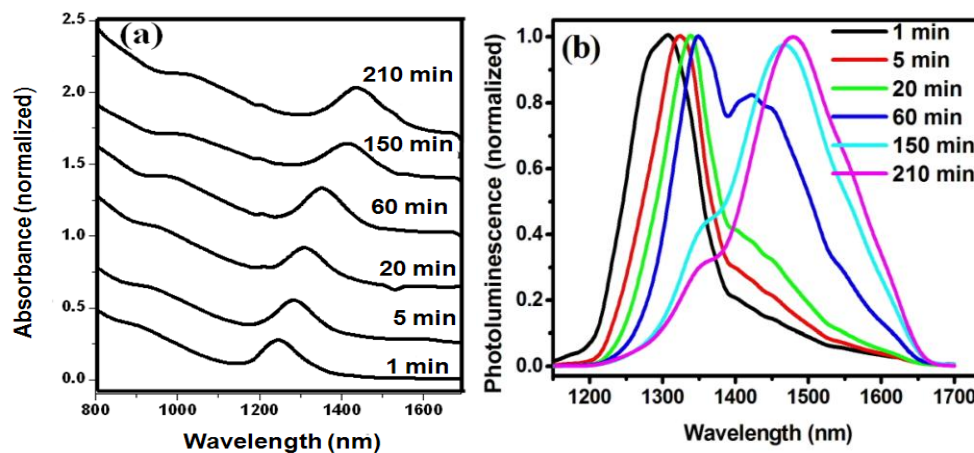


Figure 3.2 Absorption (a) and PL (b) spectra of PbS QDs prepared at 90 °C with the PbCl₂/S ratio of 3:1.

With the reaction time increasing from 1 to 210 minutes, the absorption peak shifts from 1246 nm to 1436 nm, which corresponds to the increase of the average size of PbS QDs. No evident absorption peak broadening or shape change has been observed during this period. However, the shape of the PL spectra changes significantly during the same period. Indeed, as the reaction progresses, the single PL peak with a slight red tail appearing at 1 minute gradually evolves into a double peak structure, and then into a broad peak with a shoulder on the high energy side.

In order to better understand the growth of the QDs, the PL spectra were fitted using the Gauss model (all reported data having $R^2 > 0.98$). The bimodal size distribution directly results in the bimodal PL structure which is further confirmed by TEM. As shown in Figure 3.3a, the uniform QDs synthesized at 1 minute have an average diameter of about 2 nm. Consistent with the double peaks observed in the PL spectra, the 150-minute sample shows two QD populations of different average sizes, one of about 2 nm in diameter and the other of about 6 nm (Figure 3.3b).

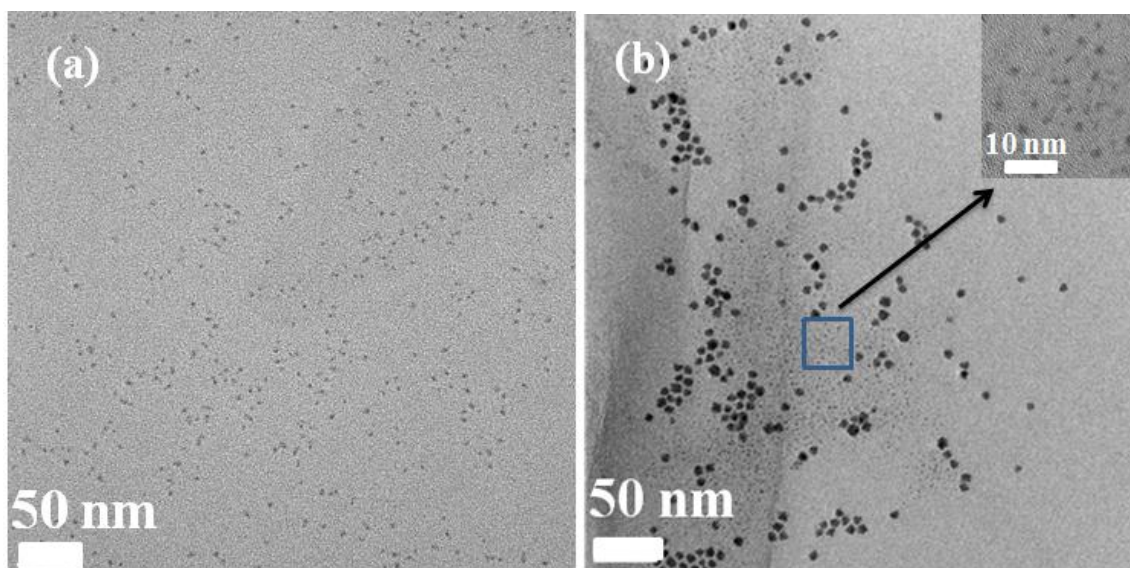


Figure 3.3 TEM images of PbS QDs synthesized at 90 °C with the PbCl_2/S ratio of 3:1. The growth time is 1 minute (a) and 150 minutes (b). Inset: a TEM image of small-sized QDs in (b).

TEM observations on the QDs synthesized at different reaction time show that only single crystalline QDs with a regular spherical shape are present. I therefore conclude that the QD growth in my system is governed by Ostwald ripening process, rather than by the oriented attachment mechanism that would otherwise lead to the formation and observation of crystals of irregular shapes [83]. Combining the PL spectra and TEM observations, the growth of the QDs can be explained as follows. The instant nucleation rapidly depletes the monomers in the solution, which initiates Ostwald ripening in the very early stage. The direct effect is the broadening of the PL peak, with a shoulder emerging at a longer wavelength. The subsequent emergence of obvious double peaks that correspond to the bimodal size distribution of the QDs can be explained by the fact that Ostwald ripening, accelerated by interparticle interactions as elaborated in reference 85, leads to a gap, developing between larger particles in growth and smaller ones in dissolution [85]. Although usually a single log-normal PL peak is reported during Ostwald ripening process [77], similar

double peaks and bimodal size distribution have been reported by Thessing *et al.* in their very recent studies on CdS QDs [85].

It is clear that high-quality PbS QDs showing a narrow size distribution can be achieved by quenching the reaction before Ostwald ripening starts. Considering that, in order to synthesize PbS QDs with different average sizes as well as narrow size distribution, I varied the molar ratios of PbCl_2/S and allowed the reaction proceeding only for a short time.

3.2.2 Effect of the molar ratio of precursors

A big difference in PL spectra (and thus size distribution) was observed for 1-minute samples when the molar ratio of precursors changes while the reaction temperature is set at 90 °C. Herein, I fixed the PbCl_2 concentration and varied the PbCl_2/S molar ratio from 2:1 to 10:1. The corresponding PL spectra are shown in Figure 3.4a. It can be seen that for the low molar ratio of 2:1, the double peaks appear at as early as 1 minute with the peak at the longer wavelength responsible for over 89% of emission according to the Gauss fitting. Although the appearance of apparent double peaks in the time-lapse PL spectra of the PbS QDs synthesized at 90 °C with the PbCl_2/S ratio of 3:1 (Figure 3.2) is not obviously reflected in their corresponding UV-visible-NIR absorption spectra, the presence of double peaks and thus bimodal size distribution seems like deteriorating the absorption spectrum of the 1-minute PbS sample prepared at the PbCl_2/S ratio of 2:1 (Figure 3.4b). The peak is much broader and weaker as compared to those of the QDs synthesized at higher PbCl_2/S ratios. The increase of the molar ratio clearly postpones the start of Ostwald ripening process which is obvious for the sample prepared with the high PbCl_2/S ratio (≥ 3).

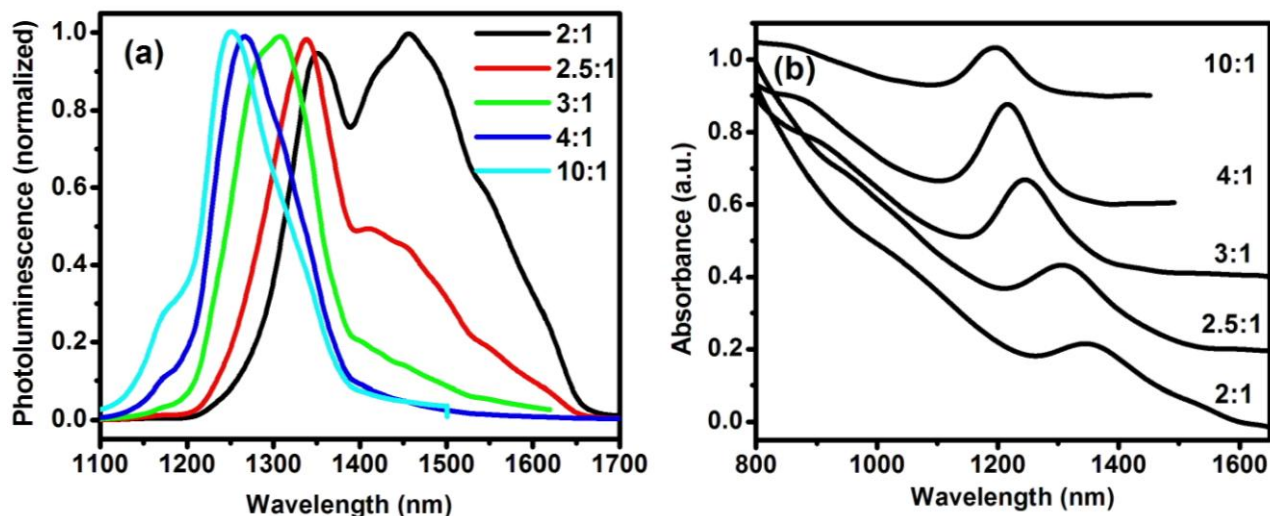


Figure 3.4 PL (a) and absorption (b) of QDs after 1-minute growth at 90 °C with the Pb/S ratio ranging from 2:1 to 10:1.

It is known that in the QD synthesis, both the higher molar ratio and the higher concentration of precursors are beneficial to the synthesis of QDs by delaying the occurrence of Ostwald ripening through increasing supersaturation in a synthesis system [79]. In my work, with increasing molar ratios, the total precursor concentration decreases. It seems like the beneficial effect of higher molar ratios largely overrides the negative effect of lower precursor concentrations. In other words, the increase in the molar ratio of precursors can effectively postpone the occurrence of Ostwald ripening, while the concentration effect on Ostwald ripening is less obvious in my system.

Although I can produce relatively small-size PbS QDs with a single-mode size distribution (reflected from a single emission peak) by applying high molar ratios, larger-size PbS QDs with a single emission peak above 1300 nm cannot be prepared in this way. In the following, I changed the reaction temperature in order to achieve larger-size PbS QDs with single and narrow size distribution.

3.2.3 Effect of reaction temperature

I have investigated the effect of reaction temperature on the growth of PbS QDs when the PbCl₂/S ratio is fixed at 3:1. For all the reaction temperatures studied herein (90 °C, 100 °C, 110 °C and 120 °C), the injection of S-OLA into PbCl₂-OLA causes immediate color change, indicating nucleation takes place rapidly right after the injection.

The PL spectra of 1-minute PbS samples synthesized at different temperatures are shown in Figure 3.5a. Evidently, there is a shoulder at the low energy side when the reaction temperature is set at 110 °C, implying that the QD growth is already greatly influenced by Ostwald ripening in such a short time. However, for all the other 1-minute samples synthesized at either lower or higher temperatures, the PL peak is basically near-single, with slight red tails, indicating that although Ostwald ripening starts to play a role, its effect on the size distribution and PL spectrum has not become very obvious. In order to understand this temperature effect, I tried to employ the UV-visible-NIR absorption spectra to relatively compare the size and molar concentration of the QDs synthesized in this early stage.

Figure 3.5b illustrates a series of absorption spectra of the PbS QDs grown at different temperatures for 1 minute. As shown in Figure 3.5b, the absorption peak of the PbS QDs shifts from 1246 nm to 1408 nm (*i.e.*, the average size increases) while the peak intensity decreases from 0.26 to 0.10 when the reaction temperature increases from 90 °C to 120 °C. It is known that the concentration of QDs with a narrow size distribution can be determined using the Beer-Lambert's law:

$$A = \varepsilon CL \quad (3.2)$$

where A is the absorbance at the peak position of the first exciton absorption peak for a given sample, C is the molar concentration of QDs, ϵ is the extinction coefficient per mole of QDs and L is the light path length [86]. For QDs with a broad size distribution, a modified value of A should be applied. Here I used A_m which is defined as the integrated absorbance obtained by integrating the absorbance over the long-wavelength side of the first exciton absorption peak and multiplying it by 2. The calculated A_m values in my work were 44.3, 37.26, 14.54 and 8.06 for the 1-minute samples prepared at 90 °C, 100 °C, 110 °C and 120 °C, respectively. The extinction coefficient of PbS QDs has been found to depend on the size of QDs according to a power law with an exponent of 2.32 [86]. Therefore, the molar concentration of the QDs synthesized at different temperatures in this work can be compared by using the following equation:

$$C = A_m / (k r^{2.32} L) \quad (3.3)$$

Since $k \cdot L$ is constant, and the average radius (r) increases while the A_m value decreases with increasing temperature, it can be deduced through simple math that, the molar concentration of the QDs synthesized at 1 minute after the reaction starts decreases with the reaction temperature increasing from 90 °C to 120 °C. It is likely that in my system, the PbCl₂-OLA interaction enhances with increasing temperature, which leads to fewer QDs formed at higher temperatures. This deduction is further supported by another observation: with the PbCl₂/S ratio of 10:1, the nucleation could not start in first 5 minutes at 120 °C although the instant nucleation can be observed at lower temperatures. Moreover, it has been reported that at 120 °C high PbCl₂/OLA ratios can induce gelling of the suspension [32].

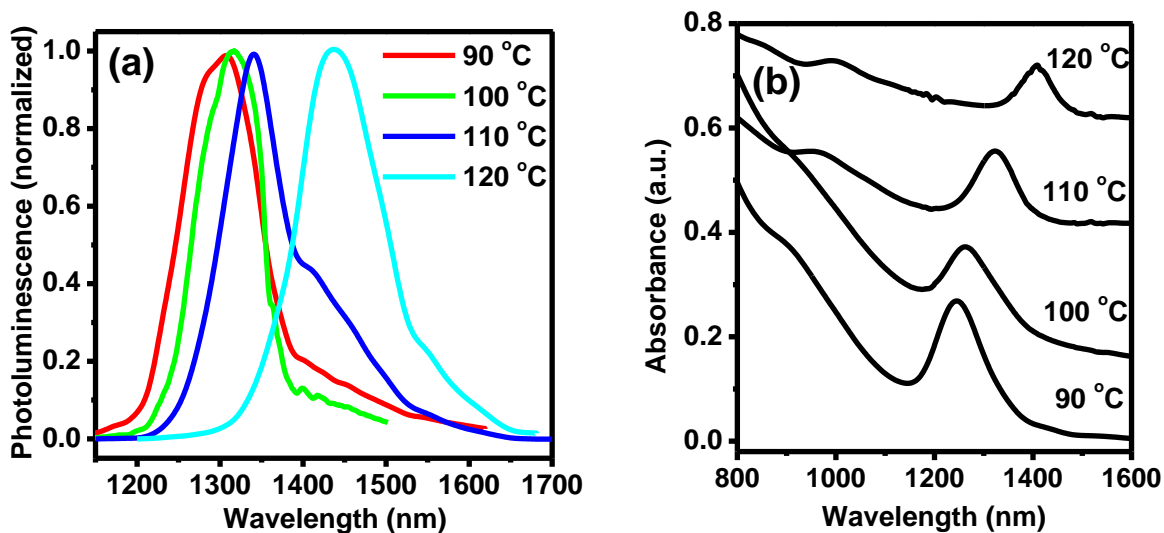


Figure 3.5 PL (a) and absorption (b) spectra of PbS QDs after 1-minute growth at different temperatures. The PbCl_2/S ratio is 3:1.

It is understood that the start of Ostwald ripening depends on the monomer concentration and the size distribution of nanoparticles present in solution. As discussed above, with temperature increasing from 90 °C to 120 °C, the average QD size increases while the molar concentration of the QDs decreases. Therefore, in my system, there is no simple monotonic relationship between the reaction temperature, the amount of consumed monomers (approximately proportional to the product of the molar concentration and the average size of QDs) and the concentration of remaining monomers. The reaction temperature of 110 °C is likely a critical point, at which the critical size exceeds the average size of the QDs at a much faster rate than at lower or higher temperatures used in this study. It is noteworthy to mention that PbS QDs synthesized at 120 °C have a narrow absorption peak with half-width at half-maximum (HWHM) as low as 22 meV that is very close to the reported best value (23 meV) [50] as far as I know for PbS QDs. In addition, as shown in Figure 3.6, several transitions in the absorption spectra can be easily identified, suggesting a good quality

of QDs [32, 86]. Together with the narrow PL peak, the results indicate that QDs with a narrow size distribution can be achieved from this preparation.

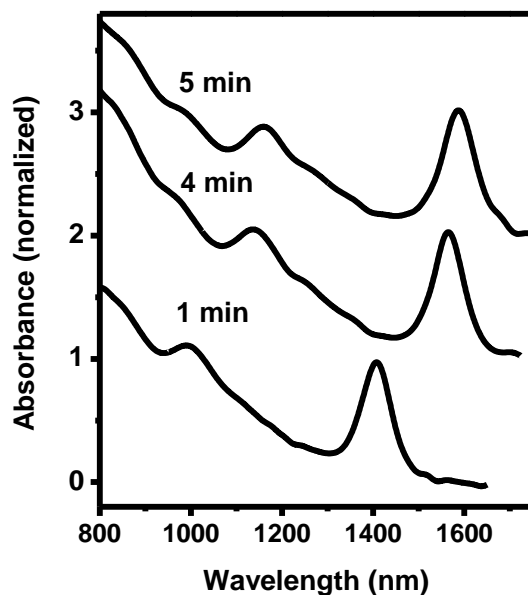


Figure 3.6 Absorption spectra of PbS QDs prepared at 120 °C with the PbCl₂/S ratio of 3:1.

In this section, I have synthesized the PbS QDs with tunable sizes in the range from 2 nm to 6 nm by changing reaction parameters. The QY of PbS QDs is as high as 40%. Very recently, Abel *et al.* reported that highly photoluminescent PbS QDs with a narrow size distribution can be achieved by using TOP as an additional capping ligand [50]. In order to further enhance the QY of PbS by my own method, I studied the TOP ligand effect on the quality of PbS QDs.

3.3 Effect of capping ligands

Herein I am interested in observing how TOP ligands affect the growth and PL band of PbS QDs when S is used as a precursor. It was found that if TOP, even as little as 200 μ L, is added, with S together to the PbCl₂ precursor solution, the nucleation will not start even if the temperature is

increased to as high as 160 °C. Alternatively, 200 μ L of the TOP ligands were injected immediately after the instantaneous nucleation of PbS QDs at 90 °C to observe their effect on the QD growth. It was found that the addition of TOP immediately initiates the bimodal PL, which otherwise will not appear until 15 minutes later (Figure 3.7a). With the reaction time increasing from 1 to 10 minutes, the peak at the shorter wavelength continuously red-shifts, while that at the longer wavelength remains nearly the same position. Meanwhile, the PL intensity under the high-energy peak gradually decreases, while that under the low-energy peak gradually increases, accounting for the variation of the fraction of PL under the high-energy peak from 64.7% to 21.5%, based on the spectra fitting. Since no red-shift is observed for the low-energy peak, the appearance of these double PL peaks does not seem to be due to Ostwald ripening; instead, I think it arises from the retarded growth caused by the strong binding effect between S (either in solution or on QD surface) and TOP. The strong binding between the precursor S and TOP decreases the chemical activity of S and simultaneously, the passivation of surface S sites by TOP increases the barrier for the QD growth. As such, it is not surprising that the growth rate is significantly decreased. Normally in the very early stage of nanoparticle synthesis, since the system is under supersaturation, smaller particles grow faster than larger ones, which lessens the size difference among and narrows the size distribution of nanoparticles. However, in my case, it appears that the sudden introduction of the strong binding TOP ligands not only results in the significant reduction in the growth rates, but also modifies the difference in the growth rates of smaller and larger QDs. As a consequence, the injection of TOP augments the instant size difference and creates a gap between smaller and larger QDs, which in turn results in the bimodal PL.

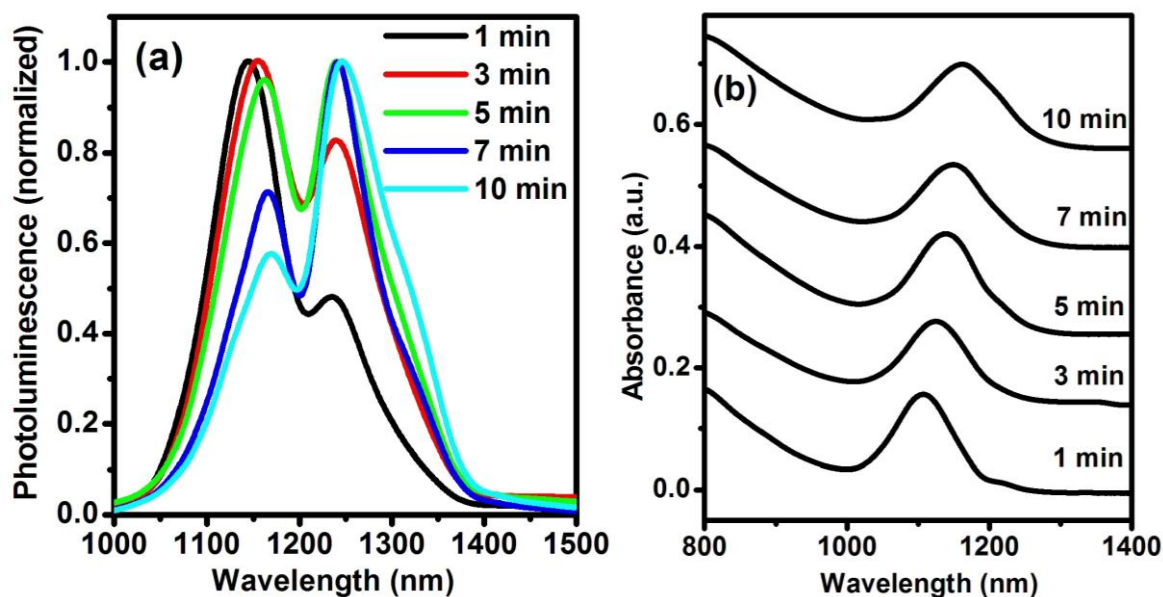


Figure 3.7 PL (a) and absorption (b) spectra of PbS QDs after the injection of 200 μl of TOP ligands. The reaction temperature is 90 $^{\circ}\text{C}$ and the PbCl_2/S ratio is 10:1.

The decrease of the growth rate is clearly reflected from the absorption spectra. As shown in Figure 3.7b, the absorption peak at 1 minute is situated at 1106 nm which is considerably shorter than that (1246 nm) obtained without the addition of TOP under otherwise same reaction conditions. Evidently, the TOP ligands affect the growth of PbS QDs significantly in my system, where S is selected as a sulfur source. The difference in the chemical reactivity between S and $(\text{TMS})_2\text{S}$ is responsible for the quite different TOP effects on the PL spectra in both systems.

It is clear that TOP ligands are not suitable as capping ligands for synthesizing high quality PbS QDs via my method.

In view of that the growth and photophysical properties of QDs may strongly depend on the purity status of involved chemicals, in the following section (3.4), I studied the purity effect of ligands and precursors on the synthesis and photophysical properties of PbS QDs.

3.4 Purity effect of ligands and precursors

Hereinbefore, the PbCl_2 precursor used has the purity of 100% and the OLA used has the content of C_{18} -amine of 70%. In the following, I studied the purity of ligands and precursors on the synthesis and photophysical properties of PbS QDs. Hereafter, I denote the OLA of a higher C_{18} -amine purity as OLA#1 (80-90 wt%) and of a lower purity as OLA#2 (70 wt%). Similarly, I denote the PbCl_2 of a higher purity as PbCl_2 #1 (100 wt%) and of a lower purity as PbCl_2 #2 (98 wt%). For all the synthesis discussed for comparing the effect of the purity status of ligands, PbCl_2 #1 is used as the Pb precursor and for comparing the effect of the purity status of the PbCl_2 precursor, OLA#2 is used as a ligand. The purities of a commonly used ligands OLA or precursor PbCl_2 affect the synthesis and photophysical properties of PbS QDs significantly under certain conditions.

3.4.1 Ligands purity effect

The absorption spectra of PbS QDs synthesized at different temperatures and quenched at the reaction time of 1 minute using OLA#1 or OLA#2 are shown in Figure 3.8a and 3.8b, respectively. With increasing the temperature from 80 °C to 120 °C, the integrated absorption (obtained by integrating the absorbance over the long-wavelength side of the first exciton absorption peak) decreases no matter OLA#1 or OLA#2 is used. The reduction is nearly 90% when OLA#2 is used at 120 °C, in clear contrast to that of less than 25% when OLA#1 is used (Figure 3.8c, error is smaller than 10%). When the synthesis temperature is set at 130 °C, the absorption peak completely disappears in the presence of OLA#2, while it is still present for the synthesis using OLA#1. As mentioned above, a higher temperature leads to less number of QDs synthesized in the very early stage, which has been attributed to enhanced PbCl_2 -amine interactions. Although the overall amine contents in OLA#1 and OLA#2 are similar (97 versus > 98 wt%), the C_{18} -amine (*i.e.*, OLA) content

differs notably (80-90 wt% versus 70 wt%) and therefore the content of other “unknown” amines differs. It is also possible that the types of other unknown amines are different in OLA#1 and OLA#2, which is not trivial to determine. Based on available OLA purity information from the companies and experimental results, I deduce that in OLA#2, there are likely some amines other than C₁₈-amine, which are at higher concentrations than those in OLA#1 (if there are any) and can bind to Pb in PbCl₂ or on the QD surface and whose interactions with Pb have strong temperature dependence that largely translates to the temperature-dependent synthesis of PbS QDs.

Another striking difference observed is the variation of the HWHM of the first exciton absorption peak at the longer wavelength side of the absorption band with temperature (Figure 3.8d, error is smaller than 5%). With temperature increasing from 80 to 120 °C, the HWHM from the synthesis using OLA#2 shows a large monotonic decrease from near 120 to about 40 nm. In contrast, the HWHM of the QDs prepared using OLA#1 shows fluctuation in between a relatively narrow range of 50-70 nm, with the minimum of about 50 nm occurring at 90 °C. It is clear that in order to achieve QDs with a very narrow absorption peak, OLA#2 needs to be used at a relatively high reaction temperature (>100 °C). However, when QDs with a narrow absorption peak at a shorter wavelength are desired, OLA#1 is a better choice. The sharp decrease in the HWHM with temperature is again likely due to the presence of a higher concentration of binding, “impurity” amines in OLA#2 than in OLA#1. The binding capability of these “impurity” amines possibly highly depends on temperature and can exert tighter control over the growth of the uniform QDs due to enhanced interactions with Pb at higher temperatures. With the same reaction temperature, OLA#2 yields the absorption peak consistently at a longer wavelength, indicating a likely larger average size of QDs. It seems that lower C₁₈-amine content favors the formation of larger QDs in the early stage. The effect of impurity amines cannot be excluded either.

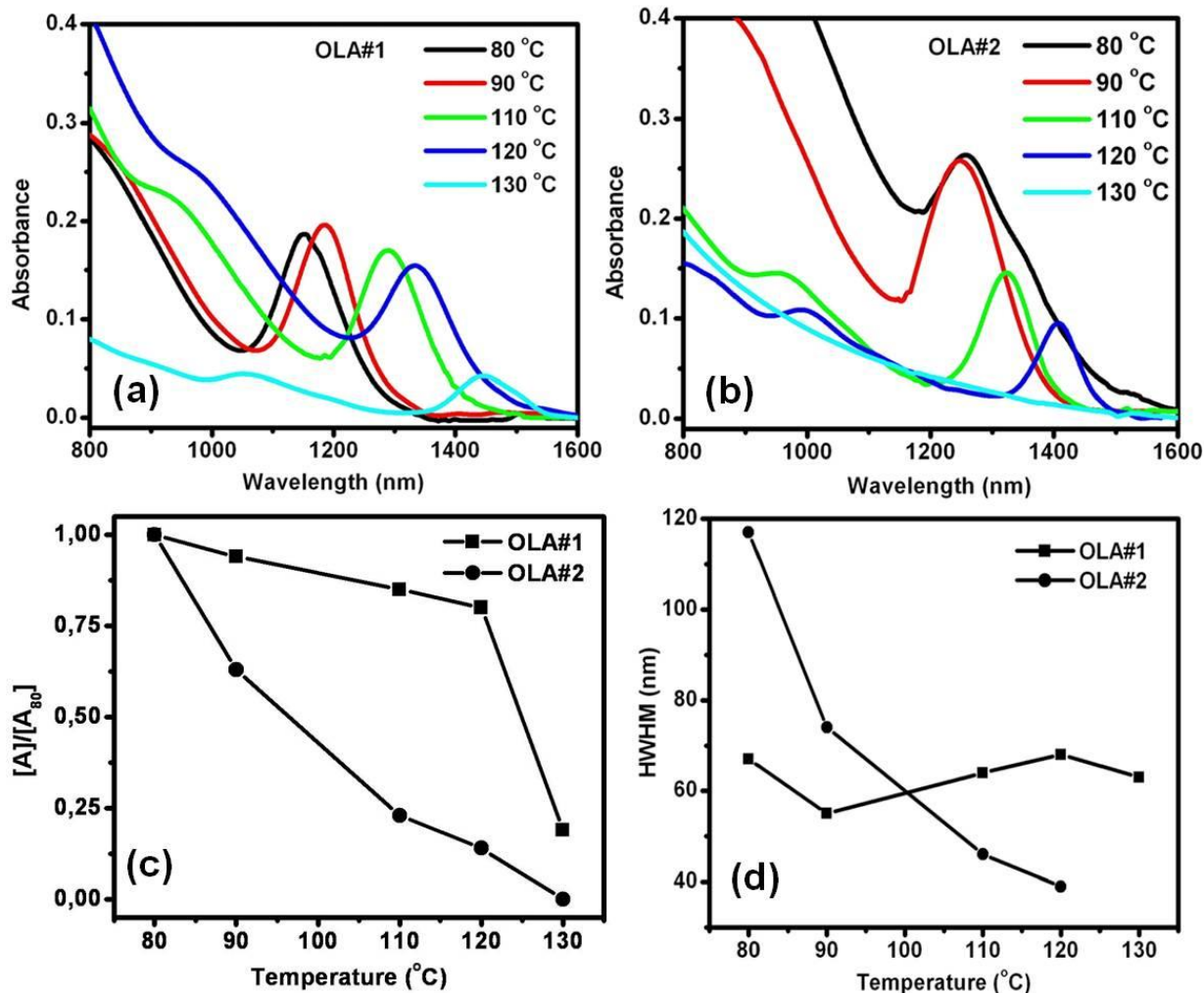


Figure 3.8 Absorption spectra of PbS QDs synthesized with the PbCl₂/S ratio of 3:1 and the reaction time of 1 minute at different temperatures by using OLA#1 (a) and OLA#2 (b) as ligands. The ratio of the integrated absorption A at different synthesis temperatures to that at 80 °C ($A/A_{(80)}$) as function of temperature (c). The integrated absorption is calculated herein by integrating the absorbance over the long-wavelength side of the first exciton absorption peak. Absorption HWHM obtained at different synthesis temperatures as function of temperature (d). The solid line is drawn to guide the eye. PbCl₂#1 was used as a precursor in both cases.

Although the growth of PbS QDs reflected from absorption or emission spectra is sensitive to the purity status of the ligand OLA, the QY of the QDs does not seem to be notably influenced by the ligand purity status. As shown in Figure 3.9a, the relative QYs, the slope of curves constructed by plotting the integrated emission intensity versus absorbance, of the QDs prepared using ligands of two different purity statuses, can be considered same at similar wavelengths within experimental

error. The slightly different lifetimes are unlikely associated with the ligand purity status, but more likely due to slightly different emission wavelengths as I have observed the wavelength-dependence of lifetimes in the PbS QDs (Figure 3.9b). Although the C₁₈-amine (*i.e.*, OLA) content differs notably (80-90 wt% versus 70 wt%), the overall amine contents in OLA#1 and OLA#2 are similar (97 versus > 98 wt%). These amines, although maybe of different molecular lengths, are likely to passivate the QD surface in a similar way and therefore contribute similarly to the QY.

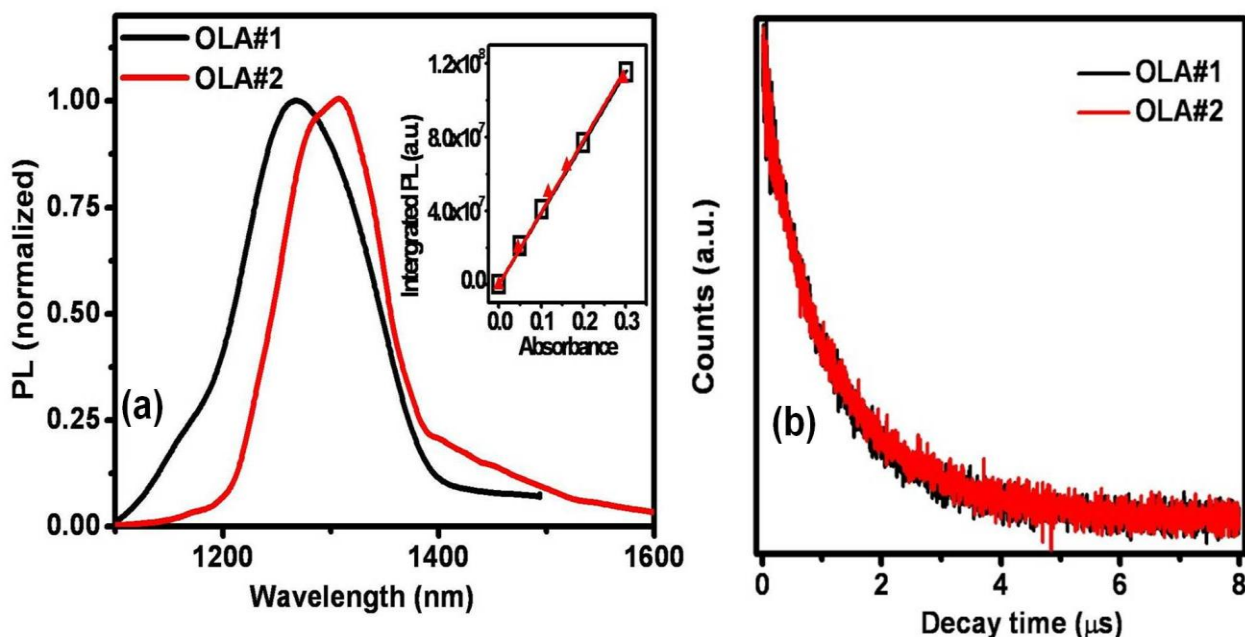


Figure 3.9 PL (a) and lifetime (b) of PbS QDs in toluene. The PbS QDs were synthesized at 90 °C with the PbCl₂/S ratio of 3:1 for 1 minute. Inset: integrated PL intensity versus absorbance at 670 nm for the QDs prepared using either OLA#1 or OLA#2 as a ligand. The linear fit of the data is also shown. PbCl₂#1 was used as a precursor in both cases.

As it is also expected that the growth and photophysical properties of PbS QDs are strongly affected by the purity of OLA ligands, in the following section (3.4.2), I present the precursor (PbCl₂) purity effect on the growth and photophysical properties of PbS QDs synthesized by my simple, constant-temperature method.

3.4.2 Precursor purity effect

I have observed remarkable difference in the absorption spectra of PbS QDs when the PbCl₂ of slightly different purities are applied. As shown in Figure 3.10, when PbCl₂#2 is used as a precursor, the bimodal PL pattern emerges as early as 1 minute after the reaction starts and consistently, the absorption peaks are weak and broad. When PbCl₂#1 is used instead, both the absorption and PL spectra are significantly improved. It is surprising that impurities of 2% can play such a significant role in the growth of PbS QDs. The exact reasons for this observation cannot yet be elaborated unambiguously within the limitations of this framework, while for sure are worth further investigation.

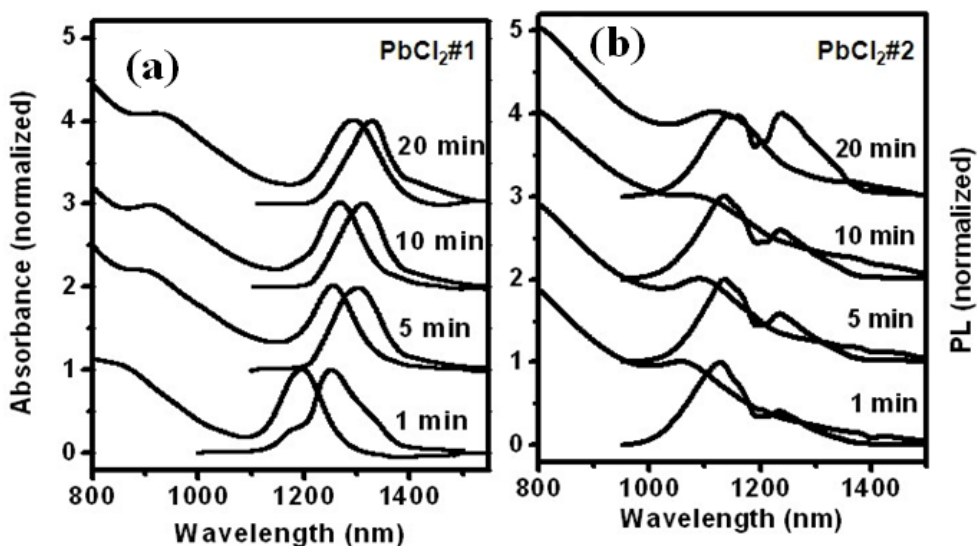


Figure 3.10 Absorption and PL of PbS QDs prepared at 90 °C with the PbCl₂/S ratio of 10:1 by using PbCl₂#1 (a) or PbCl₂#2 (b) as a precursor.

This part of work (section 3.4) indicates that the purity of chemicals may partially cause the irreproducibility problem often encountered in QD synthesis.

Based on the above investigations (sections 3.2-3.4), the growth and photophysical properties of PbS QDs are strongly affected by the reaction parameters (reaction time, temperature and molar ration of Pb-to-S), the surface capping ligands and chemical purity status. It is clear that in order to synthesize PbS QDs with high quality, we need to optimize reaction parameters as well as choose reagents of suitable purity. Figure 3.11 shows examples of optimal synthesis conditions for QDs emitting at three wavelengths.

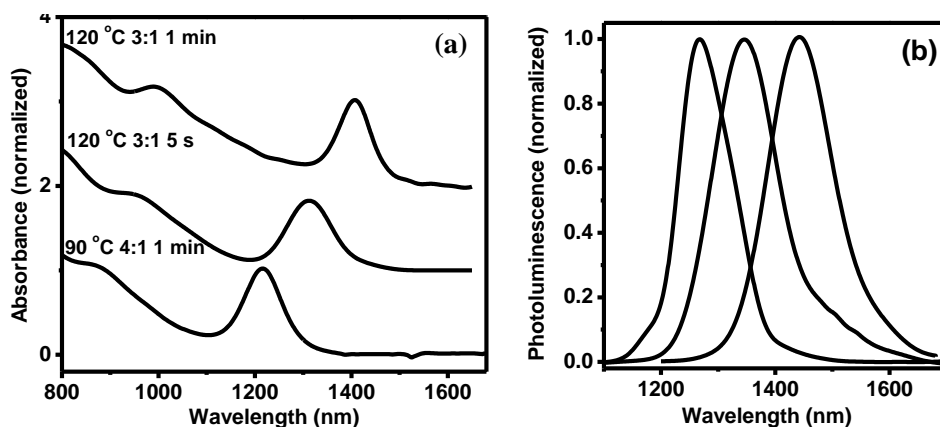


Figure 3.11 Absorption (a) and PL (b) of PbS QDs prepared at different conditions. From left to right, emission curves correspond to absorption curves. OLA#2 was used as ligands. PbCl_2 #1 was used as a precursor.

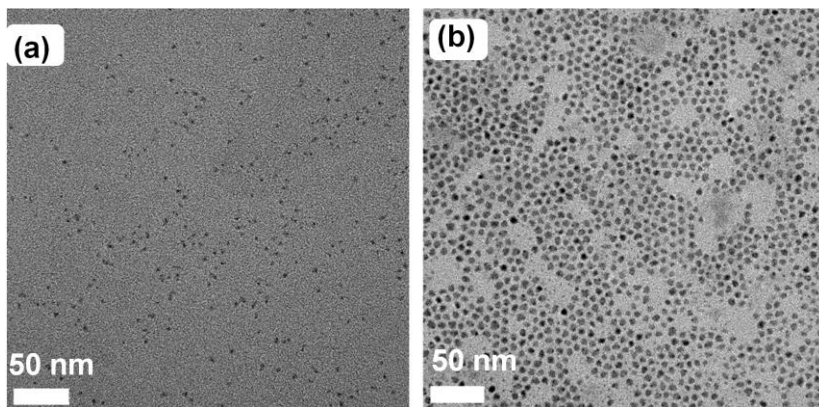


Figure 3.12 TEM images of PbS QDs synthesized at 90 °C with the PbCl_2 /S ratio of 3:1 and the reaction time of (a) 1 minute and (b) 2 hours using OLA#2 and PbCl_2 #2.

Using my simple system, I am able to synthesize PbS QDs with a narrow size distribution evidenced by the FWHM of the PL peak as low as 58 meV and TEM (Figure 3.12). The final QY of PbS QDs is as high as 40 % in the organic phase with tunable size from 2 to 6 nm.

3.5 Summary

In this chapter, the effects of reaction time (1 minute to 210 minutes), temperature (90-120 °C), molar ratio of precursors ($\text{PbCl}_2:\text{S} = 2:1$ to 10:1), capping ligands (TOP) and purity of ligands and precursors on the growth and optical properties of PbS QDs in a “non-viscous”, solvent-free, mild constant-temperature system are presented and discussed. Bimodal PL of PbS QDs has been observed and in most cases, it is due to the onset of Ostwald ripening, whose occurrence and evolution are highly affected by the reaction time and temperature, molar ratio of precursors, type of capping ligands (TOP) and purity of ligands and precursor as evidenced by the evolution of PL spectra. By adjusting reaction conditions, the PbS QDs with narrower PL peak and high QY can be achieved in my simple reaction system.

The QY of PbS QDs optimally synthesized can be as high as 40% in an organic phase. Realizing there is still space to further enhance it, I synthesized PbS/CdS core/shell QDs via cation exchange approach with an additional intention of achieving better photostability. The results are presented in the next chapter.

Chapter 4

Synthesis and characterization of PbS/CdS QDs

To be really useful in practical applications, QDs are required to exhibit a high QY and to have good photo- and thermal- stability. Certain QDs are found not very stable at high temperature or even in normal processing or operation conditions, displaying the spectral shift of the PL band and the drop in QY that in most of cases are related to surface oxidation [51, 61, 87]. The deposition of a larger-band gap, protective shell is a promising solution for the above mentioned problems.

In this chapter I discuss the synthesis and characterization of colloidal PbS/CdS core/shell QDs in the organic phase via cation exchange approach [70]. I firstly synthesized the PbS/CdS QDs with thin shell via cation exchange. The structure of PbS/CdS QDs was characterized by absorption and PL spectroscopy, TEM and XPS. In addition, ICP-OES (for estimating the Pb-to-Cd ratio) and absorption spectroscopy (for calculating band gap values) were combined to probe the chemical composition of the shell. It is likely that the shell in thin-shell PbS/CdS QDs is mainly made of CdS. Furthermore, by developing a two-step cation exchange method, I have overcome the synthesis barrier and synthesized PbS/CdS core/shell QDs with a much thicker shell. The structure of thick-shell PbS/CdS QDs was characterized by absorption and PL spectroscopy, TEM, XRD and EDX. All results strongly support the formation of crystalline CdS in thick-shell PbS/CdS QDs. Finally, I investigated the QY and photo- and thermal- stability of PbS/CdS QDs.

4.1 Core/shell structure

Recent studies have revealed that the core/shell structure can enhance the fluorescence efficiency and improve the stability of core QDs [61, 62, 63]. The growth of the shell has most commonly been achieved by exposing core nanocrystals to all the precursors of shell elements. A representative example is the use of diethylzinc (Zn precursor) and hexamethyldisilathiane (S precursor) for the synthesis of ZnS overcoated CdSe QDs [65]. In that case, the core size remains essentially constant during the overcoating process. Cation exchange has also been used for synthesizing core shell structured lead chalcogenide QDs [60, 88]. In contrast to the above-mentioned common approach, only the precursor of cationic constitute of a shell material was introduced in this approach and the shell growth proceeds through the gradual replacement of Pb cations by newly introduced cations in solution and anion sublattice remains basically un-disturbed [60, 88]. As a result, the shell grows at the expense of core nanocrystals, *i.e.*, the shell growth is accompanied by the decrease of the lead chalcogenide core size. Recently, the formation of PbSe/CdSe and PbS/CdS core/shell QDs by cation exchange has been demonstrated for the first time by Pietryga *et al.* Although it was found that the core/shell structure can enhance the QY of lead chalcogenide QDs [60], the final QY of PbS/CdS QDs is only 20% to 30%. In addition, it is still challenging to clearly resolve the core/shell morphology of these PbS/CdS QDs [60], although Lambert *et al.* have directly observed the core/shell structure of PbSe/CdSe and PbTe/CdTe QDs with high resolution TEM [88]. Also, the current cation exchange approach for the synthesis of PbS/CdS QDs in non-coordinating solvents seems to have its limitation on the maximum shell thickness attainable; relatively thick shells cannot be prepared even with larger cadmium excesses and longer reaction times [60]. The composition of the shell in the PbS/CdS system remains

unverified: is the shell composed of neat CdS or the alloy of $Pb_xCd_{1-x}S$? The optical property and thermal stability of PbS/CdS core/shell QDs are also not well studied in existing literature [60, 88].

4.2 Synthesis and characterization of PbS/CdS QDs

In this section (4.2), I am trying to address some of the above mentioned problems and focusing on understanding the structure of PbS/CdS QDs.

4.2.1 Structure of thin-shell PbS/CdS QDs

PbS QDs with varying sizes were firstly synthesized. Thin-shell PbS/CdS QDs were synthesized by adding an excess of cadmium oleate solution to PbS QD suspension in toluene at 100 °C [60]. By varying the initial core size and final shell thickness, the first exciton absorption peak of core/shell QDs can be tuned from 830 to 1960 nm and the band edge emission peak from 893 to over 1517 nm (detection limited by the NIR detector), as shown in Figure 4.1a. The experimental parameters for the synthesis of the PbS/CdS QDs presented in Figure 4.1a are listed in Table 4.1. The PbS/CdS QDs show a very uniform size distribution (Figure 4.1b). The overall size of the PbS/CdS QDs is close to the size of original PbS QDs, as previously reported [60].

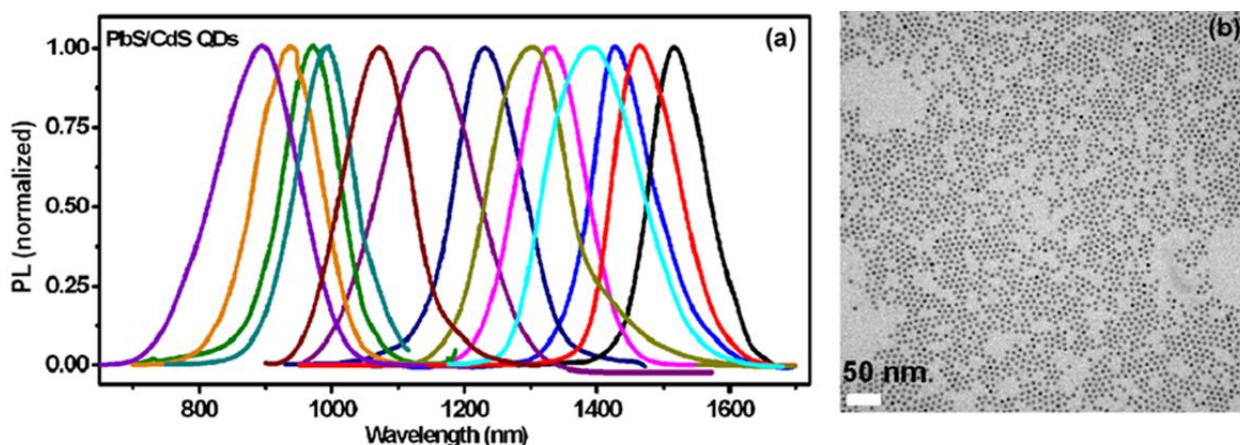


Figure 4.1 PL spectra (a) and typical TEM image (b) of PbS/CdS QDs.

The presence of cadmium element in the core/shell QDs has been confirmed by XPS and EDX (Figure 4.2 and 4.3). Although lead chalcogenide and cadmium chalcogenide have different crystal structures (for example, PbS has a rock salt structure while CdS has a zinc-blende structure), it has been reported very recently that they can grow on each other by the approach of cation exchange and the formed hybrid structure turns out to be quite stable [60]. In my investigation, it was found that during the process of lead substitution by cadmium, the particle size of PbS/CdS QDs (5.0 ± 0.3 nm) remains almost the same as that of the initial PbS QDs (5.2 ± 0.2 nm) as shown in Figure 4.4, just like the case reported for PbSe/CdSe QDs which were also prepared from cation exchange [60]. In addition, the steady blue shift of absorption peak with the reaction time indicates the gradual decrease of the effective size of the PbS “core” (Figure 4.5). This is quite likely due to the gradual replacement of lead by cadmium, leading to the formation of PbS/CdS core/shell structure.

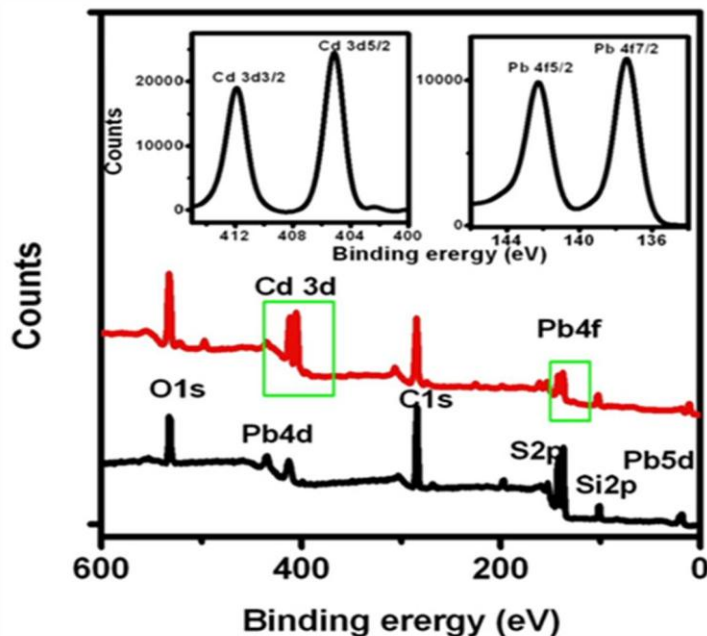


Figure 4.2 XPS spectra PbS (black line) and PbS/CdS QDs (red line). Insets: high resolution XPS spectra of Pb 4f and Cd 3d in PbS/CdS QDs.

Table 4.1 Experimental parameters for synthesizing PbS/CdS QDs presented in Figure 4.1a.

PL peak position of PbS/CdS QDs (nm)	Initial PbS size (nm)	Molar ratio of CdO to PbS	Molar ratio of OA to CdO	Reaction time (min)	Reaction temperature (°C)
893	4	300	4	360	100
939	4	300	4	120	100
972	4	150	4	10	100
994	4	150	4	2	90
1071	4.6	600	4	360	100
1147	4.6	300	4	120	100
1232	4.6	300	4	5	90
1302	4.9	300	4	60	100
1330	4.9	150	4	5	90
1393	5.4	300	4	240	100
1427	5.4	300	4	120	100
1460	5.4	150	4	10	90
1517	6.5	600	4	240	100

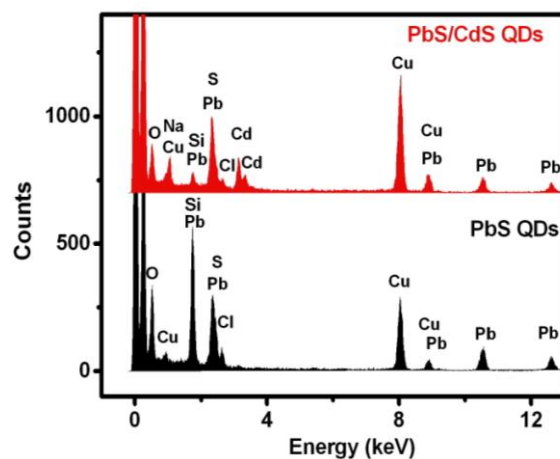


Figure 4.3 EDX spectra of PbS and PbS/CdS QDs, indicating the presence of Pb, S and Cd.

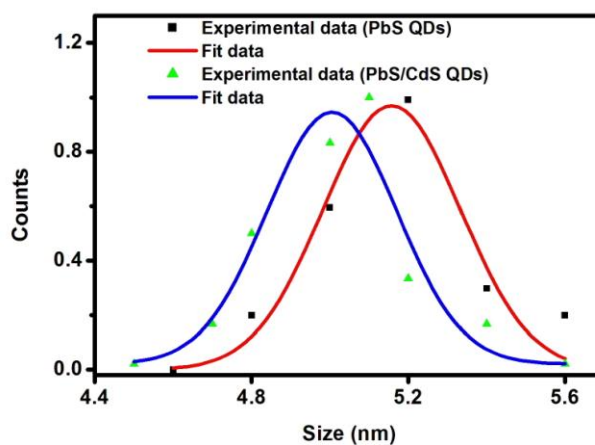


Figure 4.4 Size distribution of PbS QDs in chloroform (5.2 ± 0.2 nm) and PbS/CdS QDs after cation exchange in chloroform (5.0 ± 0.3 nm).

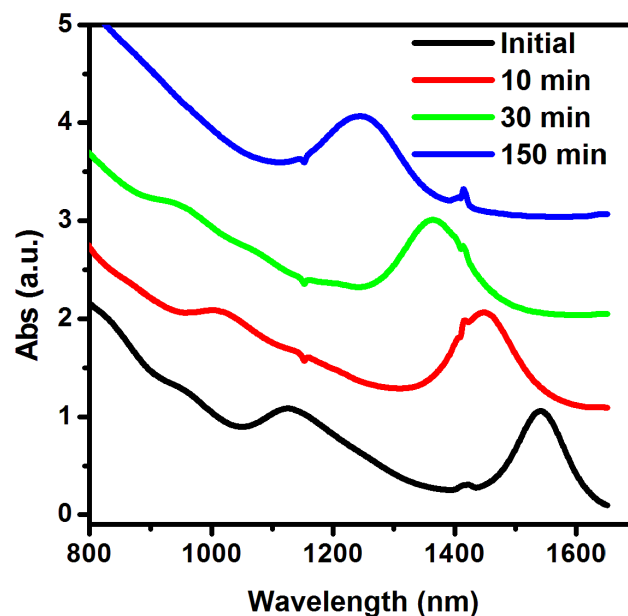


Figure 4.5 Absorption spectra of PbS during cation exchange process.

Although it is difficult to resolve the distinctive interface between the PbS core and atomically thin CdS shell through HRTEM, I have been able to observe different contrast and lattice images in individual QD (Figure 4.6), which are believed to be from the core of PbS and the shell of CdS, respectively. Figure 4.7 demonstrates that the core/shell structure is visible (indicated by arrows) in many of the QDs containing relatively large cores (>6 nm). Although it has been identified by TEM that the PbS/CdS QDs are core/shell structured, the shell composition remains unclear in thin-shell QDs. Based on the results reported in literature for PbSe/CdSe and PbTe/CdTe QDs synthesized in the same way using cation exchange [60, 88], it is expected that the shell in my thin-shell PbS/CdS QDs consists of pure CdS. As I am not able to unambiguously identify the lattice fringes of CdS in the shell by multiple HRTEM images, I made efforts to indirectly verify this by constructing band gap versus core size curves assuming the shell is entirely made of pure CdS and by comparing the curve to those of neat PbS QDs reported by others as well as obtained by

myself. If the assumed structural model (Figure 4.8a and c) is appropriate and there is no remarkable leakage of the exciton into the shell, the band gap of core/shell QDs should follow the similar relationship with the PbS size as that for shell-free PbS QDs. For comparison, I also did the same calculations on two assumed alloy-shell compositions ($\text{Pb}_x\text{Cd}_{1-x}\text{S}$ alloy, $x=0.2$ and 0.35) (Figure 4.8b).

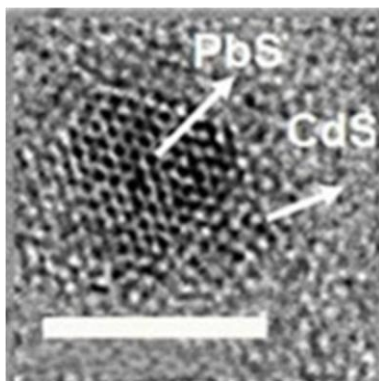


Figure 4.6 HRTEM image of an individual PbS/CdS QD. Scale bar is 5 nm.

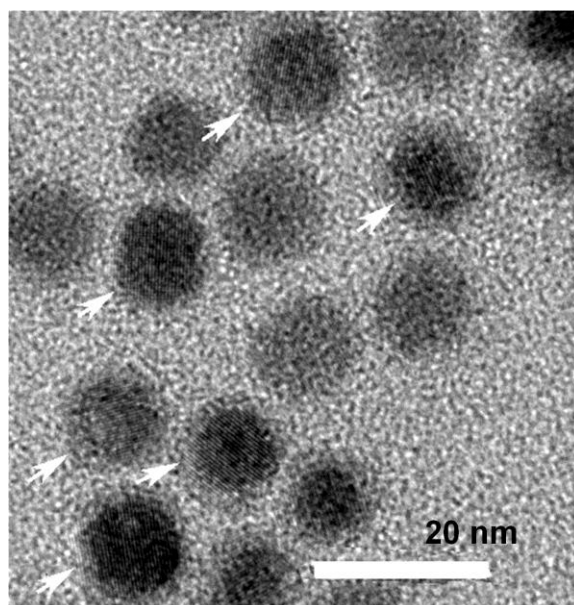


Figure 4.7 TEM image of PbS/CdS QDs. The size of parent PbS QDs is ~ 12 nm.

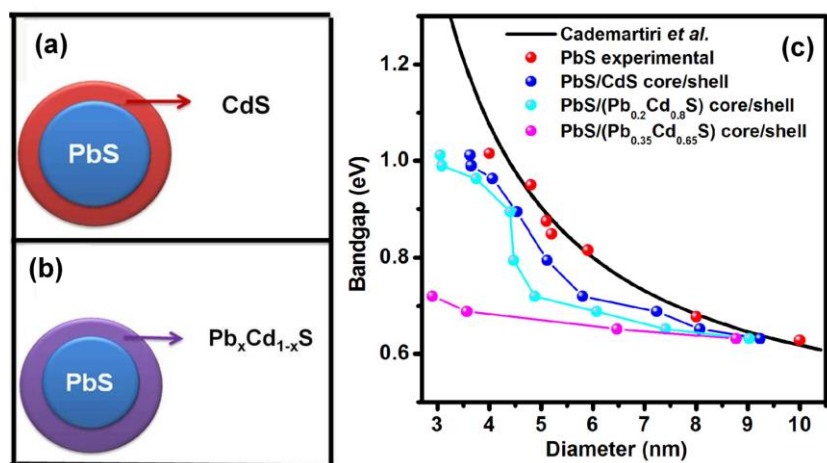


Figure 4.8 Schematic presentation of pure-CdS-shell (a) and alloy-shell structures (b) of PbS/CdS QDs. (c) Bandgap of PbS and PbS/CdS QDs as a function of PbS diameter. The black solid curve represents the data from ref 24. The blue, cyan and pink solid lines are guides to the eye.

The capability in tuning the initial PbS QD size and the final shell thickness permits me to acquire enough data to plot the band gap ~ size curves of QDs. I first synthesized pure PbS QDs with the first-exciton absorption peak spanning a large spectral range (Figure 4.9a). Then, by applying the cation exchange method with varying experimental parameters, I achieved the PbS/CdS QDs with the first-exciton absorption peak tuned in a wide wavelength range from below 1000 up to about 2000 nm (Figure 4.9b). TEM images demonstrate that both initial PbS QDs and subsequently synthesized PbS/CdS QDs are mono-dispersed with the diameter ranging from 4 nm to 10 nm (Figure 4.10 and 4.11). As stated above, the cation exchange method does not notably change the overall size of QDs. The band gap of QDs was deduced from their absorption spectra. For shell-free PbS QDs, the diameter was estimated from TEM directly. For core/shell QDs, the Pb-to-Cd ratio was first determined by ICP-OES. Then using this ratio and the overall diameter from TEM images, the diameter of the remaining PbS core and thickness of the shell were calculated for pure CdS or Cd_xPb_{1-x}S alloyed shell models assuming all QDs are spherical and contain a uniform shell.

Figure 4.8c shows the variation of the bandgap with the size of PbS QDs or PbS cores (in the case of core/shell QDs). For comparison, the data reported by Cademartiri *et al.* are also included [86].

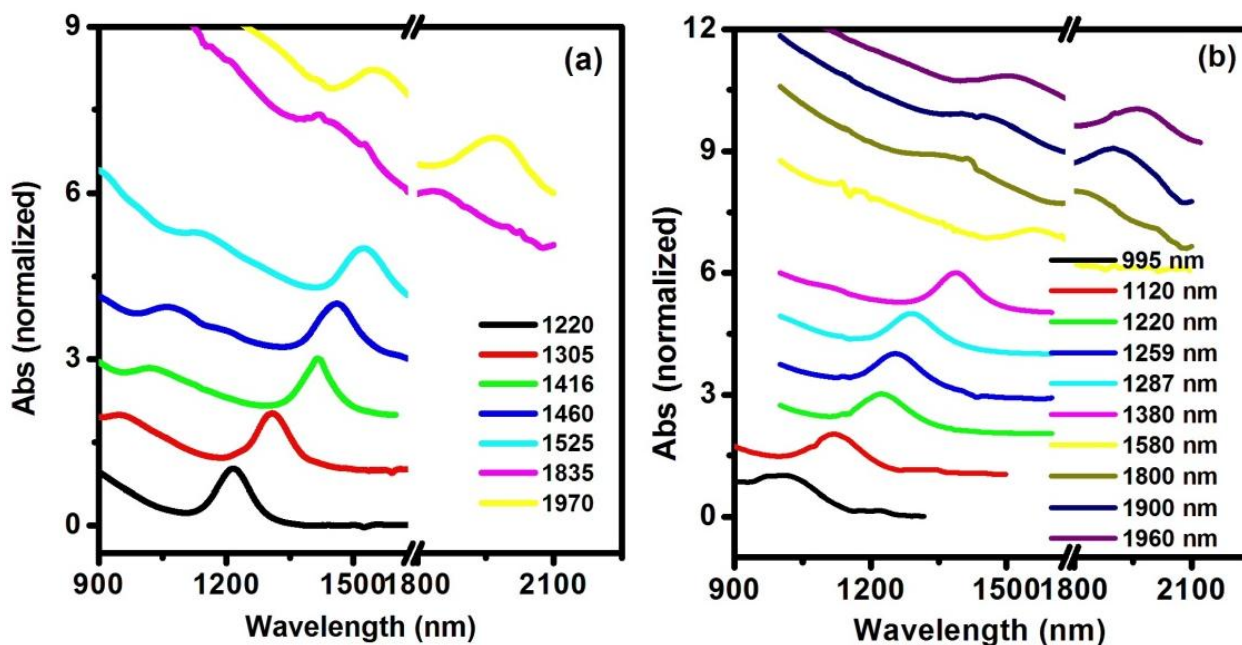


Figure 4.9 Tunable absorption spectra of (a) PbS and (b) PbS/CdS QDs.

It can be seen that my data for pure PbS QDs are in very good agreement with those reported (Figure 4.8c, black line). Among several compositional models, the pure-CdS shell model yields the closest results to the pure PbS QDs. The deviation gets more pronounced with the increasing value of x , *i.e.*, the concentration of PbS in the shell. When x reaches 35%, the deviation becomes quite obvious especially at smaller PbS sizes. These studies indicate that, most likely, the shell consists of neat CdS. It may be noted that there is a small deviation from the expected curve even for the pure-CdS shell model. Several factors may contribute to such deviation, such as the presence of a thin concentration-gradient interfacial layer between the PbS core and the CdS shell and the partial

leakage of the exciton into the shell [91]. Considering the simplicity of the compositional model, the agreement is indeed surprisingly close.

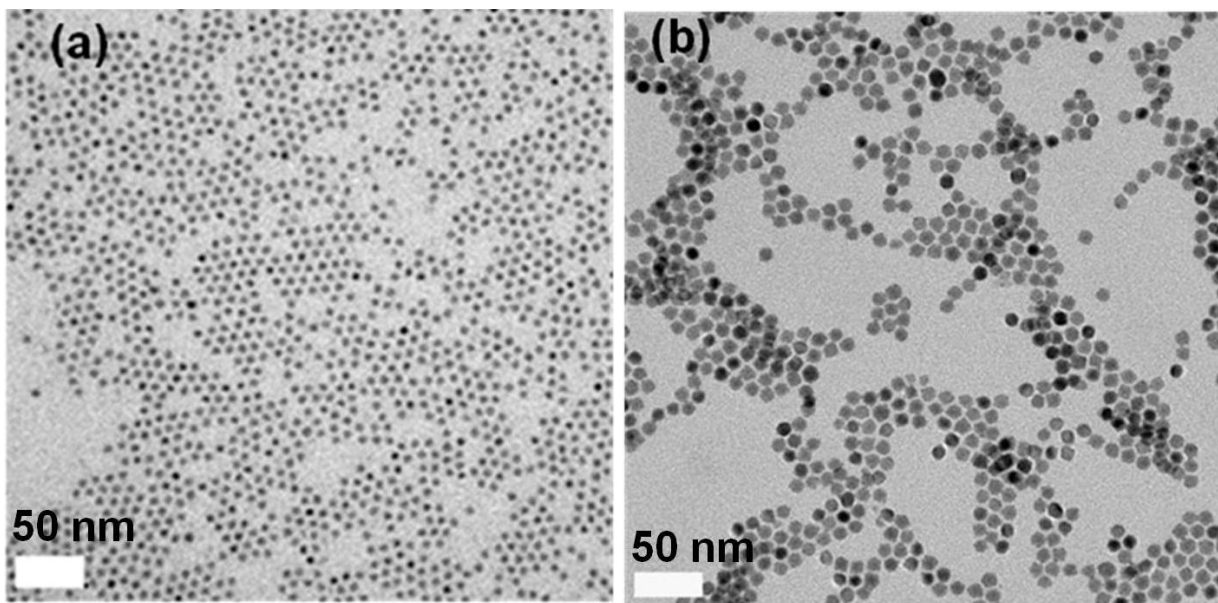


Figure 4.10 TEM images of PbS QDs with the first exciton peak at 1460 nm (a) and 1900 nm (b), respectively.

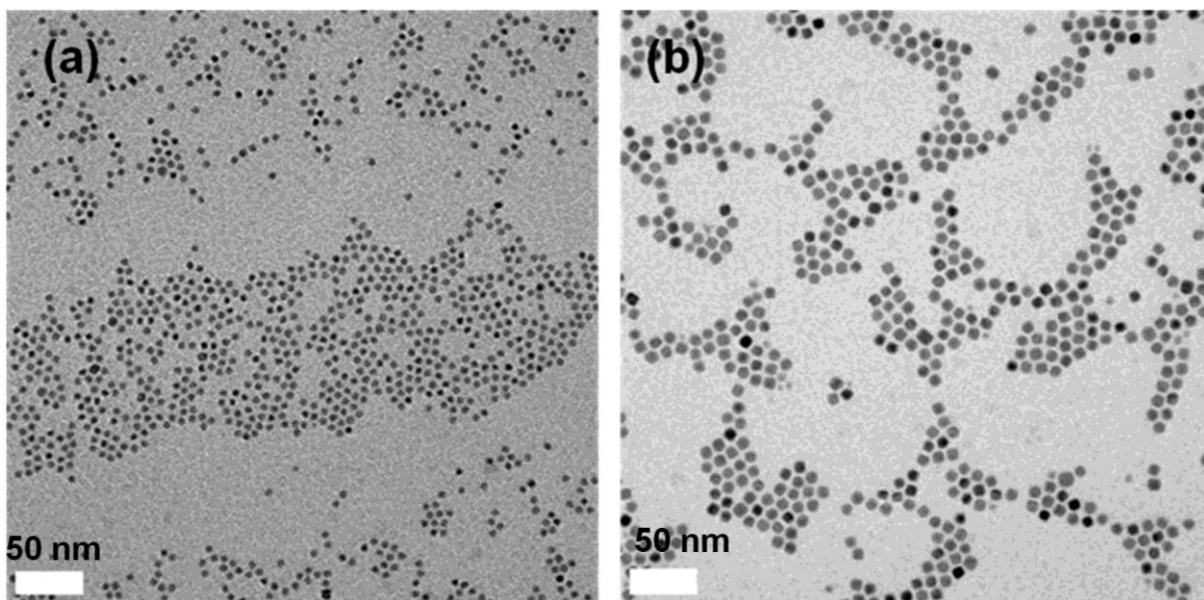


Figure 4.11 TEM images of PbS/CdS QDs with the first exciton peak at 1250 nm (a) and 1800 nm (b), respectively.

To summarize, the thin-shell PbS/CdS QDs have been synthesized and characterized. In particular, the chemical composition of the shell has been probed by using simple calculations (Section 4.2.1). In the following (Section 4.2.2), I will focus on synthesizing and characterizing thick-shell PbS/CdS QDs by a two-step cation exchange approach.

4.2.2 Structure of thick-shell PbS/CdS QDs

As reported previously, the replacement of lead by cadmium during the cation exchange reaction appears to be self-limiting [60]. The reaction does not proceed beyond a terminal shell thickness (in general below 1.5 nm) even with larger cadmium excesses and longer reaction times, regardless of initial QD diameter. As the efficiency of cation exchange is closely related to the diffusion of both types of ions and diffusion is easier at higher temperature, I expect that elevated temperature will benefit the growth of thick shells. However, it was found that directly setting the cation exchange reaction at higher temperature inevitably leads to Ostwald ripening of PbS QDs, giving rise to broader, double or even multiple size distributions (Figure 4.12a). Thereby, the key to growing a thick shell seems to be protecting PbS QDs and stabilizing them in such a way that they can resist the Ostwald ripening process at elevated temperature. I therefore performed the cation exchange reaction in two separate steps at different temperatures. As shown in Figure 4.13, in the first step, the thin layer of CdS (or $\text{Pb}_x\text{Cd}_{1-x}\text{S}$) was deposited with larger cadmium excesses at 100 °C as described above for the synthesis of thin-shell QDs, with the purpose of enhancing the stability of core QDs. After that, the reaction temperature was increased to higher than 200 °C, which is supposed to permit the cation exchange to proceed deeper into the interior of QDs. The approach is successful. Simple yet critical thin-shell deposition at relatively low temperature provides strong protection to core PbS QDs against the Ostwald ripening and allows me to attain thick-shell QDs with uniform size distribution at high temperature (Figure 4.12b and Figure 4.14).

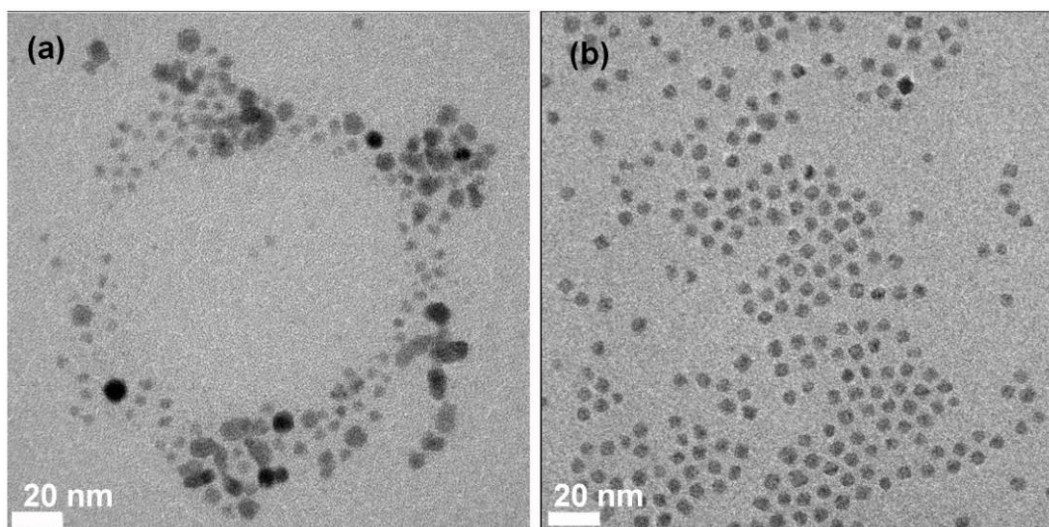


Figure 4.12 TEM images of PbS/CdS QDs (a) synthesized by cation exchange at 200 °C for 5 minutes and (b) synthesized via a two-step cation exchange (100 °C for 1 hour, following at 200 °C for 20 hours). The size of parent PbS is ~5.2 nm.

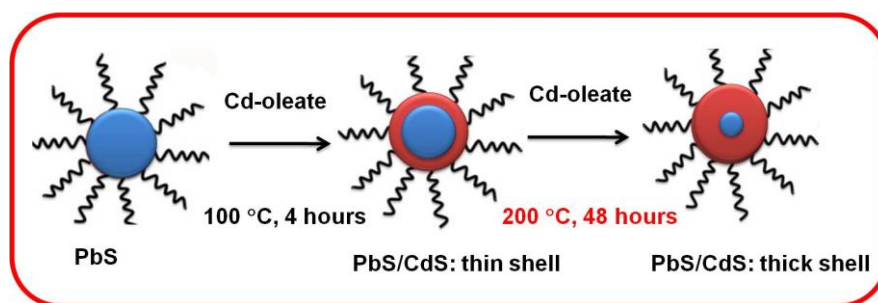


Figure 4.13 Schematic presentation of two step cation exchange to synthesize thick-shell PbS/CdS QDs.

As shown in Figure 4.15a, the thick-shell PbS/CdS QD exhibits strong contrast between the core and shell although the interface is not clear-cut. The darker part in the center shows clearly lattice fringes, which match well with the (200) planes of pure PbS, as expected (Figure 4.15a). As shown in Figure 4.14, the parent PbS QDs and all of the PbS/CdS QDs show uniform size distribution. After 4-hour reaction, the shell can be identified by TEM, although the shell thickness is not obvious. By applying a two-step approach, the thick shell is very clear, and the shell thickness

can be easily estimated by TEM. When the shell thickness reaches 1.8 nm, the QDs begin to show characteristic PL of pure CdS [89, 90] and with increasing shell thickness, it gets more distinct (Figure 4.15b and Figure 4.16).

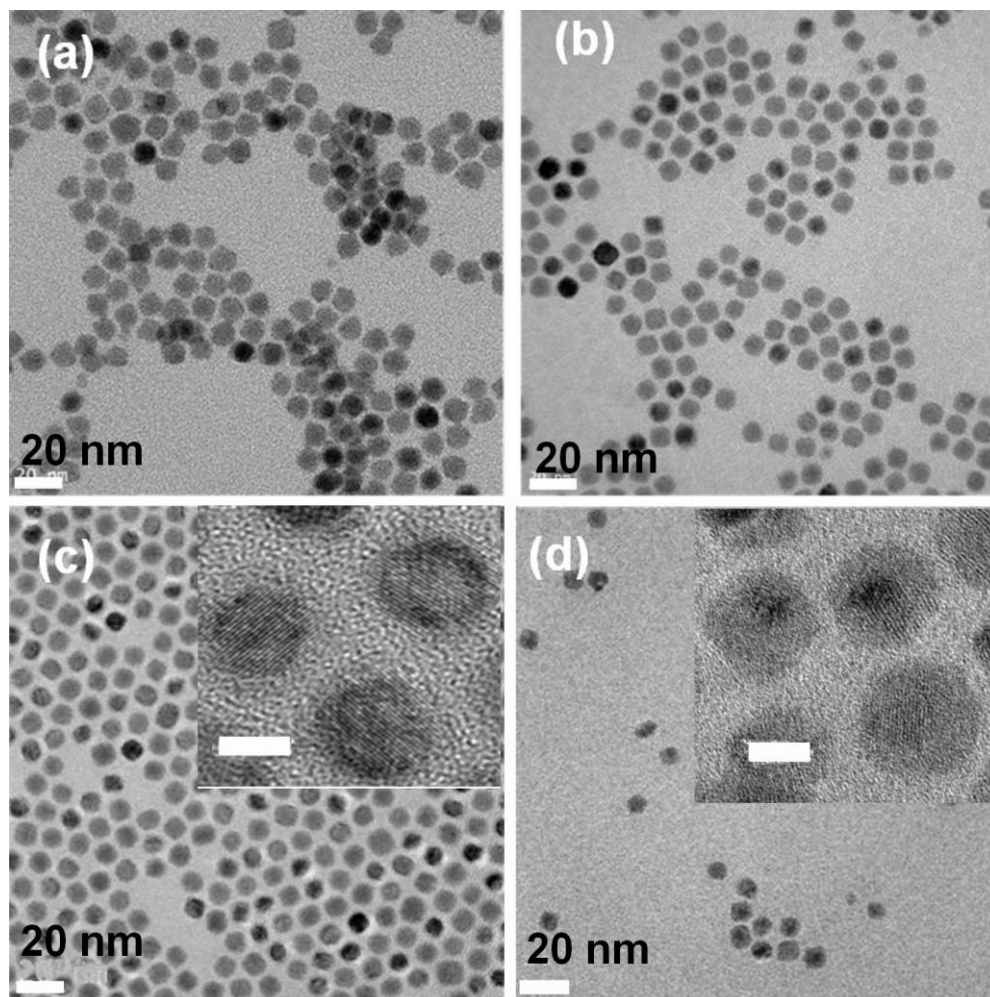


Figure 4.14 Representative TEM images of parent PbS (~ 10 nm in diameter) (a) and (b) PbS/CdS QDs synthesized at 100 °C for 1 hour (b), 4 hours (c) and PbS/CdS QDs following growth at 200 °C for another 20 hours (d). Inset of (c) and (d) are HRTEM images of (c) and (d), respectively, indicating clearly the core shell structure. Scale bar for inset images of (c) and (d) is 5 nm.

As clearly shown in Figure 4.15b, PbS/CdS QDs with a core diameter of 4.8 nm and a shell thickness of 2.4 nm exhibit both a CdS shell emission band and a PbS core emission band. The

similar phenomenon has been also found for the core/shell structured CdSe/ZnSe QDs [92]. The CdS PL band center at 510 nm and is accompanied by a broad shoulder at 580 nm, consistent with the markedly increased absorption from 500 to 600 nm in the core/shell QDs as compared with shell-free PbS QDs (Figure 4.15b). Such emission can be correlated well with pure CdS [89, 90] and is absent for bare PbS QDs. The broadness of the PL peak can be reasonably explained by the non-uniformity in the CdS shell thickness or the presence of defects in the shell. In addition, the fluorescence lifetime of these PbS/CdS QDs was measured at the wavelength of 510 nm by the TCSPC technique. The decay curve fits well into a two-component model that yields two lifetimes of 13.3 ns and 93.9 ns (Figure 4.17), which are in good agreement with the results reported recently for CdS QDs [89, 90]. The PbS/CdS QDs also emit in the NIR with the PL peak centering at 1319 nm (Figure 15b). This PL band is entirely assigned to the PbS core and from it, the core size is estimated to be 4.7 nm [86]. This estimated size is quite close to that observed in HRTEM (~4.8 nm).

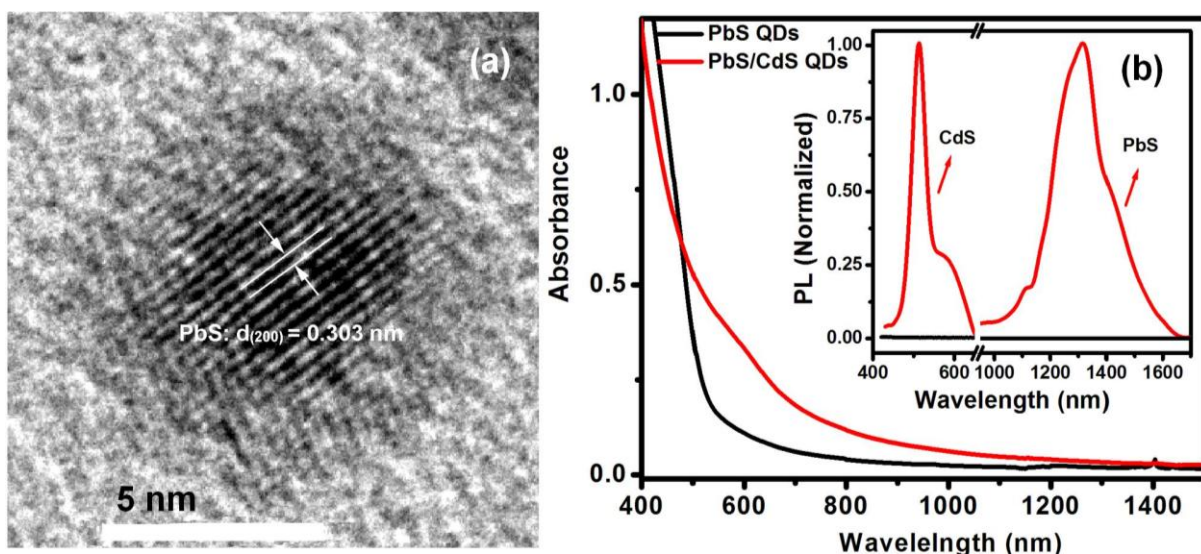


Figure 4.15 (a) HRTEM image of a thick-shell PbS/CdS QD clearly displaying the core and shell. (b) Absorption spectra of PbS and thick-shell PbS/CdS QDs in toluene. Inset of (b) is the PL spectra of PbS/CdS QDs manifesting characteristic emission from CdS and PbS.

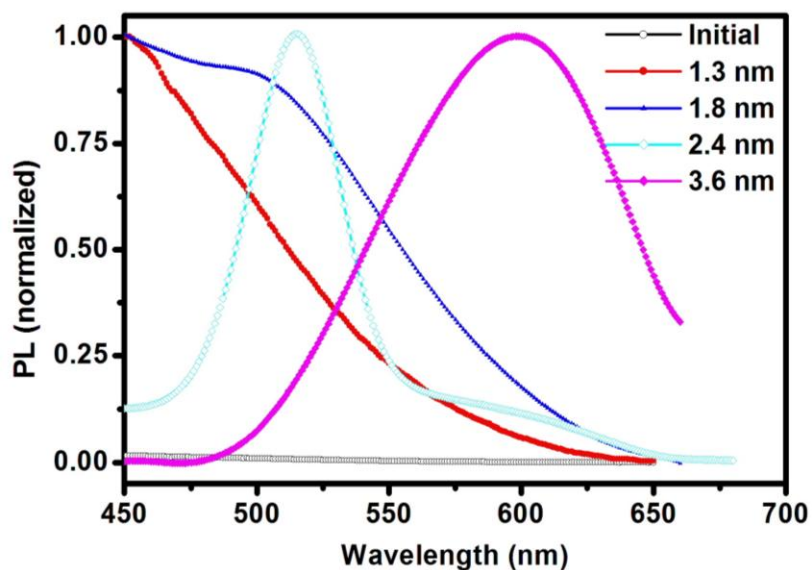


Figure 4.16 PL spectra of PbS (initial) and PbS/CdS QDs with tunable CdS shell thickness. Excitation wavelength was set at 345 nm.

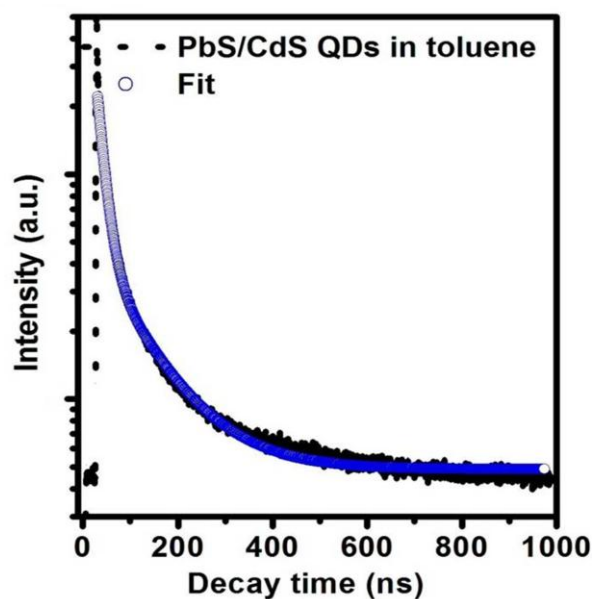


Figure 4.17 PL decay curve for thick-shell PbS/CdS QDs, measured at emission peak of ~ 510 nm in toluene, and shown on a logarithmic scale.

The PbS/CdS QDs were further characterized by XRD. As shown in Figure 4.18, the XRD patterns of the core/shell nanocrystals steadily shift from a rock-salt to a zinc-blende CdS-like

pattern with the increase of the shell thickness. When the thickness of shell reaches 3.6 nm, the PbS pattern almost totally disappears and the overall diffraction pattern is basically same as that of the CdS standard. The disappearance of the PbS pattern can be understood as that the signal from a very tiny core may be too weak to be detected. The thick-shell QDs were further analyzed by performing EDX in core (indicated by yellow circle) and shell (indicated by red circle) regions, respectively (Figure 4.19a). Although both Pb and Cd are present in the core, Pb is absent in the shell region, again strongly suggesting that the shell is made of CdS, instead of ternary $\text{Pb}_x\text{Cd}_{1-x}\text{S}$ alloy (Figure 4.19b). Since I did not observe any homogeneously nucleated CdS QDs in samples as expected for the cation exchange approach (Figure 4.14), these XRD and EDX results also strongly support the formation of the crystalline CdS shell, instead of ternary $\text{Pb}_x\text{Cd}_{1-x}\text{S}$ alloy, in the thick-shell samples, consistent with optical characterization results.

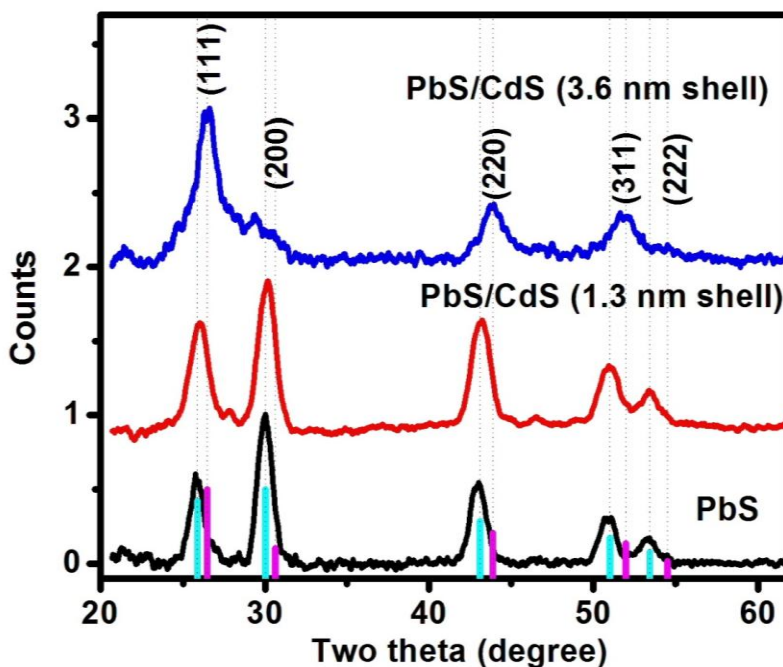


Figure 4.18 XRD patterns of PbS and PbS/CdS QDs with different shell thickness. The JCPDS card files for PbS (05-0592, cyan line) and for CdS (01 089 0440, magenta line) are shown below the spectra for identification.

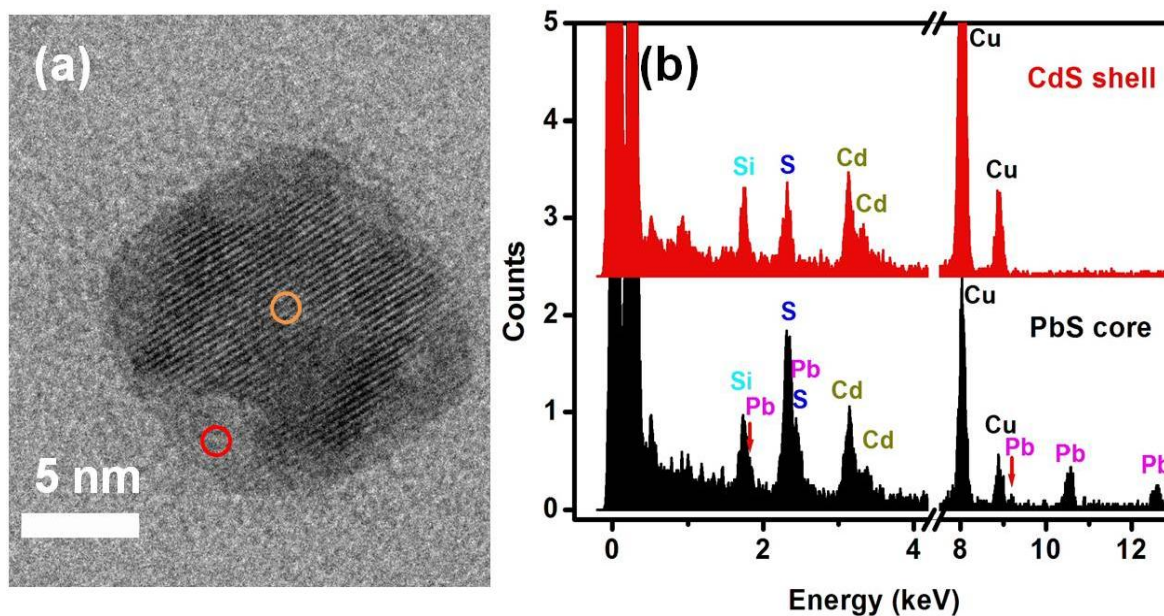


Figure 4.19 (a) TEM image of a PbS/CdS QD. (b) EDX spectra from the core (yellow circle) and shell (red circle) of the PbS/CdS QD.

In the Section 4.2, I have proved that the PbS/CdS QDs are core/shell structured and the shell is mainly made of CdS. In the following section (4.3), I will study the optical properties and stability of core/shell structured PbS/CdS QDs.

4.3 Properties of PbS/CdS QDs

4.3.1 QY

The PbS/CdS core/shell QDs show significantly improved PL efficiency. By choosing the optimal shell thickness (0.7 nm), the QY of PbS/CdS QDs can reach a value of as high as 67% which doubles that of initial, shell-free PbS QDs. It is worth mentioning that normally the QY of high-quality PbS QDs falls into the range of 20 – 40% according to literature [31, 32]. Consistently, the average PL lifetime of PbS/CdS QDs is much longer than that of parent PbS QDs (1.2 μ s versus 0.75 μ s) (Figure 4.20). The increase in the QY of PbS QDs after cation exchange is attributed to the

presence of much larger band gap material on the surface of PbS, which confines electrons and holes mainly to the PbS core and renders better passivation of surface nonradiative recombination sites. Clearly this shell deposition process reverses the dominating relaxation process in the QDs from nonradiative to radiative band edge recombination.

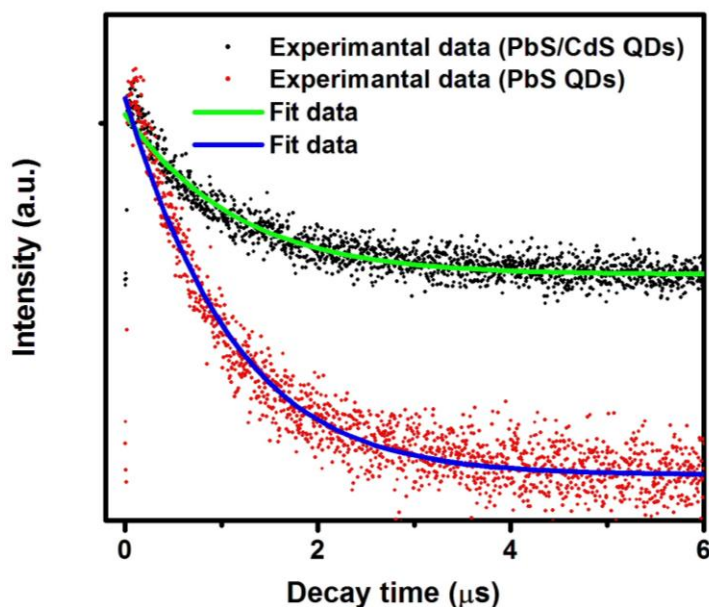


Figure 4.20 Typical PL decay curves for parent PbS QDs measured at the emission peak of ~ 1460 nm and PbS/CdS QDs measured at the emission peak of ~ 1320 nm in toluene, shown on a logarithmic scale.

4.3.2 Photostability

Even more importantly, these PbS/CdS QDs show much better photostability in the organic phase as compared to the shell-free PbS QDs under continuous UV illumination (Figure 4.21a). After 240-minute illumination, the PL intensity of the core/shell QDs keeps 85% of its original value, considerably higher than 70% of shell-free QDs. Same as the increase in QY, the enhancement of photo-stability originates from the better passivation of surface atoms due to the presence of the CdS-dominant shell.

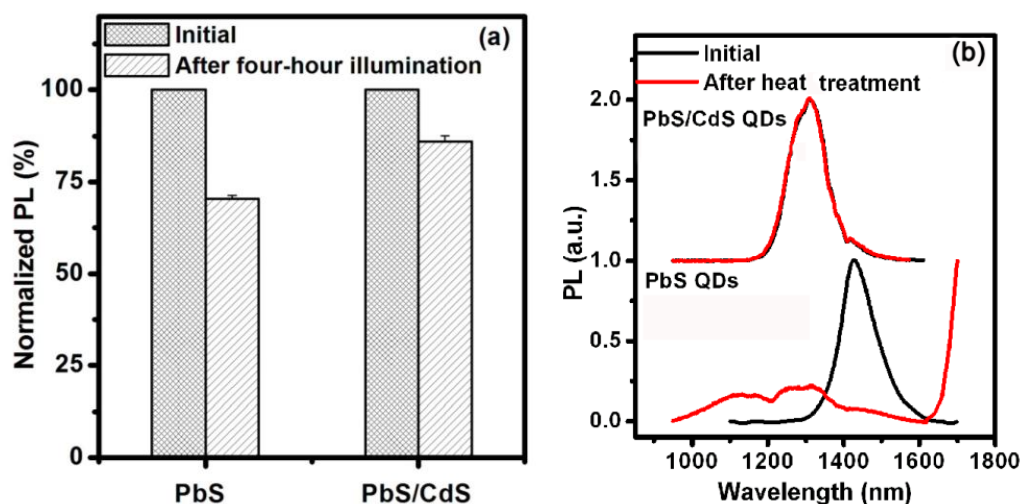


Figure 4.21 (a) The variation in the PL intensity of PbS and PbS/CdS QDs in ODE after four hours of continuous illumination. (b) The PL spectra of PbS and PbS/CdS QDs before and after heat treatment (PbS: 100 °C for 5 minutes in ODE; PbS/CdS: 150 °C for 30 minutes in ODE).

4.3.3 Thermal-stability

Meanwhile, PbS/CdS QDs show markedly better thermal stability than initial, un-shelled PbS QDs. They can remain their initial size and narrow size distribution at 150 °C for at least 30 minutes in ODE, as evidenced by essentially unchanged PL spectrum which is known to be very sensitive to the variation of the QD size distribution [85]. With the presence of excess ligands in solution, *i.e.*, in the same condition as that used for the second-step shell coating process, they are even more stable. In stark contrast, the shell-free PbS QDs of the same concentration and dispersed in the same solvent start to undergo the Ostwald ripening as short as five minutes after being held at an even lower temperature of 100 °C (Figure 4.21b). PL pattern changes dramatically from single to multi-modal with double bands between 1000 to 1400 nm corresponding to the presence of some smaller-than-initial QDs and emission above 1600 nm larger QDs. It suggests that the structure of the CdS shell is more thermally stable than that of PbS, which helps preserve the QD morphology at elevated

temperature. This is in accord with that reported for PbSe/CdSe QDs, where CdSe overcoated QDs are found to be more robust at relatively high temperature [60].

It is worth mentioning that even at room temperature; the role of the CdS shell in improving the structural tolerance of QDs to the variation of environments is pronounced. The enhanced robustness of core/shell QDs make them potentially more useful for various applications.

4.4 Summary

In this chapter, PbS/CdS QDs were synthesized via the cation exchange approach. The structure of thin-shell PbS/CdS QDs was characterized by absorption and PL spectroscopy, TEM and XPS. Comparison of compositional models based on “band gap-versus-core size” plots implies that most likely the shell in thin-shell QDs is made of pure CdS, instead of alloys. PbS/CdS QDs with a thicker shell were further synthesized via my two-step cation exchange approach, in which the first step of thin shell deposition is crucial. Owing to the preparation of a relatively thick shell, not only can the core/shell structure be directly observed by TEM, characteristic absorption and emission of CdS, distinctly different from those of the PbS core, can also be observed from such a structure, which firmly attests that the shell mainly consists of CdS. Furthermore, the XRD and EDX results strongly support the formation of the crystalline CdS shell in our thick-shell samples. Importantly, the core/shell structured PbS/CdS QDs show significantly higher QY, and better photo- and thermal stability than shell-free PbS QDs, which render them potentially more useful for a variety of applications.

The as-synthesized PbS or PbS QDs are insoluble in water, in next two chapters, I will transfer the QDs from an organic phase into water via amphiphilic polymer approach in order to achieve water-soluble high-quality PbS-based NIR emitting QDs.

Chapter 5

Synthesis and characterization of water-soluble PbS QDs

I have synthesized high quality PbS and PbS/CdS QDs in the organic phase, however, these QDs are capped by hydrophobic ligands which make QDs insoluble in water. For biomedical applications, PbS QDs are required to be soluble and bright in water.

In this chapter PbS QDs will be transferred into water via an amphiphilic polymer approach [71, 72]. I firstly transferred the PbS QDs capped by OLA ligand from chloroform into water. The PbS QDs lost their PL in 5 minutes and further automatically and partially recover their PL in water after 3 months of aging at 4 °C, an interesting phenomenon observed for the first time. I then thoroughly characterized these QDs using TEM, XRD and XPS and identified the mechanism for PL disappearance and recovery behavior of the QDs in water.

The QY of PL-recovered PbS QDs is only 10% in water. In addition, it seems that the quality of PbS QDs during the water transfer process is highly affected by OLA ligands. Motivated by this finding, I further investigated the effect of different types of surface ligands on the structure and optical property of water-soluble PbS QDs encapsulated by amphiphilic polymers in order to secure the synthetic conditions for achieving higher-quality water-soluble PbS QDs.

5.1 Synthesis approach of water-soluble QDs

NIR emitting QDs have attracted much attention in recent years due to their unique size-dependent optical properties and a wide range of potential applications in biological imaging and sensors, etc [19, 20]. The enhanced tissue penetration of lights and decreased tissue autofluorescence in the NIR range render the NIR emitting QDs highly promising for *in vivo* deep-tissue imaging [19, 20]. To date, various kinds of water-soluble NIR-emitting QDs have been synthesized directly in an aqueous solution or indirectly by an organometallic method followed by transfer into water [52, 53, 54, 55, 56, 57, 58, 93, 94, 95, 96, 97, 98].

5.1.1 Synthesis of water-soluble PbS QDs in an aqueous system

Previously, PbS QDs have been directly synthesized in water in the presence of stabilizers, such as poly(vinylalcohol), poly(vinyl pyrrolidone), gelatin and DNA [41, 42]. Furthermore, a mixture of thiols (1-thioglycerol and dithioglycerol) was used to produce water-soluble PbS QDs with tunable size [52]. However, generally these synthetic routes could not produce PbS QDs with a high QY and good photostability in buffer. High-quality PbS QDs synthesized from the organometallic approach, however, are insoluble in water due to the use of hydrophobic ligands.

5.1.2 Water transfer approach

In one approach, ligand exchange reactions strip the nanocrystal surface of their original hydrophobic organic ligands containing bulky alkyl groups, replacing them with ligands containing hydrophilic end groups (for example, hydroxyl, carboxyl) to achieve water compatibility. Over the past decade, ligand exchange approach has been widely applied for group II-VI QDs [93, 94, 95, 96, 97, 98]. Recently, this method has been applied to transfer the high quantum-yield PbS QDs from the organic phase into water [56, 57]. Currently, 26% is among the highest luminescence QY

reported to date for PbS QDs in a buffer solution achieved by ligand exchange [57]. Nonetheless, the stripping of original surface ligands from QD surfaces has been found to lead to a significant decrease of 30 ~ 60% in the QY [56, 57].

A second approach is to encapsulate the QDs in an amphiphile [58, 59]. The use of amphiphile in the water transfer process of QDs appears to be more promising. It is believed that the encapsulation of QDs into amphiphiles will not disturb the surface ligands and thus the initial high QY can be retained. In particular, some amphiphilic polymers have been proven to be good candidates for phase transfer. As compared to traditional small amphiphiles, each chain of amphiphilic polymers contains multiple hydrophobic units. As a consequence, its interaction with the native organic ligands on nanocrystals can be numerous, and thus the encapsulants can be bound more strongly than if conventional surfactants are used. In addition, polymer-capped QDs can have functionalized exteriors and be ready for further bioconjugation. Although this amphiphilic polymer approach has been successfully applied to UV-visible emitting QDs [59], as far as I know, there are no such reports on PbS QDs.

5.2 Synthesis of amphiphilic-polymer encapsulated PbS QDs

PMAO-PEG was synthesized by reacting PMAO with biocompatible PEG-OH in chloroform at the PMAO/PEG molar ratio of 1:30 [59]. The formation of PMAO-PEG was verified by FT-IR characterization (Figure 5.1). The decrease of peak 1780 cm^{-1} and the increase of peak 1710 cm^{-1} are due to the decomposition of anhydride and the formation of COOH groups. The co-polymer exhibits the major characteristic IR peaks of the original PMAO and PEG. Then PbS QDs capped by OLA ligands were transferred into water via PMAO-PEG.

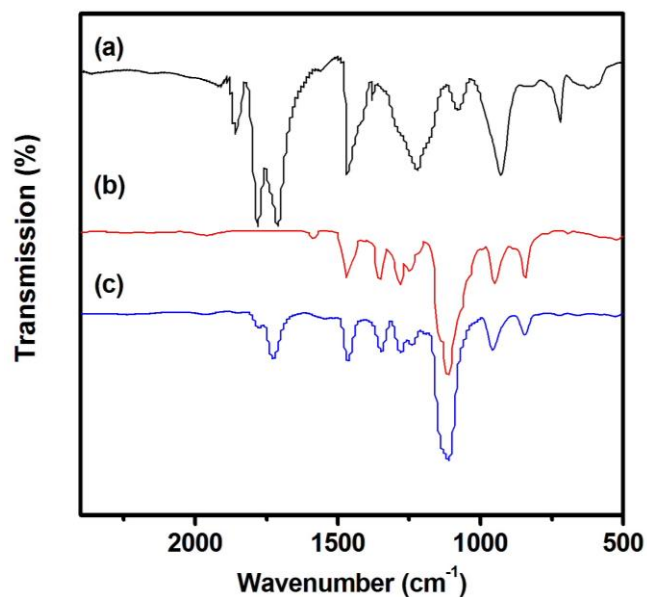


Figure 5.1 FT-IR characterizations of (a) PEG-OH, (b) PMAO and (c) PMAO-PEG.

After the PbS QDs capped by OLA ligands were transferred into water via amphiphilic polymers, I found, however, the PL totally disappeared in few minutes. In the following section (5.3), I am going to figure out the mechanism for the PL disappearance and self PL recovery of amphiphilic polymer encapsulated PbS QDs.

5.3 Self PL recovery of water-soluble PbS QDs

5.3.1 Structure variation

The structure of PbS QDs before and after transfer into water was investigated by TEM. As shown in Figure 5.2a and b, the PbS QDs maintain the structural intactness after going through the polymer encapsulation process in chloroform (5.2 ± 0.2 nm versus 5.2 ± 0.3 nm). They are, however, dissolved and broken up quickly after being transferred into water and exhibit a double size distribution (5.6 ± 0.9 nm and 2.7 ± 0.4 nm) (Figure 5.2c). In contrast, the PMAO-PEG

encapsulated PbS QDs (hereafter denoted as PbS/PMAO–PEG QDs) transferred from chloroform into ethanol still show a single size distribution while with a slight size decrease (Figure 5.2d).

The obvious variation in the size distribution of PbS QDs after transfer into water is related to ligand etching, which has been reported for thiol capped PbS QDs [99] and dodecylamine capped gold nanoparticles [100]. The etching of the PbS QD surface by OLA seems to be significantly accelerated by the co-presence of amphiphilic polymers and water since only mild ligand etching was observed for PbS/PMAO–PEG QDs transferred in ethanol, as evidenced by a slight size reduction in the latter. I postulate that it is this efficient ligand etching process in water that leads to the double size distribution of PbS/PMAO–PEG QDs. Severe ligand etching may immediately cause an important broadening of the size distribution of QDs considering that etching is often faster for smaller QDs in a group (even in a monodispersed sample, there are some QDs a little bit smaller than others).

As a result, efficient Ostwald ripening is initiated and eventually results in the two populations of QDs of distinctly different sizes [85]. This mechanism is schematically displayed in Figure 5.3. It is worth noting that both the ligand etching and Ostwald ripening processes disturb the ligands on the QD surface and modify the surface structure of PbS itself. It is highly likely that these processes simultaneously introduce considerable amounts of surface defects including unpassivated surface sites, which quench the PL of PbS QDs. This will be further discussed in the following sections.

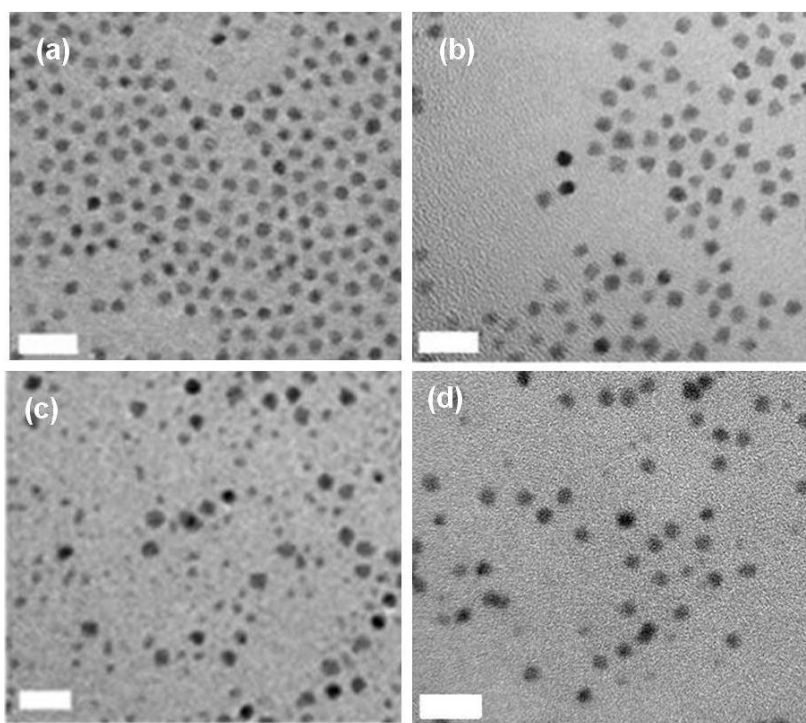


Figure 5.2 TEM images of as prepared PbS QDs in chloroform (a), and PbS/PMAO-PEG QDs in chloroform (b), immediately after transfer into water (c) and ethanol (d). Scale bar is 20 nm.

Since the polarity of ethanol is much lower than that of water (ϵ : 24.3 versus 80) and it is the hydrophilic groups of the polymer molecules that stick out from the QD surface, the interaction between the attached polymer molecules and solvent must be weaker in ethanol as compared to that in water. This is believed to be the reason for much less significant etching observed in ethanol than in water; the ligand etching may not only be directly related to the first layer of ligands, but also be indirectly related to the second layer of polymers because of the strong hydrophobic interaction between the ligands and polymers. This mild ligand etching process in alcohol does not cause any obvious broadening to the size distribution of PbS QDs and does not seem to result in any obvious Ostwald ripening. This study in alcohol confirms the important role of water in the ligand etching process.

5.3.2 Fast PL decay

The PL spectra of as prepared PbS QDs in chloroform, and those after PMAO–PEG encapsulation in chloroform, following transfer into water and further aged at 4 °C for different time are presented in Figure 5.4a, respectively. No discernable loss of QDs was observed in any of the above mentioned preparations. In other words, the QD concentration remains constant for all the samples in comparison. The PL intensity of PbS QDs after PMAO–PEG encapsulation reveals a 20% increase as compared to the initial value in chloroform. The QY reaches the value of 30%. This increase of QY is possibly due to the better isolation of PbS QDs from their environments with the introduction of an additional polymer shell. However, a large PL drop of 58% was observed after the QDs were transferred into water from chloroform. The PL peak centered at 1557 nm with a shoulder at 1380 nm rapidly evolves into a double peak structure within 1 minute, and then totally disappears within 5 minutes. The double PL peaks correlate very well with the observed double size distribution of transferred PbS QDs in water.

It is worthwhile to find out the reason for the fast PL decay of PbS/PMAO–PEG QDs after being transferred into water. As mentioned above, the optical properties of QDs are highly sensitive to surface states [56, 57]. As ligand etching and Ostwald ripening cause the change of the surface structure of QDs (including PbS surface structures and ligand capping status), they are most likely to introduce surface defects, which certainly affect the PL. The initial broadening and red shift of the PL band of PbS/PMAO–PEG QDs in water is possibly due to the degradation of size distribution [101] and surface passivation. With the rapid formation of many smaller PbS QDs and more surface defects in larger QDs, the emission at shorter wavelengths appears and that at longer wavelengths becomes weaker. As a consequence, the double PL peaks emerge shortly. With the fast Ostwald ripening process, more and more surface defects are possibly introduced which lead to the

total loss of PL eventually. The darkening of PbS QDs may also be explained from the presence of “external” molecular quenchers in water. It has been reported that water and dissolved oxygen molecules can lead to the PL quenching of QDs [102]. This has actually been further confirmed by the PL recovery behavior of QDs in environments containing less external quenchers (to be discussed below).

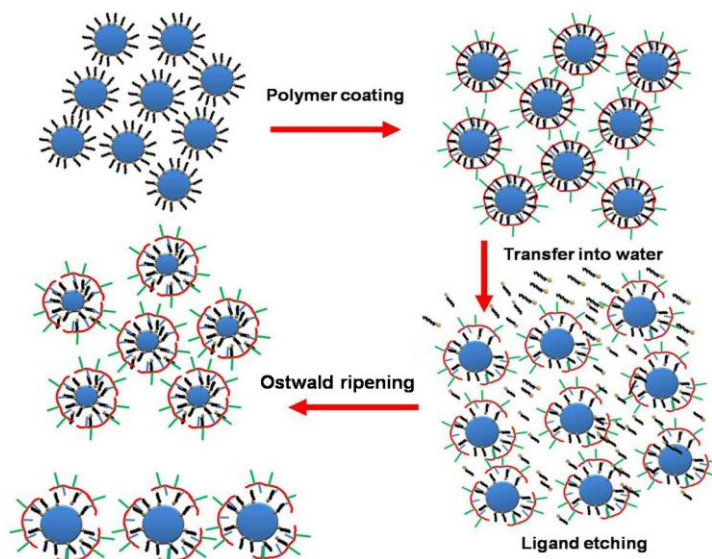


Figure 5.3 Schematic representation of the process leading to the double size distribution of PbS QDs after transfer into water.

In contrast, only a single PL peak was observed for PbS/PMAO–PEG QDs transferred into ethanol from chloroform (Figure 5.4b); this is consistent with their mono-modal size distribution as presented in Figure 5.2d. Furthermore, the blue shift of 100 nm in emission was observed for PbS/PMAO–PEG QDs with ethanol transfer. This spectral shift is believed to be mainly due to slight ligand etching, as supported also by observed slight size reduction (Figure 5.2d). Although, it has been reported that the variation of solvent polarity shifts the PL spectra of QDs, it should not be the case here since polar solvents often cause red shifts of PL spectra [103, 104]. In addition, the PL

spectrum of PbS/PMAO-PEG QDs in ethanol does not show any obvious spectral broadening, indicating the absence of Ostwald ripening in this system. It should be noted that PL spectrum broadening has often been used as a sign of the presence of the Ostwald ripening in QD studies [85]. All these results suggest that relatively strong ligand etching is necessary for the start of Ostwald ripening in the samples studied herein and the strength of ligand etching is not only determined by the type of ligands as expected, but also related to the polymer-solvent interactions.

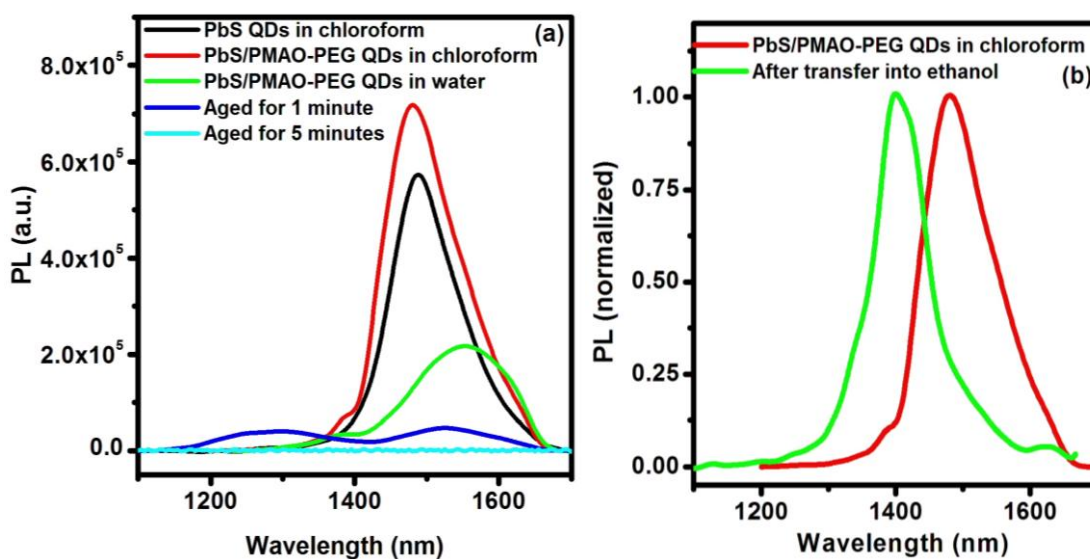


Figure 5.4 (a) PL of PbS QDs in chloroform prior to polymer encapsulation, after PMAO-PEG encapsulation in chloroform, following transfer into water and after being stored in water at 4 °C for 1 minute and 5 minutes. (b) PL of PbS/PMAO-PEG QDs in chloroform and following transfer into ethanol.

It is very clear that the disappearance of PL of PbS QDs capped by OLA liands upon water transfer is due to the ligand etching and Ostwald ripening. However, I further found that the PL of PbS QDs can be partially recovered by keeping them in the dark and the recovery behavior differs among QDs of different sizes. In the following (Section 5.3.3), I will try to figure out the reason for the size-selective PL recovery of water-soluble QDs.

5.3.3 PL recovery

Although the pronounced loss of PL can be expected considering severe QD structural variation during ligand etching and Ostwald ripening, it is interesting to observe the partial PL recovery of PMAO–PEG encapsulated QDs in water after being aged in the dark at 4 °C for 3 months. As shown in Figure 5.5a, the PL intensity of PbS QDs in water recovers to 40% of their initial value in chloroform, with the single PL peak at 1297 nm. The TEM image shows the PbS QDs are still in double size populations (6 ± 0.4 nm and 1.9 ± 0.3 nm) with slight changes of their respective average sizes as compared with those in the freshly water transferred sample (Figure 5.6a). The result suggests that Ostwald ripening continues even at a relatively low temperature of 4 °C. The number percentage of larger QDs was found to be $\sim 57\%$ based on TEM image counting, which is close to that estimated from XRD results (49%) (Figure 5.6b). In the XRD calculation, a simple equation is applied:

$$D_{\text{XRD}} = D_{\text{small}} x + D_{\text{large}} (1-x) \quad (5.1)$$

where D_{XRD} is the QD size calculated from the Scherrer equation [104], D_{small} is the average size of smaller QDs and D_{large} is the average size of larger ones based on TEM observations and x is the number percentage of smaller QDs.

According to the correlation between emission peak positions and particle sizes [86], the single emission band centered at 1297 nm was identified to be contributed from smaller QDs. It means that the larger QDs representing about half of the QDs in the sample are still non-emitting even after long time aging. The remarkably different recovery behavior in smaller and larger QDs is quite intriguing and may be explained from two aspects: the difference in the density of surface defects (“internal” quenchers) or in the compactness of the ligand/polymer structure (related to

“external” quenching events). The effective surface aging of PbS and thereby the removal of defect states and improved surface passivation due to ligand re-organization may contribute together to the recovery of PL in the smaller QDs. Nonetheless, the annealing of the surface of the larger QDs may turn out to be slower or more difficult in view of their relatively low surface activity with respect to their smaller counterparts. Furthermore, more surface defects or un-passivated surface atoms, resulting in PL quenching, may be created during the formation of less ordered crystalline surfaces in the low-temperature Ostwald growth process of larger QDs [38]. On the other hand, it is also possible that the ligand/polymer structure on larger QDs is less compact than that on smaller ones, rendering their surfaces more accessible to “external” quenchers (such as solvent or oxygen molecules) present in solution [102, 106]. Previous studies have shown that polar solvent molecules can interact with QD surfaces and lead to the decrease in PL intensity [103, 104]. In order to figure out which mechanism is mainly responsible for the non-emitting status of the larger PbS/PMAO–PEG QDs, the QDs stored in water for three months were transferred back into chloroform, which is expected to have much less numbers of “external” PL quenchers [102, 103, 104]. If it is molecular quenching that is mainly responsible for the darkening of larger QDs in water, their emission should largely recover in chloroform. Furthermore, chloroform may help improve the compactness of the amphiphilic polymer structure on the surface of QDs as the polymer is less soluble in chloroform, which will also aid in the reduction of quenching effect. As shown in Figure 5.5a, the PL intensity of PbS QDs transferred back into chloroform doubles that of the QDs in water. In addition, a shoulder located at a longer wavelength appears clearly in their PL spectrum. Gauss fitting yields two PL bands: the one situated at 1297 nm is again attributed to smaller QDs, while the one at a longer wavelength of 1486 nm is assigned to larger QDs. The integrated PL intensity ratio of larger to smaller QDs is found to be only 6.4% in chloroform, which is much lower than that (131.6%) expected from the QD number ratio (small-to-large: 76/100) extracted from

TEM observations. The value of 131.6% is obtained by assuming that each QD exhibits the same quantum efficiency whatever its size. In my studies, I found larger PbS QDs indeed have even higher quantum efficiency than smaller ones. If it also holds true here for polymer-encapsulated QDs, it means that larger QDs should contribute more than 57% of the total emission. The apparently contradictory result strongly indicates that either a significant number of larger QDs are still in the dark state or the PL efficiency of each larger QD is extremely low in chloroform. Considering the quencher concentration in chloroform is already much lower than that in water, it is clear that “external” quenching could not be a dominating factor for the total loss of PL of PbS/PMAO–PEG QDs in water although it partially contributes to the darkening of PL. It can be reasonably concluded that it is the presence of considerable numbers of surface defects or unpassivated surface atoms in larger QDs themselves that is mainly responsible for their loss in PL in water.

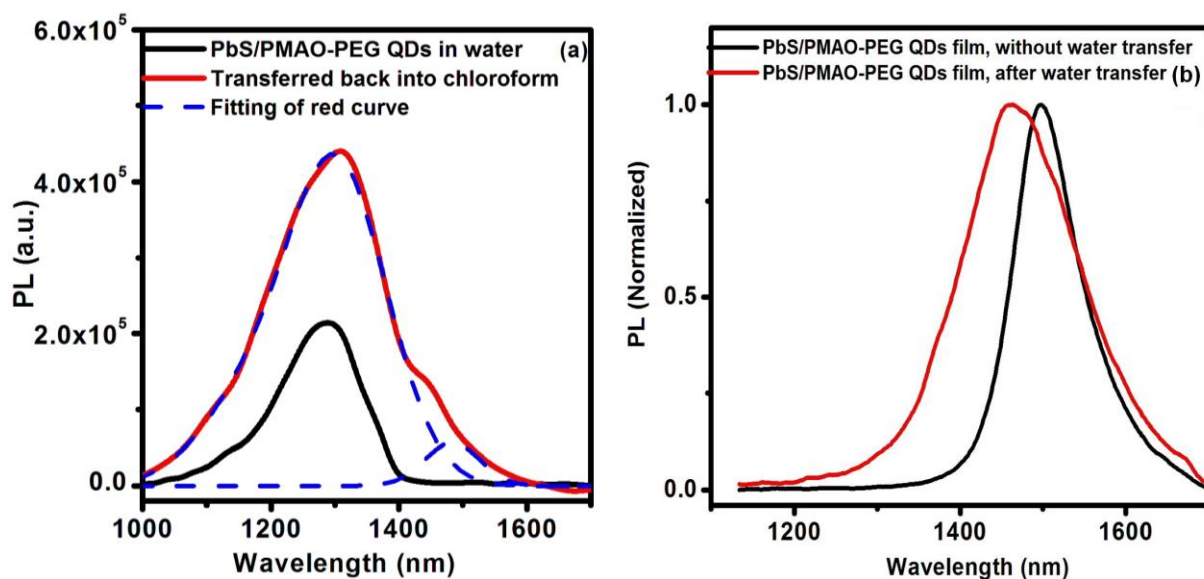


Figure 5.5 (a) PL of PbS QDs being stored at 4 °C for 3 months in water and following transfer back into chloroform. Two resolved PL peaks from the Gauss fitting for the PL curve of PbS QDs in chloroform are also shown. (b) PL of PbS solid films dried from PbS/PMAO–PEG QDs dispersed in chloroform or stored in water for 3 months.

The above conclusion is further supported by the PL investigation of dried PbS QD films, in which the molecule quenching event is eliminated or at least minimized as the collapse of amphiphilic polymers during the drying process provides QDs with good isolation from their environments. The PbS/PMAO-PEG QDs freshly prepared in chloroform show red shift from 1480 nm to 1497 nm after film preparation, which is understandable as the QD coupling in the film often leads to the red shift of PL peaks [107]. Hence, for PbS/PMAO-PEG QDs (which have gone through the 3-month storage in water) with a bimodal PL band, two emission bands situated at 1297 nm and 1486 nm in chloroform are both expected to shift to red when the QDs are dried into a film. In addition, considering the distinct difference in the size distribution of two QDs/PMAO-PEG samples (5.2 ± 0.3 nm in chloroform versus a double size distribution of 6 ± 0.4 nm and 1.9 ± 0.3 nm in water), the spectrum of the film sample of PbS/PMAO-PEG QDs that have been stored in water for three months should appear expanding towards both shorter and longer wavelengths as compared to that of the film sample of PbS/PMAO-PEG QDs from chloroform. However, it can be seen clearly in Figure 5.5b that although, as expected, there is obvious red shift of the emission peak when the PbS/PMAO-PEG QDs are dried into a film from water and a significant fraction of bluer emission as compared to that of the PbS/PMAO-PEG QDs dried from chloroform, there is only very slight spectral difference at the side of longer wavelength (above 1500 nm). This observation is a strong indication that larger QDs in the transferred sample do not make any important contribution to the PL even in the solid state. I further did simple calculation to estimate the contribution from larger QDs to PL. If we assume that all the emission above 1486 nm is contributed only by larger QDs, by comparing the integrated PL intensity above this wavelength to the PL intensity integrated over the entire PL band, it is estimated that larger QDs only account for ~30% of total emission, indicating most of PL still comes from smaller QDs. In fact, this value may even much overestimate

the contribution from larger QDs. It is known that in the solid film, the resonant electronic energy transfer from smaller to larger QDs takes place even in a nominally single-sized QD sample, which results in the quenching of higher-energy PL of smaller QDs [107]. The smaller QDs may also form clusters and show emission at much longer wavelengths, which could be mistaken as the emission from larger QDs. Considering this complexity, the above results suggest that even by almost excluding the possibility of PL quenching caused by external quenchers, the emission from the larger QDs only constitutes a much smaller fraction of the entire emission band than that expected from the molar ratio of larger-to-smaller QDs. The larger QDs must have more surface defects or unpassivated surface atoms than smaller ones.

In order to better understand the difference in the PL recovery behavior between smaller and larger QDs, I made effort to obtain the XPS spectra on smaller and large QDs, respectively, for the QD samples just after water transfer and after the 3-month aging. Although it is difficult to separate the smaller ones from larger QDs due to the very good solubility of PbS/PMAO-PEG QDs in water, I tried to achieve it by using high-speed centrifugation with the help of tiny amounts of THF. The separation is not very complete; the portion consisting of mostly smaller QDs also contains some larger QDs and vice versa. Nonetheless, useful information can still be extracted from the high resolution Pb 4f XPS spectra taken on these two portions. The peaks at 137.7 eV and 142.5 eV for all the samples are assigned to the binding energy of Pb 4f $7/2$ and Pb 4f $5/2$ of PbS, respectively [51]; while two additional peaks appearing at 136.5 eV for Pb 4f $7/2$ and 141.3 eV for Pb 4f $5/2$ (Figure 5.7) are associated with the presence of unpassivated Pb atoms. Similar phenomenon has been observed in studies of bulk PbS, in which unpassivated S atoms show slightly negative surface core-level shifts [108]. These unpassivated Pb atoms, only observed for the QDs subject to water transfer, are highly

likely responsible for the observed PL drop in PbS QDs after water transfer.

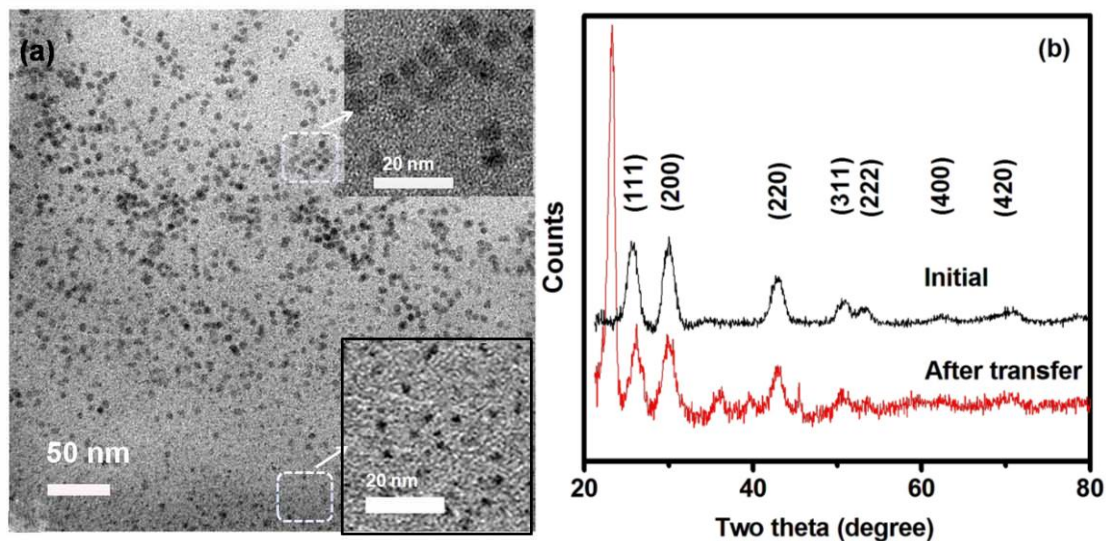


Figure 5.6 (a) Representative TEM photographs of PbS QDs stored at 4 °C for 3 months in water. (b) XRD of PbS QDs prior to water transfer and after being stored in water for 3 months. Inset of (a): enlarged TEM images of the larger and smaller QDs.

As shown in Figure 5.7, the percentage of unpassivated Pb atoms (estimated from the deconvoluted Pb 4f peak areas) from freshly transferred to three-month-aged samples varies in an opposite way in the smaller and larger QDs. The percentage of unpassivated Pb atoms of smaller QDs decreases from 21% to 9% after three-month aging; while that of larger ones increases from 7% to 11%. The significant decrease of unpassivated surface sites in the smaller QDs is a strong indication of the effective and beneficial surface re-structuring of these QDs during the aging and must be the main reason for their PL recovery. The improved surface state may arise from the surface transformation of smaller QDs themselves, thanks to their relatively high surface activity, or better passivation due to the improved organization of the ligands on the QD surface. In contrast, it seems very difficult to remove unpassivated surface states in larger QDs in the process of low-temperature aging. Moreover, more surface defects are introduced during the low-temperature

Ostwald growth. The increase of unpassivated surface atoms reasonably explains why the PL recovery behavior is absent in larger QDs stored in water.

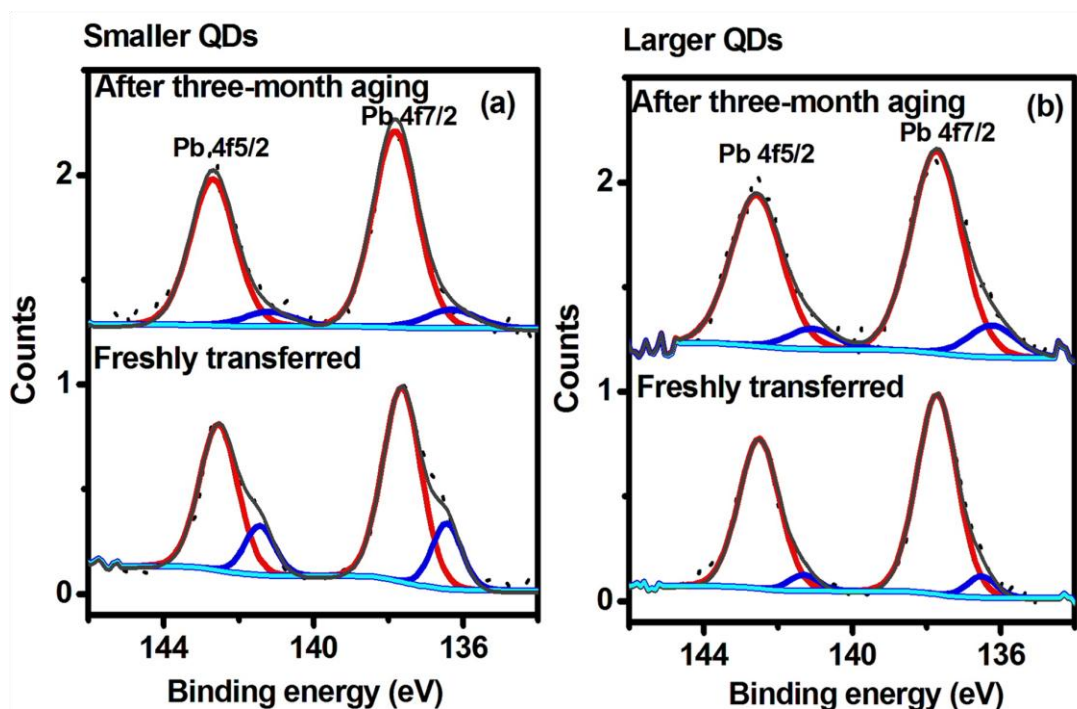


Figure 5.7 High resolution Pb 4f XPS spectra of smaller (a) and larger (b) PbS/PMAO-PEG QDs following transfer into water and after being stored in water at 4 °C for 3 months. The dots represent experimental data. The red and blue lines are fitting curves and the gray line is the sum of them. The light blue line is a background curve.

The automatic size-dependent recovery of PL was observed for the first time for PbS/PMAO-PEG QDs in water. The PL-recovered smaller PbS QDs are very stable in water for at least one year and show the QY of ~10%. However, this process is time-consuming and the final QY in water is not very high. The behavior of PbS QDs is very different from that of the UV-visible QDs which do not show any noticeable dependence on surface capping ligands during the water transfer process via amphiphilic polymer approach. Herein, the OLA ligands play a significant role on the variation of structure and optical properties of PbS QDs during the water transfer. Therefore, it is very interesting to investigate the effect of different capping ligands (OLA, OA and OA/TOP)

on the structural and optical properties of PbS QDs intending to achieve higher QY PbS QDs in water.

5.4 Ligands effect

In the following section, the PbS QDs capped by OLA, OA or OA/TOP ligands with similar PbS size were transferred into water via amphiphilic polymers (PMAO-PEG). I compared the variation of the structure and optical property of PbS QDs capped by OLA, OA or OA/TOP ligands (denoted as PbS-OLA, PbS-OA and PbS-OA/TOP) upon water transfer.

5.4.1 Synthesis of PbS QDs capped with different surface ligands

For the purpose of examining the effect of different capping ligands on the structural and optical properties of PbS QDs after they are transferred into water via PMAO-PEG, I have synthesized PbS-OLA, PbS-OA and PbS-OA/TOP QDs in the organic phase. As shown in Figure 5.8, XRD proves the crystalline nature of PbS and XPS confirms the co-presence of Pb and S. The size of PbS QDs capped by different types of surface ligands was estimated using the Scherrer formula [105]:

$$D = K\lambda/\beta\cos(\theta) \quad (5.2)$$

where D is the average crystallite size, λ is the X-ray wavelength, β is the width of a Bragg reflection in radians and θ is the diffraction angle. In my calculation, the K value of 0.90, as originally proposed by Scherrer, was applied. The calculated sizes are ~5.5, ~5.3 and ~5.4 nm for PbS-OLA, PbS-OA and PbS-OA/TOP QDs, respectively, all of which are reasonably close to those (PbS-OLA: 5.2 ± 0.2 nm; PbS-OA: 5.1 ± 0.2 nm; PbS-OA/TOP: 5.2 ± 0.3 nm) from TEM observations (Figure 5.9a-c). Despite these small discrepancies arising from different

characterization methods, the results strongly indicate that the as-prepared PbS QDs are single crystalline.

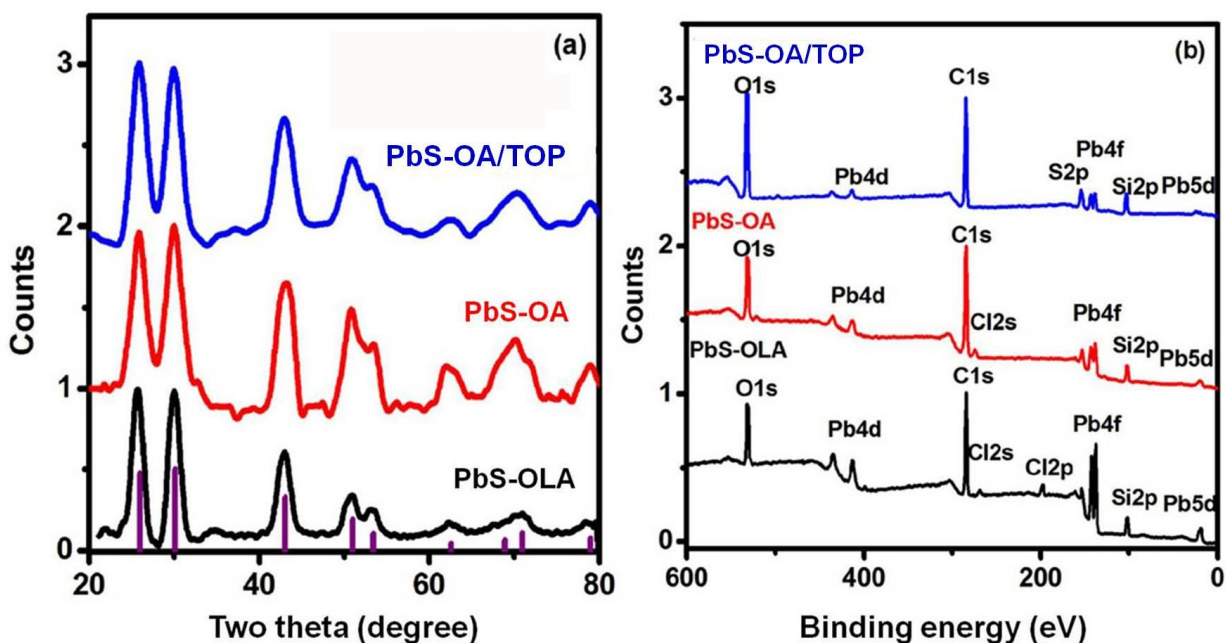


Figure 5.8 XRD (a) and XPS (b) spectra of PbS-OLA, PbS-OA and PbS-OA/TOP QDs. Data of the JCPDS card (05-0592) for PbS are also included for identification.

The hydrodynamic size of PbS QDs in chloroform, PMAO–PEG encapsulated QDs in chloroform and QDs after transfer into water was further characterized by dynamic light scattering. As shown in Figure 5.10, the diameter of PbS-OLA QDs is ~9 nm that is consistent with the TEM measurement considering the size of surface ligands (~2 nm for OLA). The addition of PMAO–PEG into chloroform leads to the hydrodynamic diameter increasing to ~16 nm, suggesting the formation of the polymer shell [59]. After water transfer, the hydrodynamic diameter of PbS-OLA QDs further increases to ~22 nm. The conformation and thus the size of polymer molecules in solution highly depends on the interaction between the polymer and solvent [109]. As the polarity of the solvent increases from chloroform to water, the interaction of the solvent with the end group,

PEG, of herein used amphiphilic polymers increases. As a result, the PEG groups in water quite possibly exhibit a more extended chain structure than those in chloroform. In addition, the increase in the interaction between the polymer and water and thus the higher solvation capacity of ligands may lead to stronger competition of water molecules as compared to the QD surface towards the polymer/ligand shell. Both of the above effects could contribute to the increase of the hydrodynamic diameter of PbS QDs after their transfer from chloroform into water.

The hydrodynamic size of PbS-OA or PbS-OA/TOP QDs exhibits the similar increase with the addition of polymers and with water transfer, which implies that these QDs have also been successfully encapsulated into the polymers. Although dynamic light scattering data serve as a good indicator for the polymer "shell" deposition, the variation of the PbS "core" size related to water transfer cannot be identified by this technique. TEM was further used to observe the actual size of PbS QDs themselves before and after water transfer. It was found that the polymer encapsulation process in chloroform does not affect the average size and size distribution of PbS QDs whatever their capping ligands. Nonetheless, the situation is quite different during the water transfer process; with the presence of different types of capping ligands, the QD size varies in a quite different way.

As I have already mentioned in Section 5.3, the size distribution of PbS-OLA QDs changes from a single (5.2 ± 0.2 nm) to double (5.6 ± 0.9 nm and 2.7 ± 0.4 nm) size distribution after transfer into water (Figure 5.9a and d). The etching of the QD surface by OLA seems to be significantly accelerated by the co-presence of polymers and water, and is stronger on slightly smaller QDs. As a result, efficient Ostwald ripening is initiated and eventually results in the two populations of QDs of distinctly different sizes. In stark contrast, PbS-OA or PbS-OA/TOP QDs can basically maintain their intactness and initial sizes (PbS-OA: from 5.1 ± 0.2 nm to 5.0 ± 0.1 nm; PbS-OA/TOP: from 5.2 ± 0.3 nm to 5.0 ± 0.2 nm) (Figure 5.9b versus 5.9e and 5.9c versus 5.9f).

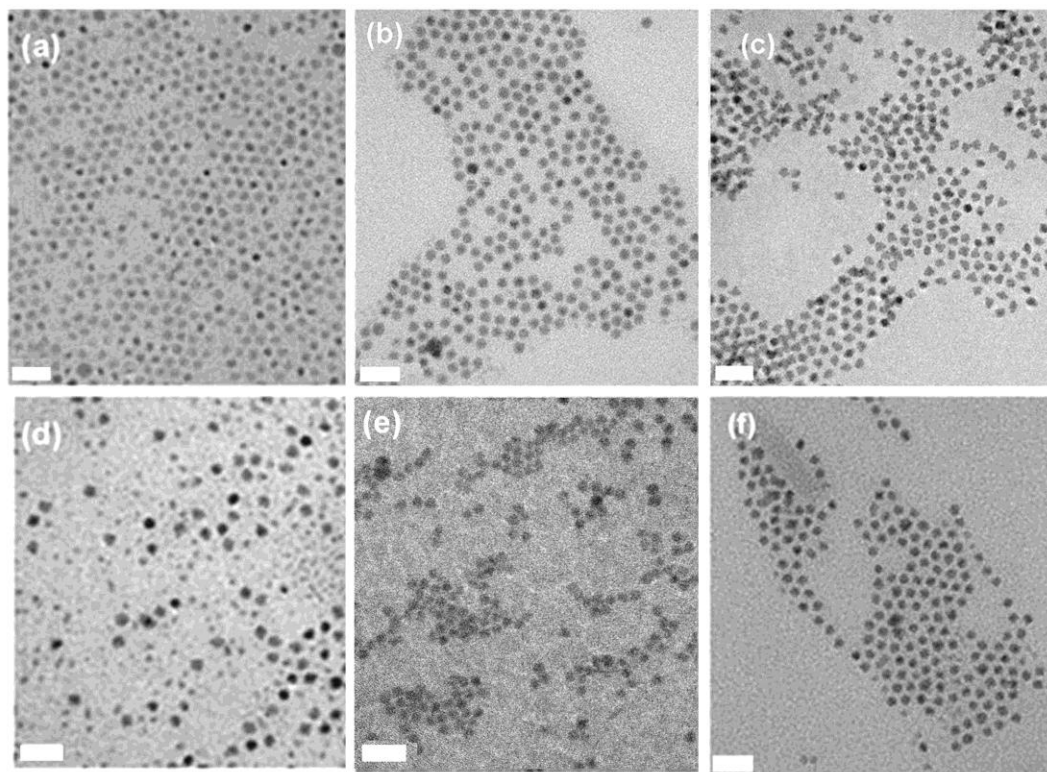


Figure 5.9 TEM images of (a,d) PbS-OLA, (b,e) PbS-OA and (c,f) PbS-OA/TOP QDs in chloroform (a, b, c) and after polymer encapsulation and transfer into water (d, e, f) via PMAO-PEG. Scale bar is 20 nm.

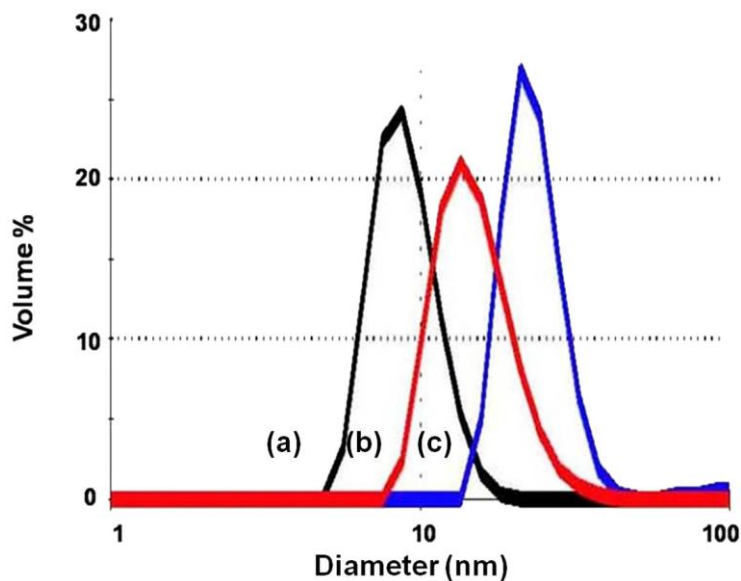


Figure 5.10 Hydrodynamic diameter of PbS-OLA QDs in chloroform (a), PMAO-PEG encapsulated PbS-OLA QDs before transfer in chloroform (b) and after transfer into water (c), measured by dynamic light scattering.

5.4.2 Ligand-dependent optical properties

Figure 5.11 shows the absorption spectra of PMAO–PEG encapsulated PbS QDs prepared in chloroform and after being transferred into water. The first exciton absorption peak of PbS-OLA QDs in chloroform is 1460 nm, 155 nm longer than that of PbS-OA QDs. As reported previously, even with the same size of 6 nm, the first exciton absorption peak of PbS-OLA QDs is situated at a wavelength of about 300 nm longer than that of PbS-OA QDs (1592 nm [32] versus ~1300 nm [31]). This may be partially related to the difference of surface capping ligands [110, 111]. Different synthesis approaches may be another reason [31, 32, 52]. The small difference in the first exciton absorption peak of PbS-OA QDs (1287 nm) and PbS-OA/TOP QDs (1301 nm) seems to mainly arise from the size dependence of optical band gaps in quantum-confined nanocrystals.

The PL spectra of PbS QDs prior to and following transfer into water via PMAO–PEG are also presented in Figure 5.11. The considerable broadening and red-shift of the PL band of PbS-OLA QDs after immediate water transfer (Figure 5.11, bottom) have been presented in section 5.2 [71]. The PL band of PbS-OA/TOP QDs shows a significant blue shift of 28 nm after transfer into water (Figure 5.11, top). The blue shift has often been explained from surface etching or surface oxidation [112, 113, 114]. As the blue shift was observed immediately after the QDs were transferred into water, while oxidation at room temperature may require longer time, I do not think the surface oxidation is a dominant factor for the observed spectral shift. The hypothesis is also supported by XPS results; no discernable signal from oxidation products was detected in the high resolution XPS spectrum of Pb 4f (Figure 5.12c), as discussed below. Furthermore, even under continuous, strong UV illumination which is normally believed to accelerate oxidation, no oxidation was observed for PbS QDs studied herein. It implies that the amphiphilic polymer can serve as a

barrier for retarding O₂ diffusion. The integration of all the above results provides a strong indication that it is the slight ligand etching, which could not even be ambiguously identified from TEM observations, that is responsible for the alteration of spectral characteristics of PbS-OA/TOP QDs. Clearly, the optical spectrum is more sensitive in mirroring the variation of QD size distribution. More interestingly, the FWHM of the PL peak becomes narrower (Table 5.1), indicating the narrowing of the size distribution after water transfer. Highly likely, the ligand etching in this sample starts with larger QDs or is at a higher rate for large QDs than smaller ones, resulting in the size focusing. This could happen when larger QDs have more surface defects than smaller ones since the etching of the surface is always faster at defective sites, as reported for gold nanoparticles [100].

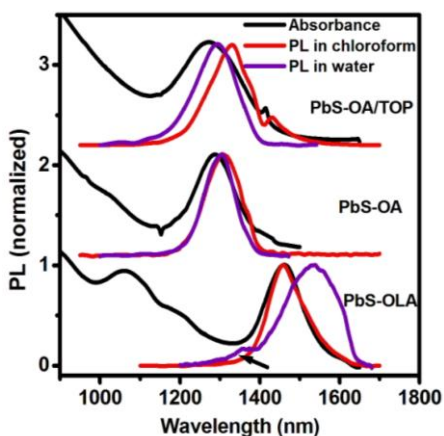


Figure 5.11 Absorption and PL spectra of PMAO–PEG encapsulated PbS QDs capped by different ligands (OLA, OA and OA/TOP) in chloroform prior to water transfer and PL spectra of QDs following transfer into water.

Table 5.1 PL maxima (λ_{em}), FWHM, lifetime (τ) and intensity variation (reflected by: PL intensity ratio = PL intensity after transfer into water/PL intensity before transfer) of PMAO–PEG encapsulated PbS QDs capped by different ligands before and after transfer into water. The fluorescence lifetime of PbS-OLA QDs in water cannot be measured due to the fast decay of PL.

	PbS-OLA		PbS-OA		PbS-OA/TOP	
Solution	chloroform	water	chloroform	water	chloroform	water
λ_{em}/nm	1480	1519	1305	1300	1339	1311
FWHM /nm	98	109	90	78	129	74
$\tau/\mu s$	0.60 ± 0.02	---	0.67 ± 0.01	0.37 ± 0.01	1.46 ± 0.08	0.72 ± 0.02
PL intensity ratio	$42 \pm 6\%$		$38 \pm 5\%$		$45 \pm 6\%$	

Among three samples, PbS-OA QDs seem to be most stable. There is only a 5-nm blue shift in their PL peak position and only trivial narrowing in their PL peak width at the side of longer wavelength after they are transferred into water (Figure 5.11, middle). These results imply that the etching effect is weakest for OA ligands and also highly likely the etching only takes place in larger QDs in this PbS-OA sample. Therefore, same as the PbS-OA/TOP QDs, larger ones of the PbS-OA QD sample are more fragile to ligand etching.

Surface etching of nanoparticles by different types of ligands has been reported recently [31, 100, 115]. For example, thiol ligands have been found to be capable of etching Au nanoparticles and thus changing their size distribution [100]. It has also been shown that trioctyl phosphine ligands can etch silver nanoparticles effectively [115]. For PbS QDs, amine ligands seem to have strong etching capacity [31]. These results clearly suggest different ligands can have different etching strength on different types of nanoparticles, likely depending on the interactions between specific ligands and nanoparticles under investigation. Although the exact mechanisms for the etching of PbS QDs by OLA, OA, or OA/TOP are still not clear at this stage, one thing is certain that OLA has much stronger etching capacity than both OA and TOP in my case. This closely contributes to the large variation in the structure and optical properties of PbS-OLA QDs upon water transfer.

Although the change of the size and steady-state PL spectra upon phase transfer differs largely among three samples, all of them exhibit a significant, similar decrease of ~60% in their PL intensity (Table 5.1). The immediate drop in the PL intensity following transfer may be explained from two aspects. One reason is that the transferred PbS QDs may have more un-passivated surface atoms introduced during the water transfer process. The other reason is that the ligand/polymer structure is not compact enough, rendering the QD surface accessible to external quenchers in water. This will be further discussed in Session 5.4.3.

With the same concentration, among three samples, PbS-OA/TOP QDs have the highest PL intensity in both chloroform and water, which is attributed to the passivation of both Pb and S sites by the use of two types of ligands [50]. Their PL intensity in water nearly doubles that of PbS-OLA and PbS-OA QDs, consistent with their doubly long lifetime (Table 5.1). Unlike PbS-OLA QDs, PbS-OA or PbS-OA/TOP QDs that are quite stable during the “dark” storage in water. I propose the much weaker ligand etching effect compared to OLA ligands, as supported by TEM observations and PL results, explains for their higher stability in water.

5.4.3 XPS characterization of PbS QDs

Peaks at 137.8 eV and 142.6 eV of PbS-OLA QDs before their transfer into water can be assigned to the binding energy of Pb 4f $7/2$ and Pb 4f $5/2$, respectively [51] (Figure 5.12a). Two additional components appearing at 136.5 eV for Pb 4f $7/2$ and 141.4 eV for Pb 4f $5/2$ after water transfer can be ascribed to the presence of unpassivated Pb atoms on the QD surface. As the PL property is highly sensitive to the surface defects, it can be reasonably concluded that it is the presence of these unpassivated Pb atoms that are primarily responsible for the PL quenching of QDs in water. This has indeed been supported by my PL studies of PMAO–PEG encapsulated PbS-OLA QDs in different environments in Section 5.2.

The high resolution XPS spectra of PbS-OA QDs collected from chloroform (Figure 5.12b) not only show the Pb 4f peaks from the Pb-S bond, but also show Pb 4f peaks from Pb atoms bonded to OA ligands at 139.0 eV and 143.8 eV [51, 116]. For water transferred QDs, the primary Pb 4f peaks (Figure 5.12b) still have double components, corresponding to Pb-S and Pb-OA bonds, respectively. Nonetheless, no lower binding energy peaks, as those observed for water-soluble PbS-OLA QDs, appear or they are below the detection limit. Similar results were

obtained for PbS-OA/TOP QDs as shown in Figure 5.12c. It strongly indicates that the water transfer process does not introduce detectable amounts of unpassivated Pb atoms in both PbS-OA and PbS-OA/TOP QDs. Therefore, the drop in PL of PbS-OA and PbS-OA/TOP QDs after water transfer is believed to be mainly due to the quenching effect by external quenchers present in water.

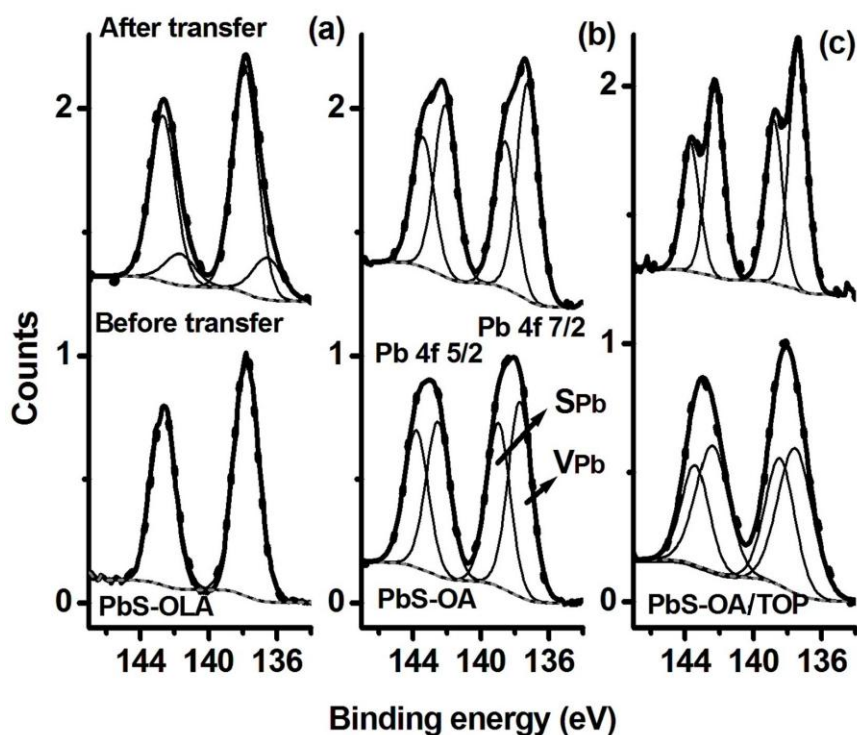


Figure 5.12 High resolution XPS spectra of Pb 4f in PbS capped by OLA (a), OA (b) and OA/TOP (c) ligands before and after transfer into water via PMAO-PEG. The dots represent experimental data. The thin lines are fitting curves and the thick line is the sum of them. The dash line is a background curve. S_{Pb} represents surface Pb atoms bonded with OA ligands and V_{Pb} the Pb atoms in the interior of QDs.

5.4.4 Photostability of PbS QDs

The photostability of freshly prepared water-soluble PbS QDs was studied and compared with that of initial polymer-encapsulated PbS QDs dispersed in chloroform by monitoring the evolution of their PL spectra under continuous UV irradiation up to 4 hours. As shown in Figure

5.13a and b, after 4 hours UV irradiation, the PL intensity of PbS-OA or PbS-OA/TOP QDs in water drops to 58% of its initial value. In large contrast, PbS-OLA QDs in water totally lose their PL just after 60 seconds of illumination (Figure 5.13b). It is straightforward that although the photostability of the PbS-OLA QDs is already worse than that of PbS-OA or PbS-OA/TOP QDs in chloroform (Figure 5.13b), the difference becomes more remarkable once they are transferred into water. In other words, the complicated interactions among water molecules, polymers, QD surfaces and different types of capping ligands significantly enlarge the difference in the PL decay behavior of differently capped QDs in water.

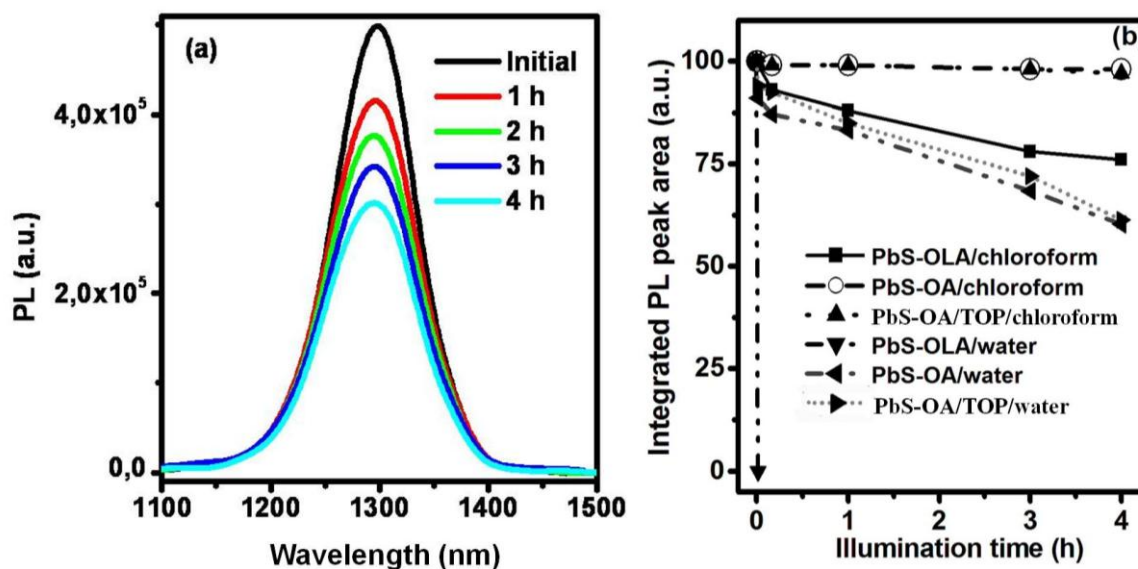


Figure 5.13 PL spectra of freshly prepared PMAO–PEG encapsulated PbS-OA QDs in water (a) and integrated PL intensity of freshly prepared PMAO–PEG encapsulated PbS QDs capped by different types of capping ligands (b) subject to UV illumination for different time. The quickly drop in PL intensity of PbS-OLA in water occurs within 1 minute.

Normally the surface oxidation is a major reason leading to the decrease of PL intensity for QDs upon illumination [112, 113]. Photo-accelerated ligand etching may be another reason [116]. Both processes lead to the reduction of the “effective” size of PbS. Therefore, they can be indirectly

yet sensitively mirrored from the blue shift in PL spectra [111, 113, 117]. In the present study, I did not notice any significant blue shift of the PL peak of the polymer encapsulated PbS-OA or PbS-OA/TOP QDs in water. This basically excludes the possibility of photooxidation and photo-accelerated ligand etching during this period and hence, neither of them is primarily responsible for the observed PL loss. This deduction is further supported by the observation that the PL of UV illuminated PbS QDs in water is recoverable by keeping the samples in dark at 4 °C for one day; it is known that the photooxidation and photo-accelerated ligand etching are irreversible processes and will cause the permanent loss of PL. I therefore infer that the temporary PL loss in the PbS-OA or PbS-OA/TOP QDs dispersed in water upon illumination is mainly attributed to the quenching event at unpassivated surface sites generated temporarily by photo-induced ligand desorption. Stouwdam *et al* reported that a strong 450 W xenon arc lamp can cause the ligand desorption from PbSe or PbSe/PbS core/shell QDs, and thus degrading their PL [106]. I believe that the similar photo-accelerated ligand desorption mechanism is dominating here. Nonetheless, unlike their QDs which are only stabilized by OA, no precipitation was found for the herein studied PbS-OA or PbS-OA/TOP QDs highly likely due to the stabilization effect of amphiphilic polymers. Similarly, the rapid PL decay of PbS-OLA QDs in water is attributed to the fast generation of many more uncapped surface atoms under UV illumination [116]. But in this case, it is not possible to follow their spectra evolution longer than 1 minute as they become dark shortly within 1 minute. In short, although the PL intensity decay of herein prepared water soluble QDs is faster than corresponding QDs in chloroform, the use of amphiphilic polymers helps retard the photooxidation of QDs under UV illumination.

5.5 Summary

In this chapter, the water-soluble PbS QDs capped by OLA were achieved by transferring monodispersed QDs from chloroform into water via PMAO–PEG. The water transfer process leads to a double size distribution (5.6 ± 0.9 nm and 2.7 ± 0.4 nm) together with the rapid disappearance of PL, due to severe ligand etching enhanced by the co-presence of water and amphiphilic polymers and thereby initiated Ostwald ripening. The PL of PbS QDs, however, can recover automatically after the storage in the dark for 3 months. The recovery behavior is found to be quite different for the smaller and larger QDs in the same sample and the primary reason consists in the difference in the variation of their surface defect states during the aging process. The effective removal of surface defect states, as evidenced by the decrease of unpassivated surface atoms from XPS studies, is a dominant factor for the observed PL recovery in the smaller QDs. In contrast, the increase of the surface defects, which are introduced during the Ostwald growth (started immediately after water transfer and continued during the low-temperature aging) and not able to be efficiently annealed out, of larger QDs is mainly responsible for their non-recovery behavior in water. The water-soluble PL-recovered PbS QDs show the minimum QY of 10%.

Furthermore, PbS QDs capped by OA or OA/TOP ligands were transferred from an organic solvent into water via amphiphilic polymer. The structure and optical properties of amphiphilic polymer-encapsulated PbS QDs after water transfer are found to highly depend on the type of initial capping ligands (OLA, OA or OA/TOP). Among all three samples in water, the PbS-OA/TOP QDs show the highest PL efficiency. As for photostability under continuous illumination, the PbS-OA and PbS-OA/TOP QDs are much better than that of the PbS-OLA QDs. It is worth noting that although the PL intensity decay of all water soluble QDs is faster than that of corresponding QDs in chloroform, the photo-induced oxidation and/or ligand etching is significantly postponed if not

eliminated due to the presence of the polymer shell in water-soluble QDs. Taking all results into consideration, PbS-OA/TOP QDs show the optimal property, with the highest QY of 20 % and good photostability.

It is still highly desirable to further improve the property of PbS QDs in water. In next chapter, I will transfer the PbS/CdS QDs into water.

Chapter 6

Synthesis and characterization of water-soluble PbS/CdS QDs

In this chapter PbS/CdS QDs will be transferred into water via the amphiphilic polymer approach [73, 74]. Firstly, a protective “shell” of the more stable material of CdS will be synthesized on the PbS QD surface and then the core/shell structured PbS/CdS QDs will be transferred into water via amphiphilic polymers. The method yields the PbS/CdS core/shell QDs with by far the best properties in water. The CdS shell around the PbS core can maintain the structural integrity and leads to high QY of the PbS/CdS QDs in buffer.

Further improvement may be made by optimizing core/shell structures. It is thus very important to study and understand the effect of CdS shell thickness on the properties of water-soluble amphiphilic polymer encapsulated PbS/CdS QDs. I firstly synthesized PbS/CdS QDs with similar core size and tunable CdS shell thickness and then transferred them from organic phase into water via amphiphilic polymers. It was found that the PbS/CdS QDs show the maximum QY of 33% when the shell thickness is around 0.7 nm. Further preparation of a series of core/shell samples with different core size and shell thickness confirms that ~ 0.7 nm is an optimal shell thickness for various core sizes investigated herein, consistently yielding the maximum QY and reasonably good photostability.

6.1 Synthesis of water-soluble PbS/CdS QDs

In Chapter 5, I have prepared water-soluble PbS QDs by transferring them from an organic phase into water via the amphiphilic polymer encapsulation approach. It was found that this method is not universal for all types of ligands [72]. In the case of OA or OA/TOP ligands, the amphiphilic polymer approach can largely keep them on the PbS QD surface during the water transfer process [72]. However, when OLA ligands are used, severe ligand etching takes place, which initiates Ostwald ripening and together they lead to significantly decreased QY and very poor photostability along with the remarkable broadening of size distribution [71, 72]. Since the CdS shell can give more surface protection to the core, I therefore, developed a novel two-step approach (PbS/CdS QDs were firstly synthesized via the cation exchange method, and then transferred into water via amphiphilic polymers). The as-synthesized water-soluble PbS/CdS QDs show a higher QY and better photostability in PBS buffer as compared with water-soluble PbS QDs described in Chapter 5.

The as-synthesized PbS/CdS QDs have a comparatively small hydrodynamic size (~22 nm in diameter, Figure 6.1). Figure 6.2 shows TEM image of PbS/CdS QDs before and after water transfer. Clearly, with the core/shell strategy, the QDs can maintain the intactness of PbS QDs after water transfer. Because CdS has a better resistance to the aqueous environment and can significantly decrease (if not eliminate) the core-environment interactions, the integrity of PbS structure after transfer into water is kept (5.0 ± 0.3 nm versus 5.0 ± 0.3 nm, Figure 6.3).

Figure 6.4 reports the PL and absorption spectra for the PbS/CdS QDs prior to and after transfer into water via PMAO-PEG. For this specific sample, the formation of the CdS shell nearly doubles the QY of PbS QDs in chloroform, up to 53%, possibly due to better surface passivation. After transfer into water, the QY of PbS/CdS QDs has a 43% decrease.

Nonetheless, since the absolute value of initial QY for PbS/CdS QDs in chloroform is almost twice that for the non-shelled PbS QDs, the retained QY value for PbS/CdS QDs after transfer into water is still as high as 30%, which has high relevance to biological applications.

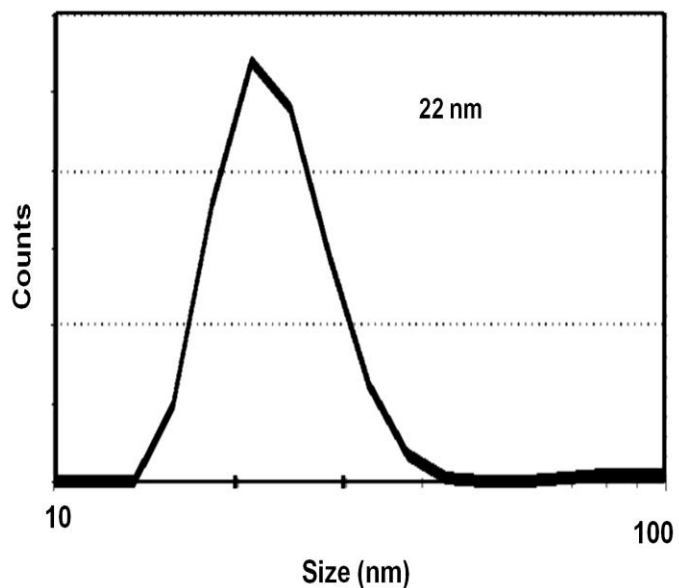


Figure 6.1 Dynamic light scattering measurement of the hydrodynamic radius of PbS/CdS QDs in water (average hydrodynamic size is ~22 nm).

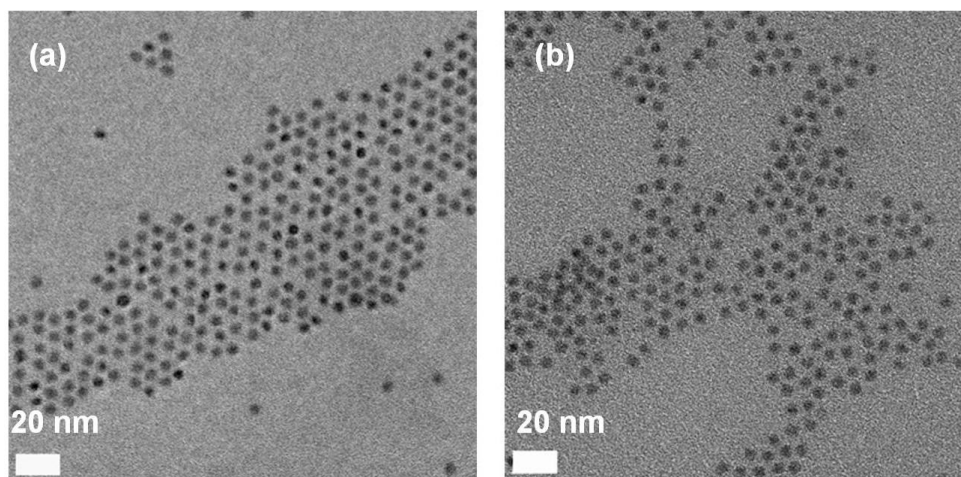


Figure 6.2 Representative TEM images of (a) PbS/CdS QDs before transfer, and (b) PbS/CdS QDs following transfer into water.

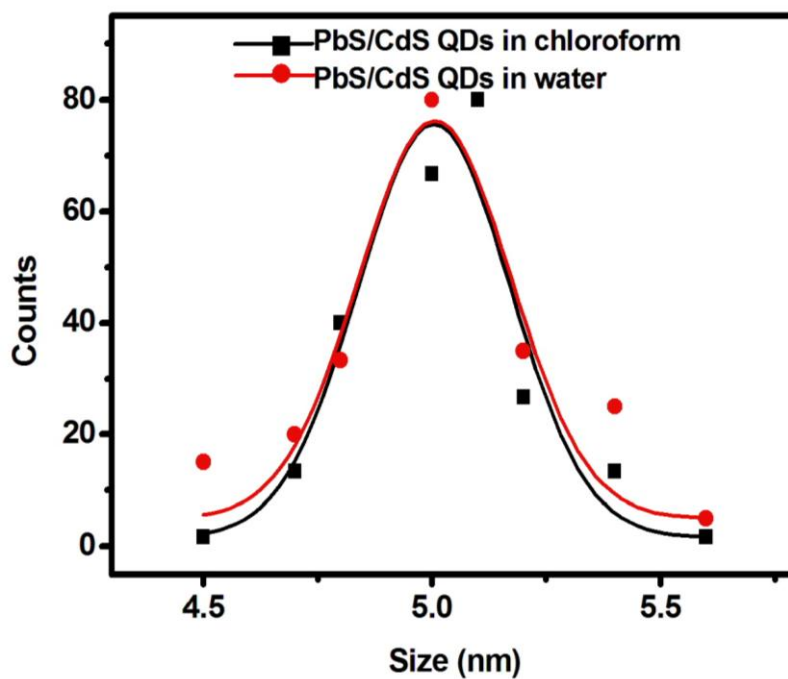


Figure 6.3 Size distribution of PbS/CdS QDs in chloroform (5.0 ± 0.3 nm) and in water (5.0 ± 0.3 nm).

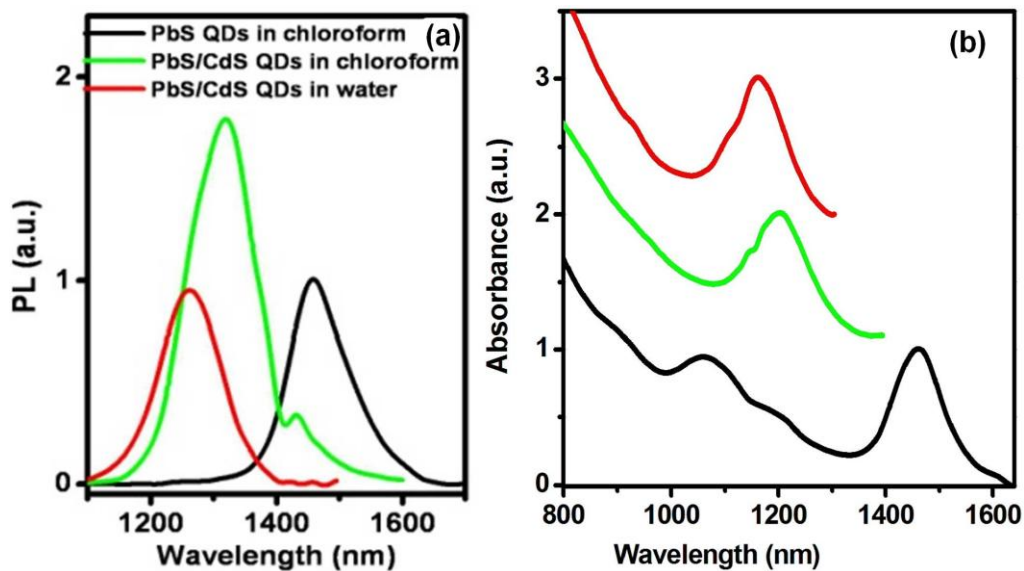


Figure 6.4 PL (a) and absorption (b) spectra of PbS, and PbS covered by a CdS shell before and after transfer into water using PMAO-PEG. Absorption curves correspond to emission curves of the same color.

Actually, the QY value of PbS/CdS QDs in water is even higher than that of the initial PbS QDs in chloroform, which represents an important improvement, as it is known that normally the water transferred QDs only keep 30 ~ 60% of the initial QY of QDs in an organic phase [57]. This is consistent with lifetime results: a slightly longer PL lifetime has been observed for PbS/CdS in water ($0.78 \pm 0.01 \mu\text{s}$) than PbS in chloroform ($0.60 \pm 0.03 \mu\text{s}$). Clearly, it is the additional core/shell formation process that aids in the formation of high QY water-soluble QDs. More importantly, the PL of PbS/CdS QDs stored in PBS buffer is quite stable. The PL band width of PbS/CdS QDs remains unchanged after transfer into water, suggesting that the narrow size distribution of PbS cores is retained. The blue-shift (37 nm) of absorption peak is apparently due to the slight decrease of the PbS core size (Figure 6.4b) [101].

In order to understand the decrease of QY of PbS/CdS QDs after their transfer into water, I have utilized XPS to characterize the effect of different media on the chemical bond status of QDs. The high resolution spectrum of Pb 4f in PbS/CdS QDs collected from chloroform (Figure 6.5) shows not only the peaks from the Pb-S bond, but also the peaks from the lead carboxylate at 139.2 eV for Pb 4f 7/2 and 144.0 eV for Pb 4f 5/2 which are formed during the reaction process [51]. After transfer into water, the primary Pb 4f and Cd 3d (Figure 6.6) do not show any significant change. However, the higher binding energy peaks of Pb 4f totally disappear, while the lower binding energy peaks similar to those for water-soluble PbS QDs appear at a lower intensity (chapter 5, Figure 5.12). These phenomena possibly imply the existence of a small amount of Pb dangling bonds transformed from the lead carboxylate due to the core-ligand-environment interactions. In other words, some of PbS/CdS QDs might have an incomplete CdS shell on the PbS surface. I think that these unpassivated Pb atoms account for the reduction of QY of the PbS/CdS QDs following their transfer into water.

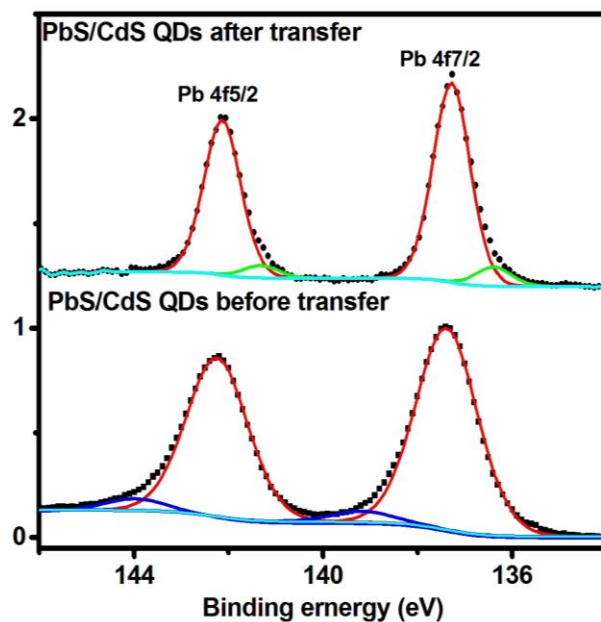


Figure 6.5 High resolution XPS spectra of Pb 4f of PbS/CdS QDs before and after transfer into water via PMAO-PEG. The black dot represents experimental data. The red, blue and green lines are fitting curves. The light blue line is a background curve.

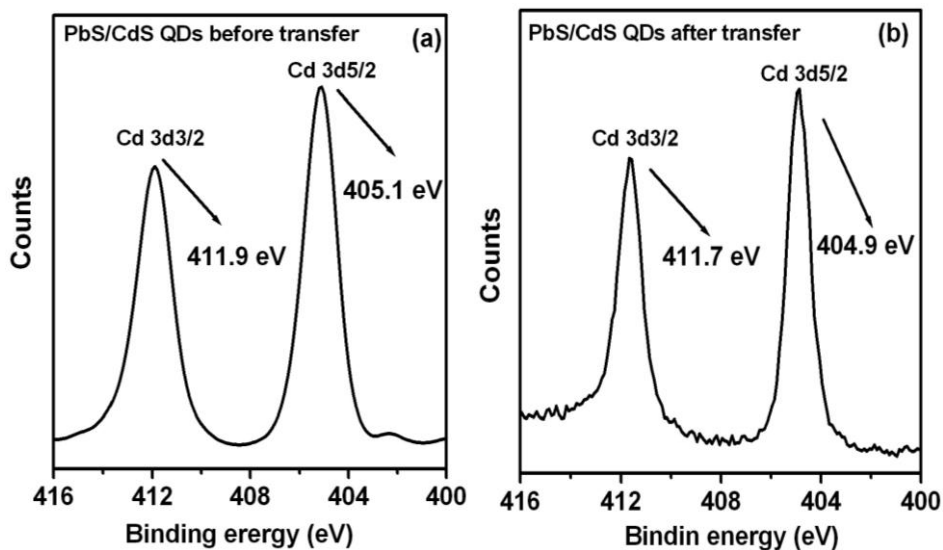


Figure 6.6 High resolution XPS spectra of Cd 3d in PbS/CdS before and after transfer into water via PMAO-PEG, indicating the CdS shell is stable during the transfer process.

Although the highest ever a high QY and good photostability have been achieved for PbS QDs dispersed in buffer, it is not clear whether and how the optical properties of PbS nanocrystals vary with the thickness of the inorganic passivating CdS shell during the water transfer process and how we can optimize these properties. In order to address these questions, the controlled synthesis of the CdS shell with varying thickness is of great importance. In the next section, I will investigate the effect of CdS shell thickness on the optical properties of PbS core QDs during water transfer process in order to choose the optimal shell thickness and achieve the best quality of water-soluble PbS/CdS QDs by this two-step approach.

6.2 CdS shell thickness effect

6.2.1 PbS/CdS core/shell QDs in an organic phase

In order to fairly investigate the effect of CdS shell thickness on the optical properties of water-soluble PbS QDs, PbS nanocrystal size has to be the same or similar for all the samples under comparison. It is known that the injection of the precursors of both shell components (such as Cd and S for CdS or Zn and S for ZnS) into a dispersion containing pre-synthesized nanocrystals, *e.g.*, CdSe, will not change the CdSe size and can give rise to the core/shell structured visible-emitting QDs (CdSe/CdS or CdSe/ZnS) whose shell thickness can be simply tuned by varying reaction time [65, 66]. However, in the cation exchange approach, only the precursor of cationic constituent of the shell material is introduced and the formation of the shell proceeds through the cationic replacement of the core material. As a consequence, this method leads to the simultaneous change of the core size during the shell formation process. Specifically, for PbS/CdS QDs, the addition of Cd-oleate causes the gradual replacement of Pb by Cd, which reacts with S to form the CdS shell accompanied by the decrease of the PbS core size [60, 88]. It thus requires more experimental control to achieve

QDs of the same PbS core size yet adjustable CdS shell thickness via the cation exchange approach. To this end, shell-free PbS QDs with tunable sizes (4 to 10 nm in diameter) were firstly synthesized [32, 68]. Then, by using PbS QDs of different initial sizes and by carefully varying the reaction parameters (Pb-to-Cd ratio, reaction time and reaction temperature), I successfully synthesized the PbS/CdS QDs with similar core sizes and different shell thickness, which were confirmed by their PL and absorption spectra. In the following, I denote the “bare” PbS QDs with starting sizes of 4.9 nm, 5.2 nm, 5.6 nm, 5.9 nm, 6.1 nm, 6.5 nm and 10 nm as PbS#1, PbS#2, PbS#3, PbS#4, PbS#5, PbS#6 and PbS#7, respectively and their corresponding core/shell structures after cation exchange as PbS/CdS#1, PbS/CdS#2, PbS/CdS#3, PbS/CdS#4, PbS/CdS#5, PbS/CdS#6 and PbS/CdS#7, respectively. The absorption peak positions of initial, shell free PbS#1-6 are in a broad range of 1361 to 1620 nm and are all blue shifted to a narrow range of 1272 ~ 1256 nm after cation exchange at different conditions which have been carefully tuned (Table 6.1 and 6.2). Representative absorption spectra can be found in Figure 6.7a. Different from others, the excitonic absorption peak, disappears, however, when PbS#7 is transformed into PbS/CdS#7. As reported previously, thick-shell lead chalcogenide QDs, formed by the cation exchange, may exhibit large core heterogeneity, even though initial lead chalcogenide nanocrystals show a narrow size distribution [88]. Such heterogeneity, or the broadening of the core size distribution, is believed to be the reason for the absence of the distinct absorption peak in PbS/CdS#7, which has a much thicker shell than all other samples. Consistently, blue shift in PL spectra was directly observed for all the samples, except for #6 and #7, after the cation exchange process (Table 6.1 and 6.2). Representative PL spectra can be found in Figure 6.7b. It is because that before the shell deposition, PbS#6 and PbS#7 emit at longer wavelengths than those can be detected by our NIR detector (up to 1700 nm). The observed blue shifts of both absorption and PL peaks after cation exchange are closely related to the shrinking of the PbS core size resulting from sacrificial replacement of lead with cadmium, which leads to the

formation of the CdS shell [60]. Since the size of PbS QDs correlates very well with their absorption and PL peak positions [86], similar absorption and PL peak positions for all the core/shell samples strongly indicate that they have the similar core sizes. Moreover, these peak positions can be used to estimate the average size of the “bare” PbS QDs or core PbS QDs [70]. As shown in Table 6.1, the estimated PbS sizes by absorption peak positions are same or quite close to those directly measured by TEM. As the overall size of PbS/CdS QDs can be measured by TEM and the average core size can be estimated from the absorption spectra, the average thickness of the CdS shell can be straightforwardly calculated.

Table 6.1 Initial PbS size based on TEM observations, PbS size estimated from absorption peak positions [86], absorption maxima (λ_{abs}), and PL maxima (λ_{em}) of PbS QDs dispersed in chloroform. PL peak positions of PbS#6-7 cannot be measured due to the limitation of our NIR detector.

Samples	Size (nm)	Estimated Size (nm)	λ_{abs} (nm)	λ_{em} (nm)
PbS#1	4.9	5.0	1361	1388
PbS#2	5.2	5.2	1414	1441
PbS#3	5.6	5.7	1496	1522
PbS#4	5.9	5.9	1538	1551
PbS#5	6.1	6.2	1580	1600
PbS#6	6.5	6.5	1620	-----
PbS#7	10.0	9.7	1980	-----

Table 6.2 The overall size of PbS/CdS QDs based on TEM observations, estimated core size and shell thickness from methods #1 and #2, absorption maxima (λ_{abs}), PL maxima (λ_{em}), PL FWHM and QY for PbS/CdS QDs in chloroform. Method#1: core size estimated from absorption peak positions and shell thickness calculated by: *overall size – core size*; Method#2: core size and shell thickness estimated from Cd/Pb ratios determined by ICP-OES measurements and overall sizes by TEM [70].

Samples	Size (nm)	Estimated Core/Shell Size (nm)				λ_{abs} (nm)	λ_{em} (nm)	FWHM (nm)	QY (%)
		Method#1		Method#2					
		Core	Shell	Core	Shell				
PbS/CdS#1	4.9	4.5	0.2	4.5	0.2	1272	1320	109	44
PbS/CdS#2	5.2	4.5	0.4	4.4	0.4	1272	1317	114	49
PbS/CdS#3	5.6	4.5	0.6	4.5	0.6	1275	1314	116	54
PbS/CdS#4	5.9	4.5	0.7	4.5	0.7	1276	1319	99	67
PbS/CdS#5	6.1	4.5	0.8	4.5	0.8	1265	1321	130	53
PbS/CdS#6	6.5	4.5	1.0	4.5	1.0	1256	1318	195	40
PbS/CdS#7	9.0	-----	-----	4.4	2.3	-----	1320	196	3

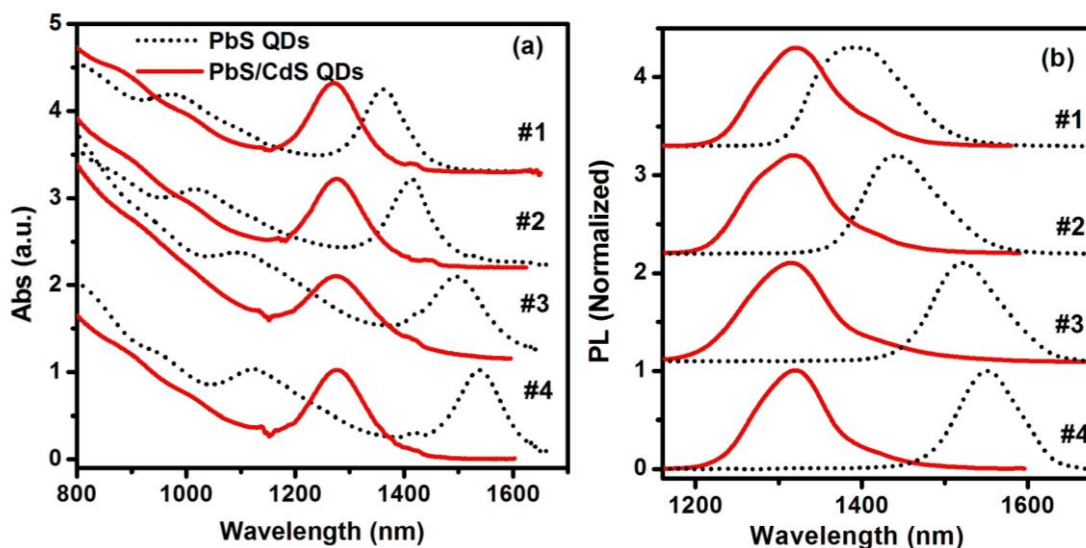


Figure 6.7 Absorption (a) and PL (b) spectra of initial PbS QDs (dot) and PbS/CdS QDs (line) dispersed in chloroform.

As shown in Figure 6.8, as-synthesized PbS/CdS QDs show a uniform size distribution. Table 6.2 lists the average overall size found from TEM as well as, the estimated average core size and shell thickness from absorption peak positions (Method 1) for all the core/shell samples, except for PbS/CdS#7. Due to the absence of the absorption peak in this sample, its core size and thus the shell thickness cannot be estimated by this method. We therefore used another technique (Method 2) to estimate the core size and shell thickness of the core/shell samples. In the method 2, we calculated the shell thickness according to the Pb-to-Cd ratio from ICP-OES measurements and the total dimension of QDs from TEM observations [60, 70]. In the calculation, it was assumed that all QDs are spherical and contain a uniform, pure CdS shell [70]. Such estimated core size and shell thickness are also included in Table 6.2. The PbS core sizes are similar, around 4.4 ~ 4.5 nm and the average thickness of shell varies from 0.2 to 2.3 nm that are in good agreement with those obtained from Method 1. As for PbS/CdS#7, the calculated average core size is comparable to that of all

other core/shell samples. Regardless of the broad core size distribution of this sample, it should be still valid for comparing it with other samples to examine the effect of shell thickness.

It is worth pointing out that all core/shell QDs in an organic phase exhibit a uniform, overall size distribution, as shown in Figure 6.8a. The lattice fringes of PbS cores can be observed in a high-resolution TEM image (Figure 6.8b). In addition, the core/shell QD samples show similar overall sizes to their respective, initial QDs before cation exchange based on TEM observations (Table 6.1 and 6.2), suggesting that the cation exchange approach does not affect the overall dimension of QDs [70].

The QY of PbS/CdS QDs increases with the increase of CdS shell thickness, approaching a maximum value of 67% at 0.7 nm (Table 6.2). This increase is attributed to steadily improved surface passivation with increasing shell thickness [60]. Further increase of the shell thickness, however, causes the decrease of the QY instead. It drops to as low as 3% at the shell thickness of 2.3 nm. This pronounced reduction is associated with the formation of new defects within the CdS shell. It is known that as the shell thickness reaches a critical value, the strain due to the lattice mismatch between CdS and PbS could lead to the formation of defects, resulting in the decrease of QY. Similar trend has been reported for CdSe/CdS and PbSe/CdSe core/shell QDs [60, 61]. As I reported in reference 70, the crystal structure of CdS is zinc blende. The shell thickness of ~ 0.7 nm thus corresponds to 1.7 monolayers of CdS on the PbS surface along the <001> direction. It is clear that 1-2 layers of CdS can offer the optimal surface passivation for PbS cores. This finding is in accord with that reported for PbSe/CdSe QDs or CdSe/ZnS QDs [57, 60].

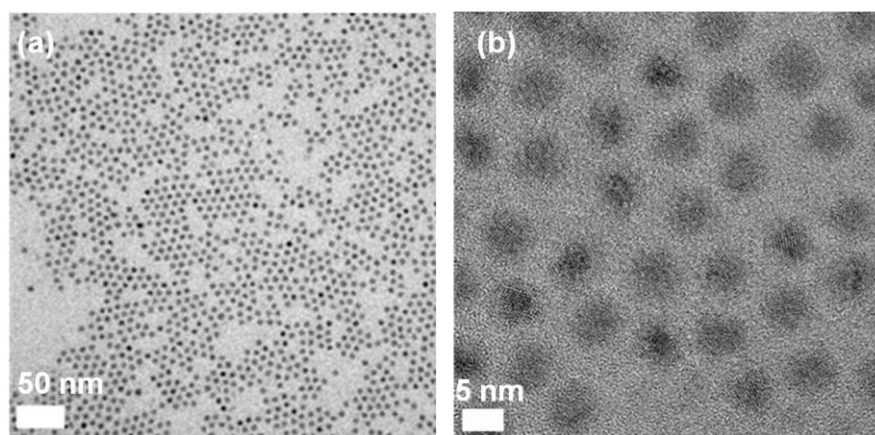


Figure 6.8 (a) Typical TEM image of PbS/CdS QDs synthesized at 100 °C for 4 hours with initial PbS size of 5.2 nm. (b) High resolution TEM image of (a).

In Section 6.2.1, by using cation exchange method, I have successfully synthesized PbS/CdS core/shell QDs with similar core size (4.4 ~ 4.5 nm) and tunable CdS shell thickness in the range from 0.2 nm to 2.3 nm in the organic phase. In the following Section (6.2.2), I will transfer them from organic phase into water via amphiphilic polymer and investigate the shell thickness effects on the optical properties of QDs during water transfer process.

6.2.2 PbS/CdS core/shell QDs transferred into water

The PbS/CdS QDs with similar core size and varying shell thickness were transferred into water via PMAO-PEG [74]. Representative TEM images of core/shell samples (PbS/CdS#1 to PbS/CdS#3) are shown in Figure 6.9. It was found that before and after water transfer the overall QD size and morphology remain same, suggesting that the QD structure in all the samples is essentially maintained during the water transfer process. This is in clear contrast to what observed for the “bare” QDs capped solely by OLA ligands [72], and is largely attributed to the structural stability of the CdS shell. The presence of the CdS shell is also expected to decrease the core-environment interactions, the extent of which depends on its compactness and thickness.

6.2.2.1 Variation of optical properties with water transfer

The absorption and PL spectra of the core/shell QDs after water transfer are shown in Figure 6.10. It can be seen that PbS/CdS#1-5 after transfer into water still show a remarkable absorption peak, however, the absorption peak completely disappears for PbS/CdS#6, which has an estimated shell thickness of about 1 nm. This change should not be related to the variation of the QD structure, instead, quite likely, it is due to the variation of immediate environments [118]. This environmental effect is believed to be more dramatic for QDs with a broader size distribution. As mentioned above, thicker-shell samples show broader core size distribution. Therefore, PbS nanocrystals in PbS/CdS#6 are expected to be less uniform than those in PbS/CdS#1-5. Same as in an organic phase, PbS/CdS#7 in water shows no characteristic absorption, due to relatively large distribution of its core size. Meanwhile, the absorption spectra for PbS/CdS#1-5 show clear blue shifts following their transfer into water. Similar blue shifts in the PL spectra were observed for all samples (Figure 6.10). Such blue shifts are a strong indication of ligand etching [73], which will be further discussed in the next section.

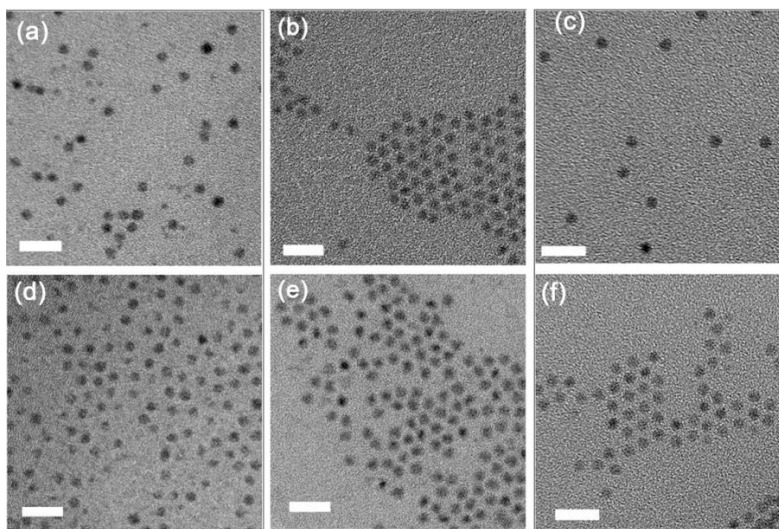


Figure 6.9 TEM images of PbS/CdS#1 (a, d), PbS/CdS#2 (b,e) and PbS/CdS#3 (c,f) before polymer encapsulation in chloroform (a, b, c) and after transfer into water (d, e, f) via PMAO-PEG. Scale bar is 20 nm.

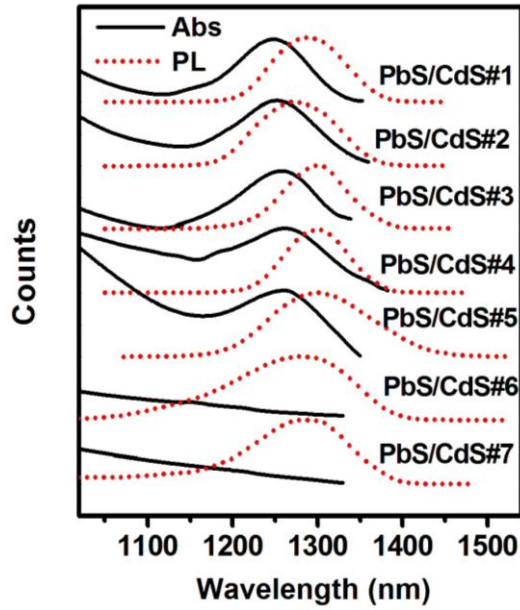


Figure 6.10 PL and absorption spectra of PbS/CdS QDs after transfer into water via PMAO–PEG.

As shown in Figure 6.11, PbS/CdS QDs show the similar trend in the variation of QYs with varying CdS shell thickness when they are transferred from chloroform into water. At the CdS shell thickness of ~ 0.7 nm, PbS/CdS QDs in water show the maximum QY of $\sim 33\%$, indicating again that the CdS shell at this thickness offers the optimal surface passivation for PbS cores.

Although it is clear that a thicker shell (> 1 nm) causes the significant drop of QYs due to the introduction of defects as already discussed above, it is unclear at which thickness the CdS shell can provide the sufficient protection to the PbS core against the change of its surroundings. Aiming to answering this question, we calculated the variation of QYs with water transfer according to the following equation:

$$QY \text{ variation} = (QY_{chloroform} - QY_{water}) / QY_{chloroform} \quad (6.1)$$

where $QY_{chloroform}$ is the QY of QDs before transfer in chloroform and QY_{water} is the QY of QDs after transfer into water. As shown in Figure 6.12, as the CdS shell thickness increases, the variation of QYs decreases monotonically from 58% to 42%. It is known that the decrease in QYs is related to the formation of new defects during water transfer [73]. Ligand etching accelerated in aqueous environments, has been considered as one of the main processes that introduce defects to polymer encapsulated PbS QDs [72, 73]. As the ligand etching only leads to a very small decrease of PbS core size, it is not possible to observe such a decrease directly by TEM. Nonetheless, the delicate variation of PbS core size after water transfer can be reflected from their optical spectra. Figure 6.12 plots the shift of absorption peaks of the samples with water transfer. The shift becomes smaller with increasing shell thickness. When the shell thickness is at 0.8 nm, the peak shift is already as small as 5 nm. Even though the absorption peak shift cannot be measured when the CdS shell thickness exceeds 0.8 nm due to the lack of characteristic excitonic absorption peaks for thick-shell samples, we expect that their absorption features will not be considerably affected by water transfer, based on the trend of my data.

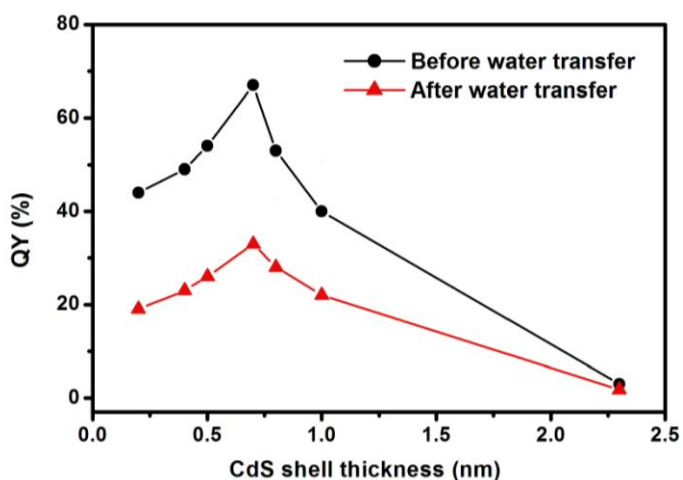


Figure 6.11 The QY of PbS/CdS QDs before and after water transfer as a function of CdS shell thickness. The solid lines are guides to the eye.

Generally, there are several reasons causing the shift of absorption peaks: the variation of solvent polarity, particle size distribution and surface capping agents [24, 71, 73, 103, 104]. For instance, Hyun *et al.* have found the absorption peaks of the water-soluble PbS QDs shift to the red by around 50 nm after transfer into water via ligand exchange [24]. Neither the variation of solvent polarity nor the change of ligands should be the dominant factor here. It is because that a more polar solvent (water versus chloroform) often causes a red shift of absorption band [103, 104], yet we observed blue shifts in our samples after transfer into water. As for the ligands, same type has been used throughout these investigations. The blue-shift of absorption peak positions in our case is thus mainly attributed to the shrink of core size by ligand etching [73]. The thicker CdS shell seems to offer the PbS core better resistance to the aqueous environment and can significantly decrease the core-environment interactions. As a result, the thicker the shell is, the larger the QDs can maintain their QYs after water transfer.

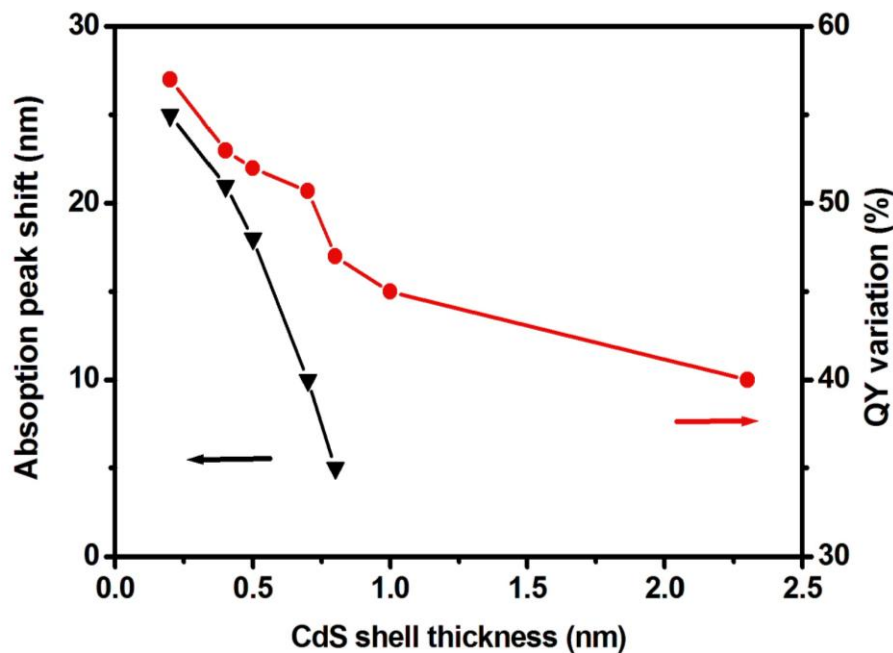


Figure 6.12 Absorption peak shifts and QY variation of PbS/CdS QDs before and after transfer into water as a function of CdS shell thickness. The solid lines are guides to the eye.

The CdS shell thickness not only affects the variation of optical properties of PbS/CdS QDs, but also the colloidal stability of QDs during the water transfer process. In the following, I will investigate the shell thickness effects on the stability of water-soluble amphiphilic polymer encapsulated PbS core QDs.

6.2.2.2 Colloidal stability

Normally, the colloidal stability of water-soluble “bare” PbS QDs is very sensitive to the variation of environments [52, 99]. Both Zhao *et al.* and Cornacchio *et al.* reported the aggregation of thiolate-capped PbS nanocrystals in water due to the oxidation of thiol capping groups [52, 99]. Although polymers are supposed to endow better colloidal stability to QDs, they may not be able to prevent QDs, themselves, from oxidation. For example, it has been found that poly(acrylic acid) capped PbS QDs gradually experienced a decrease in QY, accompanied by the blue shift of both the absorption and emission spectra, due to the surface oxidation of QDs [56]. In a big contrast, all PMAO–PEG encapsulated PbS/CdS QDs are very stable in water without any sign of QD aggregation or PbS core oxidation with time, as supported by the absence of any variations of the PL spectra. The better resistance of PbS cores to oxidation as compared to polymer encapsulated “bare” PbS QDs is believed to be due to the efficient protection from the shell of CdS.

Further dispersing PbS/CdS QDs into PBS buffers containing different NaCl concentrations does not cause any change to the PL intensity whatever the shell thickness (Figure 6.13), even at the NaCl concentration as high as 300 mM. This suggests that no severe QD agglomeration takes place with NaCl concentration up to at least 300 mM. Also no shift in absorption or PL peaks was observed for any of our samples, suggesting nanocrystal core size remains constant (Figure 6.13a) with varying salt concentrations. This observation also serves as an indication of the lack of agglomeration, which may give rise to the red shift of the PL band, especially for thin-shell QDs.

Normally, increasing the salt concentration could lead to the aggregation of QDs due to the decrease of electrostatic repulsion among QDs [119]. Our results suggest that PMAO–PEG provides sufficient and similar steric hindrance to all the samples, which prevents their aggregation and make them insensitive to a relatively high salt concentration [59]. The colloidal stability of these core/shell QDs was further proved by TEM observations; a typical TEM image of PbS/CdS#3 is shown in Figure 6.14. Such stability has important implications in biological applications.

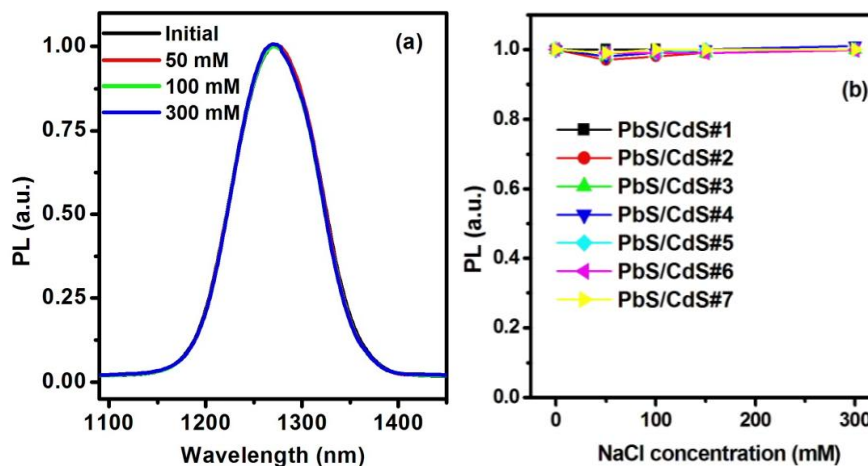


Figure 6.13 (a) PL spectra of PbS/CdS QDs in PBS buffers containing different NaCl concentrations and (b) PL intensity of PbS/CdS QDs in PBS buffer as a function of NaCl concentration.

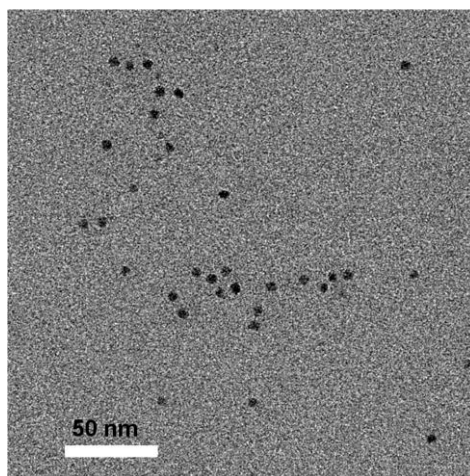


Figure 6.14 TEM image of PbS/CdS#3. PbS/CdS QDs were dispersed in PBS buffer containing 300 mM of NaCl.

6.2.2.3 Photostability

The photostability of PbS/CdS QDs, with different shell thickness, in PBS buffer was measured under continuous irradiation of a 4 W UV lamp. The PL spectra of all PbS/CdS QDs investigated herein do not exhibit any considerable peak broadening or shift (representative evolution spectra can be found in Figure 6.15a) during the irradiation period of 2 hours, suggesting that there is no detectable photooxidation or ion leaching of PbS cores [120]. The amplitude of variation of PL intensity, however, differs among samples of different shell thickness. Integrated intensity as a function of illumination time for all the samples is summarized in Figure 6.15b. It can be seen that PbS/CdS#7, with the thickest shell, is most stable. It does not lose any PL intensity after being irradiated for 2h. In contrast, PbS/CdS#1, with the thinnest shell, drops by 43% in its PL intensity after the same period of illumination. The decrease in PL intensity of QDs under illumination has often been correlated with either surface oxidation [112, 113] or photo-accelerated ligand etching [117]. Since both processes lead to the reduction of the “effective” size of PbS cores, their occurrence can be indirectly yet sensitively mirrored from the blue shift in PL spectra. As no blue shift was observed in our samples, we infer that the PL loss of PbS/CdS QDs in PBS under illumination is mainly attributed to the quenching event at unpassivated surface sites generated by photo-induced ligand desorption [73]. The differences of photostability of samples with different shell thickness are quite possible due to the amplitude of the exciton wave function at the outer interface of the shell [121]. In order to clearly demonstrate the effect of CdS shell thickness on the photostability behavior of PbS/CdS QDs in buffer, we calculated the variation of PL intensity of QDs after 2h of continuous illumination by using the following equation:

$$PL\ variation = (PL_a - PL_b) / PL_a \quad (6.2)$$

where PL_a is the PL intensity of QDs before illumination and PL_b is the PL intensity of QDs after 2h of illumination. As shown in Figure 6.15b inset, the PL variation decreases with the increase in shell thickness. It seems that the defects related to thicker shells do not exert significant effect on the photostability [122] and thicker shells lead to better isolation of core QDs from their aqueous environment. Similar finding was reported by Mekis *et al* for CdSe QDs, which also show gradually enhanced luminescence stability with increasing CdS shell thickness [122].

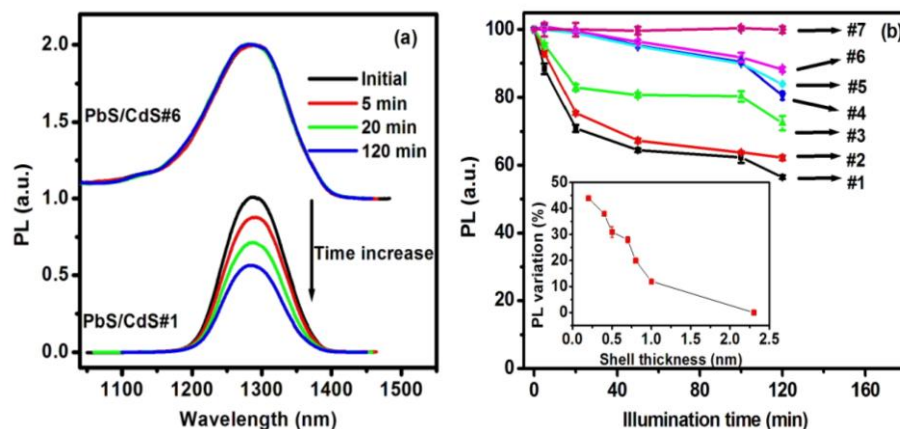


Figure 6.15 (a) PL spectra of PbS/CdS QDs in PBS buffer under continuous illumination and (b) PL intensity of PbS/CdS QDs in PBS buffer as a function of illumination time. Inset of (b) is the PL variation of PbS/CdS QDs after 2-hour of illumination as a function of CdS shell thickness.

6.2.2.4 Identifying optimal shell thickness

Based on all of data of core/shell QDs dispersed in aqueous solutions, we identify that the optimal CdS shell thickness is 0.7 nm at which, the PbS core QDs (~4.5 nm in diameter) reach the maximum in their QYs and as well as show reasonable photostability. In order to testify whether this also holds true for PbS QDs of other sizes, we have synthesized series of PbS/CdS QDs with PbS core size tuning from 2.6 nm to 5 nm. As expected, all samples yield the highest QYs in water when their shell thickness is about 0.7 nm. As examples, the PL spectra of 0.7-nm-thick-shell QDs are shown in Figure 6.16a. These high-quality water-soluble PbS/CdS QDs, with PL peak positions

spanning from 830 nm to 1400 nm, show QYs in the range of 26~33 % in PBS buffer with a narrow PL FWHM of as low as 65 meV. Their narrow size distribution has been confirmed by TEM observations (Figure 6.16b).

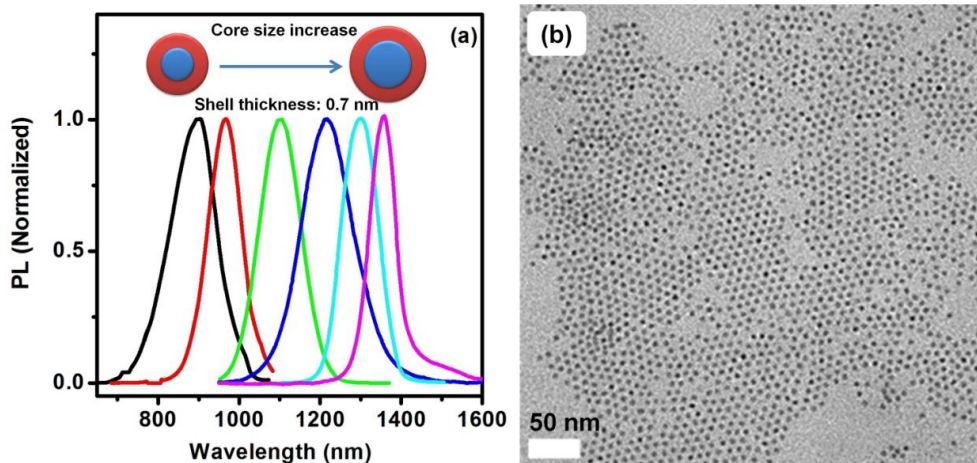


Figure 6.16 (a) PL spectra of water-soluble PbS/CdS QDs with varying core size and constant CdS shell thickness of 0.7 nm. (b) Typical TEM image of water-soluble, 0.7-nm-thick-shell PbS/CdS QDs.

6.3 Summary

In this chapter, a novel two-step approach has been developed to synthesize monodisperse, stable and water-soluble NIR-emitting PbS/CdS QDs with a high QY of 30%. The CdS shell around the PbS core can maintain the structural integrity and leads to high QY and photostability of the QDs in buffer.

Furthermore, the water-soluble PbS/CdS QDs with similar core size and varying shell thickness were successfully synthesized. It was found that the QY of PbS/CdS QDs (with the core size of ~4.5 nm in diameter) reaches the maximum at an intermediate shell thickness. The considerable decline in the QY in relatively thick-shell QDs is due to the formation of new defects within thick shells. These defects, however, do not show any overwhelmingly negative effects on

the variation of QY with environments and QD photostability. A thicker shell offers the PbS core better protection from their environments and renders them more photostable. The colloidal stability of PbS/CdS QDs bears no relation with the CdS shell thickness. Similarly high colloidal stability of all the samples is attributed to the effective steric stabilization provided by the amphiphilic polymer. In view of all results, it was found that ~0.7 nm is optimal shell thickness at which 4.5-nm PbS core QDs show the highest QY and reasonably good photostability. Further preparation and investigations of series of core/shell QDs of varying core size and shell thickness confirm that 0.7 nm is indeed an universally optimal value for the shell thickness for all QDs, with the core size ranging from 2.6 to 5 nm, investigated herein.

Chapter 7

Conclusions and perspectives

7.1 Conclusions

Colloidal PbS QDs have attracted much attention due to their unique size-dependent photophysical properties that are distinctly different from corresponding bulk materials, in the NIR range. They are currently exploited for various applications, such as NIR biomedicine and NIR solar energy conversion. In particular, in the field of biomedicine, they are attractive for in vivo deep-tissue imaging. For all these applications, they are required to show high quantum efficiency and good photostability. It is still a big challenge to synthesize high-quality NIR-emitting PbS QDs stable in an organic phase or in aqueous environments and our knowledge on these QDs are also quite limited. The objectives of this thesis were to synthesize high-quality NIR-emitting PbS QDs in an organic phase and in water by developing new approaches as well as to gain more understanding of these QDs.

In Chapter 3, I describe a simple and relatively green approach to synthesize PbS QDs in an organic phase. The effects of reaction time, temperature (90 ~ 120 °C), molar ratio of precursors (PbCl₂/S: 2:1 to 10:1), capping ligands and purity of ligands and precursors on the growth of PbS QDs in a “non-viscous”, solvent-free, mild constant-temperature system and the optical properties

of such prepared QDs are presented and discussed. Bimodal PL has been observed and in most cases, it is due to the onset of Ostwald ripening, whose occurrence and evolution are highly affected by reaction parameters, such as temperature and molar ratio of precursors, as evidenced by the evolution of PL spectra. This observation is interesting since Ostwald ripening usually result only in broadening of a single peak. The injection of additional, another type of ligands TOP has a significant effect on the PL spectra; it immediately initiates the bimodal PL, which however is not believed to be related with Ostwald ripening based on spectra characteristics. Aging can clearly enhance the emission at the shorter wavelength, while does not influence the emission at the longer wavelength. By adjusting parameters, the narrowest PL peak achieved in this simple system has PL FWHM of 58 meV with the QY as high as 40% in the organic phase.

Chapter 4 details a new two-step cation exchange method to synthesize PbS/CdS core/shell QDs with varying shell thickness in the organic phase. The first exciton absorption peak of PbS/CdS QDs can be tuned from 830 to 1960 nm and the band edge emission peak from 850 to over 1600 nm (detection limited by our NIR detector) by varying the size of starting PbS QDs and the thickness of the shell. As direct experimental identification of the shell composition in thin-shell QDs is difficult, experimental data and calculations are combined to indirectly probe this issue. The comparison of band gap versus core size plots of different compositional models indicates that highly likely, the thin shell is mainly made of CdS. A two-step cation exchange procedure has been developed for synthesizing PbS/CdS core/shell QDs with a much thicker shell than previously reported, which expands the flexibility of the current cation exchange approach. The thick-shell QDs allow relatively easy observation of the core/shell morphology by transmission electron microscopy as well as exhibit characteristic absorption and emission of CdS when the shell thickness reaches 1.8 nm. X-ray diffraction patterns show gradual transformation from a rock salt

PbS pattern to a zinc blende CdS pattern with increasing shell thickness and the overall diffraction pattern is indeed same as that of the CdS standard when the shell is thicker than 3.6 nm. The thick-shell QDs were further analyzed by energy dispersive X-ray spectrometry. It is found that Pb only exists in the core region and is essentially absent in the shell region. All of these results consistently suggest that the shell is made of CdS, instead of ternary $\text{Pb}_x\text{Cd}_{1-x}\text{S}$ alloy in thick-shell QDs. Importantly, these core/shell PbS/CdS QDs not only show significantly increased quantum yield up to 67% at the optimal shell thickness of about 0.7 nm, they are also much more photostable and thermally stable than the shell-free PbS QDs.

The as-synthesized PbS and PbS/CdS QDs are insoluble in water. Chapter 5 and Chapter 6 focus on the phase transfer process of these QDs from the organic phase into water via the amphiphilic polymer approach in order to achieve high-quality PbS-based NIR emitting QDs stable in aqueous solutions.

In Chapter 5, PbS QDs capped by three types of most commonly used capping ligands were synthesized and transferred from an organic solvent into water via amphiphilic polymers of PMAO-PEG. For PbS QDs capped by OLA (~ 5.2 nm in diameter), the water transfer process leads to a double size distribution (5.6 ± 0.9 nm and 2.7 ± 0.4 nm) together with the rapid disappearance of PL, due to severe ligand etching enhanced by the co-presence of water and PMAO-PEG and thereby initiated Ostwald ripening. The PL of PbS QDs, however, was found to recover automatically after the storage in the dark for 3 months. The recovery behavior was found to be quite different for the smaller and larger QDs in the same sample and the primary reason consists in the difference in the variation of their surface defect states during the aging process. The effective removal of surface defect states, as evidenced by the decrease of unpassivated surface atoms from XPS studies, is a dominant factor for the observed PL recovery in the smaller QDs. In contrast, the

increase of the surface defects, which are introduced during the Ostwald growth (starting immediately after water transfer and continuing during the low-temperature aging) and not able to be efficiently annealed out, of larger QDs is mainly responsible for their non-recovery behavior in water. The water-soluble PL-recovered PbS QDs show the minimum QY of 10%.

Similarly, PbS QDs with slimier core size capped by OA or OA/TOP ligands were transferred from an organic solvent into water via PMAO-PEG. The structure and optical properties of amphiphilic polymer-encapsulated PbS QDs after water transfer were found to highly depend on the type of initial capping ligands (OLA, OA or OA/TOP). Among all three samples in water, the PbS-OA/TOP QDs show the highest QY of 20%. As for photostability under continuous illumination, the PbS-OA and PbS-OA/TOP QDs are much better than that of the PbS-OLA QDs. It is worth noting that although the PL intensity decay of all water soluble QDs is faster than that of corresponding QDs in chloroform, the photo-induced oxidation and/or ligand etching are significantly postponed if not eliminated due to the presence of the polymer shell in water-soluble QDs. Taking all results into consideration, PbS-OA/TOP QDs show the optimal properties in water. Our study strongly suggests that, owing to the crucial role played by the capping ligands in the process of water transfer of PbS QDs via the amphiphilic polymer approach, the “correct” capping ligands should be chosen in order to obtain high-quality water-soluble QDs. Quite likely, this newly discovered concept can be applied to other types of NIR-emitting QDs as well.

In Chapter 6, a new two-step approach (formation of a PbS/CdS core/shell structure followed by water transfer via amphiphilic polymers) to synthesize high-quality water-soluble NIR QDs is described. The CdS shell efficiently increases the structural stability of PbS QDs during water transfer and leads to good photostability and a significantly enhanced QY. Further improvement may be made by optimizing core/shell structures. By carefully varying the initial size

of PbS QDs and finely tuning cation exchange experimental conditions, I am able to synthesize PbS/CdS core/shell QDs with a similar PbS core size of 4.4 ~ 4.5 nm yet different CdS shell thickness from 0.2 to 2.3 nm via a cation exchange approach. This enables me to study the effect of the shell thickness on the optical properties of these near infrared emitting PbS/CdS core/shell QDs after their transfer from an organic solvent into water via PMAO-PEG. It was found that the QY of PbS/CdS QDs (with the core size of ~4.5 nm in diameter) reaches the maximum at an intermediate shell thickness. The considerable decline in the QY in relatively thick-shell QDs is due to the formation of new defects within thick shells. These defects, however, do not show any overwhelmingly negative effects on the variation of QY with environments and QD photostability. A thicker shell offers the PbS core better protection from their environments and renders them more photostable. The colloidal stability of PbS/CdS QDs bears no relation with the CdS shell thickness. Similarly high colloidal stability of all the samples is attributed to the effective steric stabilization provided by the amphiphilic polymer. In view of all results, it is found that ~0.7 nm is optimal shell thickness at which 4.5-nm PbS core QDs show the highest QY and reasonably good photostability. Further preparation and investigations of series of core/shell QDs of varying core size and shell thickness confirm that 0.7 nm is indeed an universally optimal value for the shell thickness for all QDs, with the core size ranging from 2.6 to 5 nm, investigated in the current work.

7.2 Perspectives

Toxicity is an important factor that is required to consider, in many cases, before QDs can be put into practical use. The toxicity of QDs is affected by many parameters such as chemical composition, size, shape, aggregation status, surface coating, and dose [120, 123, 124]. Although some types of QDs can be presently prepared with tight size and shape control and various surface

chemistries, to date systematic and thorough investigations of QD toxicity is still lacking, which largely limits the use of QDs in biomedicine.

To be specific about PbS QDs, *in vitro* studies have suggested that they may induce negative responses through mechanisms such as particle breakdown and the subsequent release of toxic metals [54]. L. Turyanska *et al* have assessed the biocompatibility of a nanocomposite based on a PbS QD entrapped in the hollow core of an apoferritin protein cage [54]. They found that apoferritin-PbS nanocomposites have lower level of toxicity toward healthy cells compared to that reported in the literature for other colloidal QDs, and show differential toxicity between healthy and cancerous cells [125, 126]. Native polyacrylamide gel-electrophoresis (PAGE) studies demonstrate that the PbS QDs do not alter the external surface of apoferritin and its migratory behavior. Nonetheless, the biocompatibility and toxicity of amphiphilic polymer-encapsulated PbS-based QDs are still largely unexplored. Although the CdS shell can largely enhance the QY of PbS core QDs and the core/shell QDs show overall higher structural stability and less sensitivity to environments, in general the Cd^{2+} is more toxic than Pb^{2+} [127]. It is thus very important to investigate the biocompatibility and toxicity of amphiphilic polymer-encapsulated PbS or PbS/CdS QDs *in vitro* before further exploring their bio-applications. In addition to simply studying the response of various cells to the presence of these QDs at different dosages, it is also necessary to evaluate the toxicity of QDs during and after illumination, especially for PbS/CdS QDs, as their bio-applications often involve photons which may interact with QDs and lead to their harmful interactions with cells at both molecular and cellular levels. Since toxicology data derived from *in vitro* studies may not accurately reflect *in vivo* responses, it is essential to further assess and compare the toxicity of PbS and PbS/CdS core/shell QDs systematically in animals.

On the other hand, as PbS and PbS/CdS QDs contain toxic elements (Cd, Pb), their toxicity is a major concern in practical applications, particularly *in vivo* applications. Therefore, their toxicity needs to be thoroughly investigated and systematically evaluated at various levels and minimized by coating their surface with inorganic, relatively safe materials such as ZnS and silica, or organic, biocompatible molecules such as bovine serum albumin. Depending on the nature of applications, the QDs may be further attached with specific biomolecules via covalent bonding and/or electrostatic interaction.

The actual interest of these QDs is much broader. For example, they may be used as light-harvesting components for photovoltaic devices. Recently, I have collaborated with other researchers to fabricate a PbS QDs/carbon-nanotube nano-architecture, which after being integrated with a hole transporting polymer shows a photoconversion efficiency of ~3.03% under 1 sun AM1.5 solar simulator [128]. Since the CdS shell can largely improve the optical properties of PbS, it is interesting to explore the use of the PbS/CdS QDs in the photovoltaic devices. But since the charge transfer between the PbS core and carbon nanotubes (or polymers) may be decreased or even blocked by the CdS shell depending on its thickness and uniformity, systematic investigations are required in order to optimize their photovoltaic performance.

Bibliography

- [1] P. Alivisatos. Semiconductor Clusters, Nanocrystals, and Quantum Dots. *Science*, 271:933–937, 1996.
- [2] L. E. Brus. Electron-electron and Electron-hole Interactions in Small Semiconductor Crystallites - the Size Dependence of the Lowest Excited Electronic State. *Journal of Chemical Physics*, 80:4403–4409, 1984.
- [3] X. Michalet, F. F. Pinaud, L. A. Bentolila, J. M. Tsay, S. Doose, J. J. Li, G. Sundaresan, A. M. Wu, S. S. Gambhir, and S. Weiss. Quantum Dots for Live Cells, in Vivo Imaging, and Diagnostics. *Science*, 307:538–544, 2005.
- [4] M. Bruchez, M. Moronne, P. Gin, S. Weiss, and A. P. Alivisatos. Semiconductor Nanocrystals as Fluorescent Biological Labels. *Science*, 281:2013–2016, 1998.
- [5] D. Gerion, F. Pinaud, S. C. Williams, W. J. Parak, D. Zanchet, S. Weiss, and A. P. Alivisatos. Synthesis and Properties of Biocompatible Water-Soluble Silica-Coated CdSe/ZnS Semiconductor Quantum Dots. *Journal of Physical Chemistry B*, 105:8861–8871, 2001.
- [6] W. W. Yu, J. C. Falkner, B. S. Shih, and V. L. Colvin. Preparation and Characterization of Monodisperse PbSe Semiconductor Nanocrystals in a Noncoordinating Solvent. *Chemistry of Materials*, 16:3318–3322, 2004.

- [7] A. Guzelian, U. Banin, A. V. Kadavanich, X. Peng, and A. P. Alivisatos. Colloidal Chemical Synthesis and Characterization of InAs Nanocrystal Quantum Dots. *Applied Physics Letters*, 69:1432–1434, 1996.
- [8] A. Guzelian, J. E. B. Katari, A. V. Kadavanich, U. Banin, K. Hamad, E. Juban, and A. P. Alivisatos. Synthesis of Size-Selected, Surface-Passivated InP Nanocrystals. *Journal of Physical Chemistry*, 100:7212–7219, 1996.
- [9] W. W. Yu, and X. Peng. Formation of High Quality CdS and Other II-VI Semiconductor Nanocrystals in Non-Coordinating Solvent, Tunable Reactivity of Monomers. *Angewandte Chemie International Edition*, 41:2368–2371, 2002.
- [10] W. W. Yu, Y. A. Wang, and X. Peng. Formation and Stability of Size-, Shape-, and Structure-Controlled CdTe Nanocrystals: Ligand Effects on Monomers and Nanocrystals. *Chemistry of Materials*, 15:4300–4308, 2003.
- [11] J. M. Tsay, M. Pflughoeft, L. A. Bentolila, and S. Weiss. Hybrid Approach to the Synthesis of Highly Luminescent CdTe/ZnS and CdHgTe/ZnS Nanocrystals. *Journal of the American Chemical Society*, 126:1926–1927, 2004.
- [12] M. Nirmal, B. O. Dabbousi, M. G. Bawendi, J. J. Macklin, J. K. Trautman, T. D. Harris and L. E. Brus. Fluorescence Intermittency in Single Cadmium Selenide Nanocrystals. *Nature*, 383:802–804, 1996.
- [13] S. Hennig, S. van de Linde, M. Heilemann, and M. Sauer. Quantum Dot Triexciton Imaging with Three-Dimensional Subdiffraction Resolution. *Nano Letters*, 9:2466–2470, 2009.
- [14] L. Rogach, A. Eychmüller, S. G. Hickey, and S. V. Kershaw. Infrared-Emitting Colloidal Nanocrystals: Synthesis, Assembly, Spectroscopy, and Applications. *Small*, 3:536–557, 2007.

- [15] J. Joo, H. B. Na, T. Yu, J. H. Yu, Y. W. Kim, F. Wu, J. Z. Zhang, and T. Hyeon. Generalized and Facile Synthesis of Semiconducting Metal Sulfide Nanocrystals. *Journal of the American Chemical Society*, 125:11100–11105, 2003.
- [16] X. Peng, L. Manna, W. D. Yang, J. Wickham, E. Scher, A. Kadavanich, and A. P. Alivisatos. Shape Control of CdSe Nanocrystals. *Nature*, 404:59–61, 2000.
- [17] R. Weissleder. Progress Continues in the Development of Smaller, More Penetrable Probes for Biological Imaging. *Nature Biotechnology*, 19:316–317, 2001.
- [18] F. W. Wise. Lead Salt Quantum Dots: the Limit of Strong Quantum Confinement. *Accounts of Chemical Research*, 33:773–780, 2000.
- [19] Y. He, and R. Wang. Dynamic Optical Clearing Effect of Tissue Impregnated with Hyperosmotic Agents and Studied with Optical Coherence Tomography. *Journal of Biomedical Optics*, 9:200–206, 2004.
- [20] X. Gao, L. Yang, J. A. Petros, F. F. Marshall, J. W. Simons, and S. Nie. In Vivo Molecular and Cellular Imaging with Quantum Dots. *Current Opinion in Biotechnology*, 16:63–72, 2005.
- [21] M. Hintersteiner, A. Enz, P. Frey, A. L. Jaton, W. Kinzy, R. Kneuer, U. Neumann, M. Rudin, M. Staufienbiel, M. Stoeckli, K. H. Wiederhold, and H. U. Gremlich. In Vivo Detection of Amyloid- β Deposits by Near-infrared Imaging Using an Oxazine-Derivative Probe. *Nature Biotechnology*, 23:577–583, 2005.
- [22] A. Zaheer, R. E. Lenkinski, A. Mahmood, A. G. Jones, L. C. Cantley, and J. V. Frangioni. In Vivo Near-infrared Fluorescence Imaging of Osteoblastic Activity. *Nature Biotechnology*, 19:1148–1154, 2001.
- [23] P. Alivisatos, W. W. Gu, and C. Larabell. Quantum Dots as Cellular Probes. *Annual Review of Biomedical Engineering*, 7:55–76, 2005.

- [24] B. B. Hyun, H. Chen, D. A. Rey, F. W. Wise, and C. A. Batt. Near-Infrared Fluorescence Imaging with Water-Soluble Lead Salt Quantum Dots. *Journal of Physical Chemistry B*, 111:5726–5730, 2007.
- [25] R. G. Aswathy, Y. Yoshida, T. Maekawa, and D. S. Kumar. Near-infrared Quantum Dots for Deep Tissue Imaging. *Analytical and Bioanalytical Chemistry*, 397:1417–1435, 2010.
- [26] K. T. Yong, I. Roy, H. Ding, E. J. Bergey, and P. N. Prasad. Biocompatible Near-Infrared Quantum Dots as Ultrasensitive Probes for Long-Term in vivo Imaging Applications. *Small*, 5:1997–2004, 2009.
- [27] S. V. Kershaw, M. Harrison, A. L. Rogach, and A. Kornowski. Development of IR-Emitting Colloidal II-VI Quantum-Dot Materials. *IEEE Journal of Selected Topics in Quantum Electronics*, 6:534–543, 2000.
- [28] L. Rogach, S. V. Kershaw, M. Burt, M. Harrison, A. Kornowski, A. Eychmüller, and H. Weller. Colloidally Prepared HgTe Nanocrystals with Strong Room Temperature Infrared Luminescence. *Advanced Materials*, 11:552–555, 1999.
- [29] M. Green, G. Wakefield, and P. J. Dobson. A Simple Metalorganic Route to Organically Passivated Mercury Telluride Nanocrystals. *Journal of Materials Chemistry*, 13:1076–1078, 2003.
- [30] B. Murray, D. J. Norris, and M. G. Bawendi. Synthesis and Characterization of nearly Monodisperse CdE (E = sulfur, selenium, tellurium) Semiconductor Nanocrystallites. *Journal of the American Chemical Society*, 115:8706–8715, 1993.
- [31] M. A. Hines, and G. D. Scholes. Colloidal PbS Nanocrystals with Size-tunable Near-Infrared Emission: Observation of Post-synthesis Self-narrowing of the Particle Size Distribution. *Advanced Materials*, 15:1844–1849, 2003.

- [32] L. Cademartiri, J. Bertolotti, R. Sapienza, D. S. Wiersma, V. Kitaev, and G. A. Ozin. Multigram Scale, Solventless, and Diffusion-controlled Route to highly Monodisperse PbS Nanocrystals. *Journal of Physical Chemistry B*, 110:671–673, 2006.
- [33] C. B. Murray, S. H. Sun, W. Gaschler, H. Doyle, T. A. Betley, and C. R. Kagan. Colloidal Synthesis of Nanocrystals and Nanocrystal Superlattices. *IBM Journal of Research and Development*, 45:47–56, 2001.
- [34] E. Lifshitz, M. Bashouti, V. Kloper, A. Kigel, M. S. Eisen, and S. Berger. Synthesis and Characterization of PbSe Quantum Wires, Multipods, Quantum Rods, and Cubes. *Nano Letters*, 3:857–861, 2003.
- [35] W. G. Lu, J. Y. Fang, K. L. Stokes, and J. Lin. Shape Evolution and Self Assembly of Monodisperse PbTe Nanocrystals. *Journal of the American Chemical Society*, 126:11798–11799, 2004.
- [36] N. Y. Morgan, S. English, W. Chen, V. Chernomordik, A. Russo, P. D. Smith, and A. Gandjbakhche. Real Time in Vivo Non-invasive Optical Imaging Using Near-infrared Fluorescent Quantum Dots. *Academic Radiology*, 12:313–323, 2005.
- [37] S. Kim, B. Fischer, H. J. Eisler, and M. Bawendi. Type-II Quantum Dots: CdTe/CdSe(Core/Shell) and CdSe/ZnTe (Core/Shell) Heterostructures. *Journal of the American Chemical Society*, 125:11466–11467, 2003.
- [38] V. G. Savitskii, N. N. Posnov, A. M. Malyarevich, K. V. Yumashev, E. L. Raaben, and A. A. Zhilin. Relaxation of Bleaching in Lead Sulfide Nanoparticles at Different Pump Powers. *Journal of Applied Spectroscopy*, 71:83–88, 2004.
- [39] P. T. Guerreiro, S. Ten, N. F. Borrelli, J. Butty, G. E. Jabbour, and N. Peyghambarian. PbS Quantum-dot Doped Glasses as Saturable Absorbers for Mode Locking of A Cr:Forsterite Laser. *Applied Physics Letters*, 71:1595–1598, 1997.

- [40] S. Joshi, S. Sen, and P. C. Ocampo. Nucleation and Growth Kinetics of PbS Quantum Dots in Oxide Glass: Spectroscopic and Microscopic Studies in the Dilute Range. *Journal of Physical Chemistry C*, 111:4105–4110, 2007.
- [41] A. Patel, F. Wu, J. Z. Zhang, C. L. Torres-Martinez, R. K. Mehra, Y. Yang, and S. H. Risbud. Synthesis, Optical Spectroscopy and Ultrafast Electron Dynamics of PbS Nanoparticles with Different Surface Capping. *Journal of Physical Chemistry B*, 104:11598–11605, 2000.
- [42] D. Kim, N. Teratani, H. Nishimura, and M. Nakayama. Photo-Irradiation Effects on Preparation of Colloidal Quantum Dots and Their Surface Modification. *International Journal of Modern Physics B*, 15:3829–3832, 2001.
- [43] E. Leontidis, M. Orphanou, T. Kyprianidou-Leodidou, F. Krumeich, and W. Caseri. Composite Nanotubes Formed by Self-Assembly of PbS Nanoparticles. *Nano Letters*, 3:569–572, 2003.
- [44] L. Bakueva, I. Gorelikov, S. Musikhin, X. Zhao, E. H. Sargent, and E. Kumacheva. PbS Quantum Dots with Stable Efficient Luminescence in the Near-IR Spectral Range. *Advanced Materials*, 16:926–929, 2004.
- [45] V. S. Gurin. Nucleation and Growth of PbS Nanocrystals and Simulation of X-ray Diffraction Patterns. *Journal of Crystal Growth*, 191:161–165, 1998.
- [46] M. Flores-Acosta, M. Sotelo-Lerma, H. Arizpe-Chavez, F. F. Castillon- Barraza, and R. Ramirez-Bon. Excitonic Absorption of Spherical PbS Nanoparticles in Zeolite-A. *Solid State Communications*, 128:407–411, 2003.
- [47] N. M. Huang, R. Shahidan, P. S. Khiew, L. Peter, and C. S. Kan. In Situ Synthesis of PbS Nanorods Using Reverse Hexagonal HII Liquid Crystals. *Colloids and Surfaces A*, 247:55–60, 2004.

- [48] Z. Hens, D. Vanmaekelbergh, E. J. A. J. Stoffels, and H. van Kempen. Effects of Crystal Shape on the Energy Levels of Zero-Dimensional PbS Quantum Dots. *Physics Review Letters*, 88:236803–236807, 2002.
- [49] J. J. Zhu, S. W. Liu, O. Palchik, Y. Kolytyn, and A. Gedanken. A Novel Sonochemical Method for the Preparation of Nanophasic Sulfides: Synthesis of HgS and PbS Nanoparticles. *Journal of Solid State Chemistry*, 153:342–348, 2000.
- [50] K. A. Abel, J. N. Shan J. C. Boyer, F. Harris, and F. C. J. M. Van Veggel. Highly Photoluminescent PbS Nanocrystals: The Beneficial Effect of Trioctylphosphine. *Chemistry of Materials*, 20:3794–3796, 2008.
- [51] A. Lobo, T. Möller, M. Nagel, H. Borchert, S. G. Hickey, and H. Weller. Photoelectron Spectroscopic Investigations of Chemical Bonding in Organically Stabilized PbS Nanocrystals. *Journal of Physical Chemistry B*, 109:17422–17428, 2005.
- [52] X. S. Zhao, I. Gorelikov, S. Musikhin, S. Cauchi, V. Sukhovatkin, E. H. Sargent, and E. Kumacheva. Synthesis and Optical Properties of Thiol-Stabilized PbS Nanocrystals. *Langmuir*, 21:1086–1090, 2005.
- [53] B. Hennequin, L. Turyanska, T. Ben, A. M. Beltran, S. I. Molina, M. Li, S. Mann, A. Patane, and N. R. Thomas. Aqueous Near-Infrared Fluorescent Composites Based on Apoferritin-Encapsulated PbS Quantum Dots. *Advanced Materials*, 20:3592–3596, 2008.
- [54] L. Turyanska, T. D. Bradshaw, J. Sharpe, M. Li, S. Mann, N. R. Thomas, and A. Patane. The Biocompatibility of Apoferritin-Encapsulated PbS Quantum Dots. *Small*, 15:1738–1741, 2009.
- [55] W. Deng, W. H. Zhang, X. Y. Chen, F. Liu, J. Zhang, Y. Q. Gu, and J. M. Hong. Facile Synthesis of High-Quality, Water-Soluble, Near-Infrared-Emitting PbS Quantum Dots. *European Journal of Inorganic Chemistry*, 23:3440–3446, 2009.

- [56] W. Lin, K. Fritz, G. Guerin, G. R. Bardajee, S. Hinds, V. Sukhovatkin, E. H. Sargent, G. D. Scholes, and M. A. Winnik. Highly Luminescent Lead Sulfide Nanocrystals in Organic Solvents and Water through Ligand Exchange with Poly(acrylic acid). *Langmuir*, 24:8215–8219, 2008.
- [57] S. Hinds, S. Myrskog, L. Levina, G. Koleilat, J. Yang, S. O. Kelley, and E. H. Sargent. NIR-Emitting Colloidal Quantum Dots Having 26% Luminescence QY in Buffer Solution. *Journal of the American Chemical Society*, 129:7218–7219, 2007.
- [58] H. Y. Fan, E. W. Leve, C. Scullin, J. Gabaldon, D. Tallant, S. Bunge, T. Boyle, M. C. Wilson, and C. J. Brinker. Surfactant-Assisted Synthesis of Water-Soluble and Biocompatible Semiconductor Quantum Dot Micelles. *Nano Letters*, 5:645–648, 2005.
- [59] W. W. Yu, E. Chang, J. C. Falkner, J. Zhang, A. M. Al-Somali, C. M. Sayes, J. Johns, R. Drezek, and V. L. Colvin. Forming Biocompatible and Nonaggregated Nanocrystals in Water Using Amphiphilic Polymers. *Journal of the American Chemical Society*, 129:2871–2879, 2007.
- [60] J. M. Pietryga, D. J. Werder, D. J. Williams, J. L. Casson, R. D. Schaller, V. I. Klimov, and J. A. Hollingsworth. Utilizing the Lability of Lead Selenide to Produce Heterostructured Nanocrystals with Bright, Stable Infrared Emission. *Journal of the American Chemical Society*, 130:4879–4885, 2008.
- [61] X. Peng, M. C. Schlamp, A. V. Kadavanich, and A. P. Alivisatos. Epitaxial Growth of Highly Luminescent CdSe/CdS Core/Shell Nanocrystals with Photostability and Electronic Accessibility. *Journal of the American Chemical Society*, 119:7019–7029, 1997.
- [62] A. Aharoni, T. Mokari, I. Popov, and U. Banin. Synthesis of InAs/CdSe/ZnSe Core/Shell1/Shell2 Structures with Bright and Stable Near-Infrared Fluorescence. *Journal of the American Chemical Society*, 128:257–264, 2006.
- [63] M. Smith, and S. Nie. Semiconductor Nanocrystals: Structure, Properties, and Band Gap Engineering. *Accounts of Chemical Research*, 43:190–200, 2009.

- [64] J. McBride, J. Treadway, L. C. Feldman, S. J. Pennycook, and S. J. Rosenthal. Structural Basis for Near Unity QY Core/shell Nanostructures. *Nano Letters*, 6:1496–1501, 2006.
- [65] O. Dabbousi, J. Rodriguez-Viejo, F. V. Mikulec, J. R. Heine, H. Mattoussi, R. Ober, K. F. Jensen, and M. G. Bawendi. (CdSe)/ZnS Core-shell Quantum Dots: Synthesis and Characterization of a Size Series of Highly Luminescent Nanocrystallites. *Journal of Physical Chemistry B*, 101:9463–9475, 1997.
- [66] M. A. Hines, and P. Guyot-Sionnest. Synthesis and Characterization of Strongly Luminescing ZnS-capped CdSe Nanocrystals. *Journal of Physical Chemistry*, 100:468–471, 1996.
- [67] M. Brumer, A. Kigel, L. Amirav, A. Sashchiuk, O. Solomesch, N. Tessler and E. Lifshitz, PbSe/PbS and PbSe/PbSe_xS_{1-x} Core/Shell Nanocrystals. *Advanced Functional Materials*, 15:1111–1116, 2005.
- [68] H. Zhao, M. Chaker, and D. Ma. Bimodal Photoluminescence during the Growth of PbS Quantum Dots. *Journal of Physical Chemistry C*, 113:6497–6504, 2009.
- [69] H. Zhao, T. Zhang, M. Chaker, and D. Ma. Ligand and Precursor Effects on the Synthesis and Optical Properties of PbS Quantum Dots. *Journal of Nanoscience and Nanotechnology*, 10:4897–4905, 2010.
- [70] H. Zhao, M. Chaker, N. Wu, D. Ma. Towards Controlled Synthesis and Better Understanding of Highly Luminescent PbS/CdS Core/shell Quantum Dots. 21:8898–8904, 2011.
- [71] H. Zhao, M. Chaker, and D. Ma. Self-selective Recovery of Photoluminescence in Amphiphilic Polymer Encapsulated PbS Quantum Dots. *Physical Chemistry Chemical Physics*, 12:14754–14761, 2010.

- [72] H. Zhao, D. Wang, M. Chaker, and D. Ma. Photoluminescence Effect of Different Types of Surface Ligands on the Structure and Optical Property of Water-soluble PbS Quantum Dots Encapsulated by Amphiphilic Polymers. *Journal of Physical Chemistry C*, 115:1620–1626, 2011.
- [73] H. Zhao, D. Wang, T. Zhang, M. Chaker, and D. Ma. Two-step Synthesis of High-quality Water-soluble Near-infrared Emitting Quantum Dots via Amphiphilic Polymers. *Chemical Communications*, 46:5301–5303, 2010.
- [74] H. Zhao, M. Chaker, and D. Ma. Effect of CdS Shell Thickness on the Optical Properties of Water-soluble Amphiphilic Polymer Encapsulated PbS/CdS Quantum Dots. *Journal of Materials Chemistry*, 21:17483–17491, 2011.
- [75] R. C. Benson, and H. A. Kues. Absorption and Fluorescence Properties of Cyanine Dyes. *Journal of Chemical & Engineering Data*, 22:379–383, 1977.
- [76] R. Rossetti, S. Nakahara, and L. E. Brus. Quantum Size Effects in the Redox Potentials, Resonance Raman-Spectra, and Electronic-Spectra of CdS Crystallites in Aqueous-Solution. *Journal of Chemical Physics*, 79:1086–1088, 1983.
- [77] X. Peng, J. Wickham, and A. P. Alivisatos. Kinetics of II-VI and III-V Colloidal Semiconductor Nanocrystal Growth: “Focusing” of Size Distributions. *Journal of the American Chemical Society*, 120:5343–5344, 1998.
- [78] R. L. Penn, and J. F. Banfield. Imperfect Oriented Attachment: Dislocation Generation in Defect-Free Nanocrystals. *Science*, 281:969–971, 1998.
- [79] R. L. Penn, and J. F. Banfield. Oriented Attachment and Growth, Twinning, Polytypism, and Formation of Metastable Phases: Insights from Nanocrystalline TiO₂. *American Mineralogist*, 83:1077–1082, 1998.
- [80] Z. Wagner. Theorie der Alterung von Niederschlägen durch Umlösen (Ostwald-Reifung). *Elektrochemie*, 65:581–591, 1961.

- [81] M. Lifshitz, and V. V. Slyozov. The Kinetics of Precipitation from Supersaturated Solid Solutions. *Journal of Physics and Chemistry of Solids*, 19:35–50, 1961.
- [82] V. Talapin, A. L. Rogach, M. Haase, and H. Weller. Evolution of an Ensemble of Nanoparticles in a Colloidal Solution: Theoretical Study. *Journal of Physical Chemistry B*, 105:12278–12285, 2001.
- [83] F. Huang, H. Zhang, and J. F. Banfield. Two-Stage Crystal-Growth Kinetics Observed during Hydrothermal Coarsening of Nanocrystalline ZnS. *Nano Letters*, 3:373–378, 2003.
- [84] J. Zhang, Z. Lin, Y. Lan, G. Ren, D. Chen, F. Huang, and M. Hong. A Multistep Oriented Attachment Kinetics: Coarsening of ZnS Nanoparticles in Concentrated NaOH, *Journal of the American Chemical Society*, 128:12981–12987, 2006.
- [85] J. Thessing, J. H. Qian, H. Y. Chen, N. Pradhan, and X. Peng. Interparticle Influence on Size/Size Distribution Evolution of Nanocrystals. *Journal of the American Chemical Society*, 129:2736–2737, 2007.
- [86] L. Cademartiri, E. Montanari, G. Calestani, A. Migliori, A. Guagliardi, and G. A. Ozin. Size-Dependent Extinction Coefficients of PbS Quantum Dots. *Journal of the American Chemical Society*, 128:10337–10346, 2006.
- [87] J. D. Klem, D. D. MacNeil, L. Levina, and E. H. Sargent. Solution Processed Photovoltaic Devices with 2% Infrared Monochromatic Power Conversion Efficiency: Performance Optimization and Oxide Formation. *Advanced Materials*, 20:3433–3439, 2008.
- [88] K. Lambert, B. De Geyter, I. Moreels, and Z. Hens. PbTe/CdTe Core/Shell Particles by Cation Exchange, a HR-TEM Study. *Chemistry of Materials*, 21:778–780, 2009.
- [89] S. Karan, and B. Mallik. Tunable Visible-Light Emission from CdS Nanocrystallites Prepared under Microwave Irradiation. *Journal of Physical Chemistry C*, 111:16734–16741, 2007.

- [90] Y. Wada, H. Kuramoto, J. Anand, T. Kitamura, T. Sakata, H. Mori, and S. Yanagida. Microwave-assisted Size Control of CdS Nanocrystallites. *Journal of Materials Chemistry*, 11:1936–1940, 2001.
- [91] P. Reiss, M. Protière, and L. Li. Core/Shell Semiconductor Nanocrystals. *Small*, 5:154–168, 2009.
- [92] F. Li, D. I. Son, T. W. Kim, E. Ryu, S. W. Kim, S. K. Lee, and Y. H. Cho. Photovoltaic Cells Fabricated Utilizing Core-shell CdSe/ZnSe Quantum Dot/Multiwalled Carbon Nanotube Heterostructures. *Applied Physics Letters*, 95:061911–3, 2009.
- [93] Z. Zhelev, R. Bakalova, H. Ohba, R. Jose, Y. Imai, and Y. Baba. Uncoated, Broad Fluorescent, and Size-Homogeneous CdSe Quantum Dots for Bioanalyses. *Analytical Chemistry*, 78:321–330, 2006.
- [94] W. C. W. Chan, and S. M. Nie. Quantum Dot Bioconjugates for Ultrasensitive Nonisotopic Detection. *Science*, 281:2016–2018, 1998.
- [95] D. M. Willard, L. L. Carillo, J. Jung, and A. Van Orden. CdSe–ZnS Quantum Dots as Resonance Energy Transfer Donors in a Model Protein–Protein Binding Assay. *Nano Letters*, 1:469–474, 2001.
- [96] H. Mattoussi, J. M. Mauro, E. R. Goldman, G. P. Anderson, V. C. Sundar, F. V. Mikulec, and M. G. Bawendi. Self-Assembly of CdSe–ZnS Quantum Dot Bioconjugates Using an Engineered Recombinant Protein. *Journal of the American Chemical Society* 122:12142–12150, 2000.
- [97] Y. A. Wang, J. J. Li, H. Chen, and X. Peng. Stabilization of Inorganic Nanocrystals by Organic Dendrons. *Journal of the American Chemical Society*, 124:2293–2298, 2002.

- [98] Q. Wang, Y. Xu, X. Zhao, Y. Chang, Y. Liu, L. Jiang, J. Sharma, D. K. Seo, and H. Yan. A Facile One-Step in situ Functionalization of Quantum Dots with Preserved Photoluminescence for Bioconjugation. *Journal of the American Chemical Society*, 129: 6380–6381, 2007.
- [99] A. L. P. Cornacchio, and N. D. Jones. Thiolate-capped PbS Nanocrystals in Water: Sensitivity to O₂, pH and Concentration, an Alternate Pathway for Crystal Growth and A Top-down Synthesis. *Journal of Materials Chemistry*, 16:1171–1177, 2006.
- [100] L. V. Prasad, S. I. Stoeva, C. M. Sorensen, and K. J. Klabunde. Digestive-Ripening Agents for Gold Nanoparticles: Alternatives to Thiols. *Chemistry of Materials*, 15:935–942, 2003
- [101] I. Kang, and F. W. Wise. Electronic structure and optical properties of PbS and PbSe Quantum Dots. *Journal of the Optical Society America B: Optical Physics*, 14:1632–1646, 1997.
- [102] S. C. Cui, T. Tachikawa, M. Fujitsuka, and T. Majima. Solvent-Polarity Dependence of Electron-Transfer Kinetics in a CdSe/ZnS Quantum Dot–Pyromellitimide Conjugate. *Journal of Physical Chemistry C*, 114:1217–1225, 2010.
- [103] R. Jose, M. Ishikawa, V. Thavasi, Y. Baba, and S. Ramakrishna. Dependence of Luminescence Efficiency of CdSe Quantum Dots on Chemical Environments. *Journal of Nanoscience and Nanotechnology*, 8:5615–5623, 2008.
- [104] S. W. Buckner, R. L. Konold, and P. A. Jelliss. Luminescence Quenching in PbS Nanoparticles. *Chemical Physics Letters*, 394:400–404, 2004.
- [105] I. Langford, and A. J. C. Wilson. Scherrer after Sixty Years: A Survey and some new Results in the Determination of Crystallite Size. *Journal of Applied Crystallography*, 11:102–113, 1978.
- [106] W. Stouwdam, J. Shan, F. C. J. M. vanVeggel, A. G. Pattantyus-Abraham, J. F. Young, and M. Raudsepp, Photostability of Colloidal PbSe and PbSe/PbS Core/Shell Nanocrystals in Solution and in the Solid State. *Journal of Physical Chemistry C*, 111:1086–1092, 2007.

- [107] S. W. Clark, J. M. Harbold, and F. W. Wise. Resonant Energy Transfer in PbS Quantum Dots. *Journal of Physical Chemistry C*, 111:7302–7305, 2007.
- [108] A. Leiro, K. Laajalehto, I. Kartio, and M. H. Heinonen. Surface Core-level Shift and Phonon Broadening in PbS(100). *Surface Science*, 412/413:L918–923, 1998.
- [109] Z. Xu, H. Tsai, H. Wang, and M. Cotlet. Solvent Polarity Effect on Chain Conformation, Film Morphology, and Optical Properties of a Water-Soluble Conjugated Polymer. *Journal of Physical Chemistry B*, 114:11746–11752, 2010.
- [110] G. Kalyuzhny, and R. W. Murray. Ligand Effects on Optical Properties of CdSe Nanocrystals. *Journal of Physical Chemistry B*, 109:7012–7021, 2005.
- [111] J. Tang, L. Brzozowski, D. A. R. Barkhouse, X. Wang, R. Debnath, R. Wolowiec, E. Palmiano, L. Levina, A. G. Pattantyus-Abraham, D. Jamakosmanovic, and E. H. Sargent. Quantum Dot Photovoltaics in the Extreme Quantum Confinement Regime: The Surface-Chemical Origins of Exceptional Air- and Light-Stability. *ACS Nano*, 4:869–878, 2010.
- [112] M. Smith, H. Duan, M. N. Rhyner, G. Ruan, and S. Nie. A Systematic Examination of Surface Coatings on the Optical and Chemical Properties of Semiconductor Quantum Dots. *Physical Chemistry Chemical Physics*, 8:3895–3903, 2006.
- [113] J. J. Peterson, and T. D. Krauss. Photobrightening and Photodarkening in PbS Quantum Dots. *Physical Chemistry Chemical Physics*, 8:3851–3856, 2006.
- [114] D. L. Nida, N. Nitin, W. W. Yu, V. L. Colvin, and R. Richards-Kortum. Photostability of Quantum Dots with Amphiphilic Polymer-Based Passivation Strategies. *Nanotechnology*, 19:035701–035707, 2008.
- [115] B. Smetana, K. J. Klabunde, and C. M. Sorensen. Synthesis of Spherical Silver Nanoparticles by Digestive Ripening, Stabilization with Various Agents, and their 3-D and 2-D Superlattice Formation. *Journal of Colloid and Interface Science*, 284:521–526, 2005.

- [116] G. Konstantatos, L. Levina, A. Fischer, and E. H. Sargent. Engineering the Temporal Response of Photoconductive Photodetectors via Selective Introduction of Surface Trap States. *Nano Letters*, 8:1446–1450, 2008.
- [117] V. Biju, R. Kanemoto, Y. Matsumoto, S. Ishii, S. Nakanishi, T. Itoh, Y. Baba, and M. Ishikawa. Photoinduced Photoluminescence Variations of CdSe Quantum Dots in Polymer Solutions. *Journal of Physical Chemistry C*, 111:7924–7932, 2007.
- [118] A. Martucci, J. Fick, S. mile LeBlanc, M. LoCascio, and A. Haché Optical Properties of PbS Quantum Dot Doped Sol–gel Films. *Journal of Non-Crystalline Solids*, 345&346:639–642, 2004.
- [119] R. Koole, P. Liljeroth, C. M. Donega, D. Vanmaekelbergh, and A. Meijerink. Electronic Coupling and Exciton Energy Transfer in CdTe Quantum-Dot Molecules. *Journal of the American Chemical Society*, 128:10436–10441, 2006.
- [120] A. Derfus, W. C. W. Chan, and S. N. Bhatia. Probing the Cytotoxicity of Semiconductor Quantum Dots. *Nano Letters*, 4:11–18, 2004.
- [121] T. Blaudeck, E. I. Zenkevich, F. Cichos, and C. von Borczyskowski. Probing Wave Functions at Semiconductor Quantum-Dot Surfaces by NON-FRET Photoluminescence Quenching. *Journal of Physical Chemistry C*, 112:20251–7462, 2008.
- [122] I. Mekis, D. V. Talapin, A. Kornowski, M. Haase, and H. Weller. One-Pot Synthesis of Highly Luminescent CdSe/CdS Core–Shell Nanocrystals via Organometallic and “Greener” Chemical Approaches. *Journal of Physical Chemistry B*, 107:7454–7462, 2003.
- [123] C. Kirchner, T. Liedl, S. Kudera, T. Pellegrino, A. Javier, H. Gaub, S. Stölzle, N. Fertig, and W. Parak. Cytotoxicity of Colloidal CdSe and CdSe/ZnS Nanoparticles. *Nano Letters*, 5:331–338, 2005.

- [124] R. Hardman. A Toxicologic Review of Quantum Dots: Toxicity Depends on Physicochemical and Environmental Factors. *Environmental Health Perspectives*, 114:165–172, 2006.
- [125] A. Shiohara, A. Hoshino, K. Hanaki, K. Suzuki, and K. Yamamoto. On the Cytotoxicity Caused by Quantum Dots. *Microbiology and Immunology*, 48:669–675, 2004.
- [126] S. Cho, D. Maysinger, M. Jain, B. Roder, S. Hackbarth, and F. Winnik. Long-Term Exposure to CdTe Quantum Dots Causes Functional Impairments in Live Cells. *Langmuir*, 23:1974–1980, 2007.
- [127] A. Fargasová Toxicity of metals on *Daphnia magna* and *Tubifex tubifex*. *Langmuir*, 27:210–213, 1994.
- [128] D. F. Wang, J. K. Baral, H. Zhao, B. A. Gonfa, V. Truong, M. A. E. Khakani, R. Izquierdo, and D. Ma. Controlled Fabrication of PbS Quantum-Dot/Carbon-Nanotube Nanoarchitecture and its Significant Contribution to Near-Infrared Photon-to-Current Conversion. *Advanced Functional Materials*, 21:4010–4018, 2011.

Appendix A

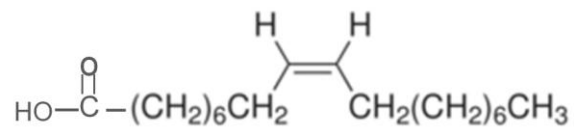
List of acronyms

PbS	lead sulfide
CdS	cadmium sulfide
FT-IR	Fourier transform infrared spectroscopy
ICP-OES	inductively coupled plasma optical emission spectrometry
NIR	near infrared
OA	oleic acid
OLA	oleylamine
PbS	lead sulfide
PL	photoluminescence
PEG	poly(ethylene glycol) methyl ethers
PMAO	poly(maleic anhydride-alt-1-octadecene)
PMAO-PEG	poly(maleic anhydride-alt-1-octadecene-co-poly(ethylene glycol))
QD	quantum dot
QY	quantum yield
TEM	transmission electron microscopy
TOP	trioctylphosphine
XRD	X-ray diffraction
XPS	X-ray photoelectron spectrometry

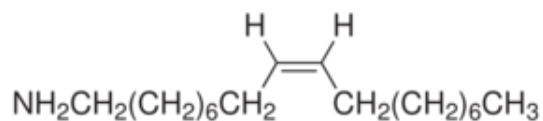
Appendix B

List of chemical formulas

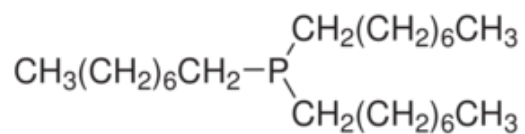
OA



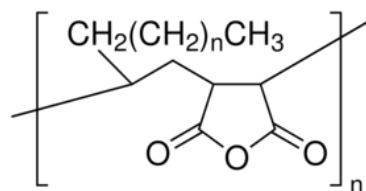
OLA



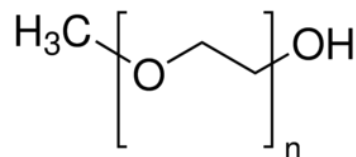
TOP



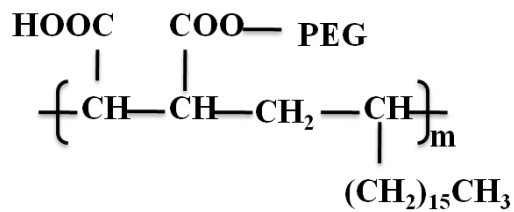
PMAO



PEG



PMAO-PEG



Appendix C

Résumé de la thèse

Introduction

L'imagerie optique in vivo dans le domaine biomédical nécessite l'utilisation de longueurs d'onde d'excitation et d'émission de fluorophores dont l'absorption et la diffusion par les fluides et les tissus biologiques (eau, hémoglobine, lipides) sont aussi faibles que possible [19, 20]. Une longueur d'onde d'émission dans la gamme proche infrarouge de 700–900 nm et 1200–1600 nm répond à ces exigences assurant d'une part la pénétration de la lumière dans les tissus et d'autre part une diminution de leur autofluorescence. Les premiers candidats pour cette application furent les colorants organiques [21, 22]. Cependant, la plupart de ces colorants ont une mauvaise photostabilité et leurs longueurs d'onde d'émission sont limitées à moins de 950 nm [23].

Au cours des dix dernières années, les points quantiques PbS émettant dans le proche infrarouge ont fait l'objet d'un intérêt croissant à travers le monde pour l'imagerie in vivo des cellules vivantes [19, 24, 25] car ils ont potentiellement plusieurs avantages par rapport aux colorants. Ils ont en particulier un spectre d'absorption plus large et des longueurs d'onde d'émission accordables dans le domaine du proche infrarouge (700 nm-2000 nm). Pour cette application, ces points quantiques devraient cependant avoir un très bon rendement quantique et une excellente

photostabilité. De plus, ils devraient être solubles dans l'eau tout en étant biocompatibles. Pour ce faire, de nombreux défis demeurent pour synthétiser de tels points quantiques

En utilisant différentes approches telles que les techniques électrochimiques [48] et sonochimique [49], des points quantiques à base de PbS ont été synthétisés dans divers médias: verres [38, 39, 40], matrices polymères [41, 42], solution aqueuse [43, 44], composés organiques [45], zéolithes [46], des cristaux liquides [47], monocouches auto-assemblés. Cependant, ceux qui produisent les rendements quantiques les plus élevés sont exclusivement synthétisés à haute température en utilisant un procédé d'injection (hot injection method) [31, 32]. Par exemple, Hines et Scholes ont rapporté pour la première fois la synthèse organométallique de points quantiques de PbS avec une émission et une taille ajustables en utilisant l'acide oléique comme ligand, de l'oxyde de plomb et le bis (triméthylsilyl) sulfure comme précurseurs. Pour ce faire, une certaine quantité de PbO dissous dans l'acide oléique est purgé via un écoulement d'azote et chauffée par la suite dans un ballon de réaction à 150 °C. Les solutions de bis (triméthylsilyl) sulfure et octadécène sont ajoutées dans le ballon et mélangées avec une agitation vigoureuse. La température est par la suite maintenue à 100 °C durant la croissance de nanocristaux. Des aliquotes de la solution de réaction sont alors retirées de la fiole à intervalle de temps régulier afin d'obtenir des points quantiques de différentes tailles. Cette approche permet la production de nanocristaux de PbS ayant un seuil d'absorption allant de 800 nm à 2000 nm [31]. Cette méthode de synthèse est à l'heure actuelle utilisée d'une manière courante pour la production de points quantiques de PbS. Elle implique donc l'emploi du bis (triméthylsilyl) sulfuré, qui est toxique, odorant et chimiquement instable [31, 50, 51]. Une approche plus écologique, dans lequel le bis (triméthylsilyl) est remplacé par le sulfure de soufre, a été rapportée récemment par le groupe d'Ozin. Grâce à cette nouvelle méthode, des nanocristaux de PbS de haute qualité ont été produits en grande quantité soit à échelle du

multigramme. Toutefois, la réaction s'effectue dans un système visqueux à très forte concentration de précurseurs de plomb avec un rapport molaire Pb/S supérieur à 10 [32].

Pour être utilisé dans les systèmes biologiques, les points quantiques sont tenus d'avoir une bonne solubilité dans l'eau. Aujourd'hui, plusieurs méthodes ont été proposées pour synthétiser dans l'eau des points quantiques de PbS [44, 59, 60, 61, 62, 63, 64, 65, 66]. Une approche basée sur la synthèse directe de points quantiques de PbS dans l'eau, aboutit malheureusement à un faible rendement quantique et des spectres d'émission très larges [44, 59, 60, 61, 62, 63, 64, 65, 66]. De plus, la stabilité dans l'eau des points quantiques de PbS est en général très mauvaise car leur surface est très sensible à l'oxygène [59].

Une méthode de préparation permettant de produire des points quantiques solubles dans l'eau est nommé échange de ligands [56, 57]. Elle est basée sur la préparation dans une phase organique de points quantiques de PbS de bonne qualité, entouré d'un premier ligand hydrophobe (capping agent). Au cours du transfert dans l'eau, le premier ligand est remplacé par un nouveau ligand qui est hydrophile. Au cours de la dernière décennie, cette approche a été largement utilisée pour modifier les surfaces de diverses nanoparticules, y compris des points quantiques pour des applications biologiques. Cependant, en général, il a été constaté que cette méthode pourrait conduire à une diminution significative du rendement quantique après le transfert dans l'eau dû au décapage des ligands présents sur la surface des points quantiques. Notons que le rendement quantique est très sensible à la chimie de surface des points quantiques en raison de leur très grand rapport surface/volume [56, 57]. Dans le cas du PbS, Sargent et ses collègues ont réussi à synthétiser des points quantiques de PbS/acide oléique solubles dans l'eau en les traitant directement avec (1-mercaptopundec-11-yl) tétraéthylène glycol. Ces points quantiques de PbS montrent un rendement quantique maximum de 26% et au meilleur de notre connaissance, ces points quantiques de PbS semblent également être assez stables dans l'eau [57]. Cependant, le décapage des ligands acide

oléique de la surface des nanoparticules mène à une diminution du rendement quantique pour atteindre jusqu'à 30% de sa valeur initiale.

Bon nombre de problèmes mentionnés ci-dessus pourraient être surmontés en utilisant des polymères amphiphiles en plus des ligands [58, 59]. La méthode d'encapsulation avec des polymères pourrait, en principe, offrir plus de possibilités en permettant l'ajustement des interactions hydrophobes et hydrophiles tout en ne perturbant pas les ligands qui sont présents originalement à la surface des points quantiques. Parce qu'une chaîne de polymère amphiphile peut avoir plusieurs chaînes hydrophobes, leurs interactions avec les ligands natifs organiques sur les points quantiques peuvent être nombreuses [58, 59]. Par ailleurs, à l'autre extrémité, les chaînes hydrophiles de ce polymère confèrent aux points quantiques une bonne solubilité dans l'eau. De plus, d'autres composants chimiques peuvent être incorporés dans la chaîne de polymère pour augmenter la biocompatibilité (tels que le PEG), afin de permettre de nouvelles conjugaisons (tels que des amines, carboxyles, etc), ou faciliter la réticulation. Récemment, cette approche basée sur les polymères amphiphiles a été appliquée avec succès sur des points quantiques émettant dans le domaine de l'ultraviolet-visible. Le rendement quantique des points quantiques n'a pas varié après le transfert dans l'eau [59].

Par ailleurs, les points quantiques entourés par des ligands organiques sont très sensibles à l'état de surface en raison du grand rapport volume sur surface. Des études récentes ont montré qu'une structure cœur/coquille peut stabiliser et maximiser la fluorescence des points quantiques [60, 61, 62, 63]. Un matériau coquille (ou enveloppe) ayant une plus grande bande interdite, passive les atomes de surface et les gardant ainsi loin de la surface et du milieu environnant [61, 62, 63]. En conséquence, les défauts de surface, les sites de piégeage et les facteurs environnementaux ont dans ce cas un impact réduit sur l'efficacité de fluorescence et de la stabilité des points quantiques. Le premier exemple connu d'une structure cœur/coquille concerne les points quantiques de CdSe/ZnS.

Dans ce cas, le ZnS ayant une large bande interdite non seulement isole le noyau CdSe mais dispose d'un S^{2-} avec un potentiel d'oxydation beaucoup plus faible que Se^{2-} , ce qui entraîne une plus grande résistance de l'ensemble d'une part à la dégradation due à la photo-oxydation et d'autre part à la formation de défauts de surface, conduisant ainsi à une amélioration notable du rendement quantique atteignant des valeurs de 50 %.

L'échange cationique est également utilisé pour la synthèse de la structure cœur/coquille des points quantiques. La réalisation d'une structure cœur/coquille des points quantiques de PbSe/CdSe par échange de cation a été démontré pour la première fois par Pietryga *et al.* Ils ont constaté que la structure cœur/coquille améliore grandement le rendement quantique du PbSe à cause de l'effet de "passivation inorganiques" du noyau de PbSe par la coquille de CdSe, d'une manière similaire au système bien connu de CdSe/ZnS. En outre, la structure cœur/coquille de CdSe présente une stabilité plus élevée dans les conditions ambiantes, résultant en grande partie de la protection des nanocristaux PbSe par les nanocristaux de CdSe [60]. Bien que les structures cœur/coquille électroluminescentes dans le visible aient été largement étudiées, le nombre de travaux sur des points quantiques émettant dans l'infrarouge, en particulier pour les structures cœur/coquille à base de PbS demeure extrêmement limité

Objectives

Comme nous l'avons déjà précisé, les points quantiques de PbS sont synthétisés dans une phase organique. Cependant dans cette approche, ceci implique soit l'utilisation comme précurseur de soufre de sulfure de bis-(triméthylsilyl) qui est très toxique, soit une réaction qui s'effectue dans un système visqueux formé en utilisant une très forte concentration de chlorure de plomb dans l'oléylamine [31, 32]. Il serait donc souhaitable de développer une approche simple et plus verte avec une bonne reproductibilité. De plus, le revêtement des points quantiques de PbS avec un matériau ayant une plus grande bande interdite pourrait accroître le rendement quantique, toutefois, pour les

points quantiques de PbS/CdS de type cœur/coquille, le rendement quantique demeure encore assez faible à savoir typiquement de 20 à 30 % [60]. Il serait donc important d'optimiser cette approche dans le but d'obtenir un meilleur rendement quantique. De plus comme nous venons de le mentionner la méthode faisant appel aux polymères amphiphiles a été appliquée récemment avec succès sur des points quantiques solubles dans l'eau et émettant dans le domaine de l'ultraviolet-visible. Il serait donc également intéressant d'explorer cette méthode pour voir s'il est possible de synthétiser des points quantiques PbS ou PbS/CdS solubles dans l'eau.

Dans ce contexte, nous nous sommes donnés comme défi de synthétiser et de caractériser des points quantiques de PbS ou/et de PbS/CdS de haute qualité dans une phase organique et dans de l'eau. Par conséquent, les objectifs de mon projet sont:

1. Synthèse et caractérisation de points quantiques de PbS de haute qualité dans une phase organique dans une approche simple et plus écologique.
2. Synthèse et caractérisation de points quantiques cœur/coquille de PbS/CdS de haute qualité
3. Synthèse et caractérisation de points quantiques de PbS et de points quantiques cœur/coquille PbS/CdS de haute qualité émettant dans le proche infrarouge soluble dans l'eau par une approche utilisant des polymères amphiphiles.

Grâce à des études systématiques mettant en jeu de nombreuses caractérisations, nous avons été en mesure d'améliorer la compréhension du comportement des points quantiques de PbS et des structures cœur/coquille PbS/CdS dans différents milieux. Les résultats obtenus dans le cadre des travaux de recherche de mon doctorat sont présentés dans 4 chapitres. Le chapitre 3 décrit la synthèse et la caractérisation de points quantiques PbS dans une phase organique basé sur une

nouvelle méthode plus simple et plus verte. En particulier, la synthèse est réalisée pour la première fois dans un système non-visqueux, utilisant des faibles concentrations de PbCl_2 et de S [68, 69]. Dans le chapitre 4, nous rapportons la synthèse et la caractérisation des points quantiques de PbS/CdS dans une phase organique. Nous montrons que cette structure cœur/coquille permet d'améliorer d'une manière significative d'une part le rendement quantique à savoir 67 % et d'autre part la photostabilité [70]. Le chapitre 5 est consacré à l'étude de la synthèse de points quantiques de PbS dans l'eau où nous avons utilisé pour la première fois l'approche basée sur les polymères amphiphiles. Ceci nous a permis d'obtenir des points quantiques ayant une excellente photostabilité et un rendement quantique de 20% dans l'eau [71, 72]. Enfin dans le chapitre 6, nous avons reporté la synthèse de points quantiques de PbS/CdS obtenus pour la première fois dans l'eau en utilisant la méthode des polymères amphiphiles. Un rendement quantique aussi élevé que 33% dans l'eau a été ainsi obtenu avec des points quantiques exhibant également une excellente photostabilité [73, 74].

Chapitre 3: Synthèse et caractérisation de points quantiques de PbS dans une phase organique

Des points quantiques de PbS ont été synthétisés dans une approche simple, plus écologique dans une phase organique. Dans ce chapitre, les effets du temps de réaction, de la température (90 à 120 °C), du rapport molaire des précurseurs (PbCl_2/S : 2:1 à 10:1), des ligands, de la pureté des ligands et des précurseurs sur la croissance et les propriétés optiques des points quantiques de PbS dans un système "non-visqueux", sans solvant et à une température constante sont présentés et discutés. Nous avons en particulier tenté d'optimiser les spectres de photoluminescence de ces points quantiques qui idéalement devraient avoir un seul pic étroit. Cependant, la photoluminescence bimodale a été observée dans la plupart des cas. Elle est due à l'apparition de la maturation d'Ostwald [80, 81, 82]. Comme le montrent les spectres obtenus, l'apparition et l'évolution de cette

maturation dépend du temps de réaction, de la température, du rapport molaire des précurseurs, des ligands de surface et de la pureté des ligands et de précurseurs. Sous certaines conditions, les spectres de photoluminescence montrent un élargissement initial dû essentiellement à la maturation d'Ostwald, puis se transforment graduellement en une structure bimodale. Dans d'autres cas, les pics bimodaux apparaissent rapidement une minute après le début de réaction. En ajustant les conditions de réaction, nous avons été en mesure d'éviter la structure bimodale et de synthétiser donc des points quantiques de PbS avec une distribution de taille étroite.

Figure R.1 présente les pics d'absorption et de photoluminescence de points quantiques de PbS variant entre 1240 nm et 1450 nm. Comme le montre cette figure, l'optimisation des conditions de synthèse nous ont permis d'obtenir un seul pic étroit pour chacune de ces longueurs d'onde. La figure R.2 montre deux tailles standard (2 et 5 nm) de points quantiques de PbS obtenus pour deux temps de réaction (1 min et 120 min) à une température de 90 °C et un rapport de PbCl₂/S de 3:1. Le rendement quantique final des points quantiques de PbS est d'environ 20% à 40% en phase organique avec une taille ajustable de 2 à 6 nm.

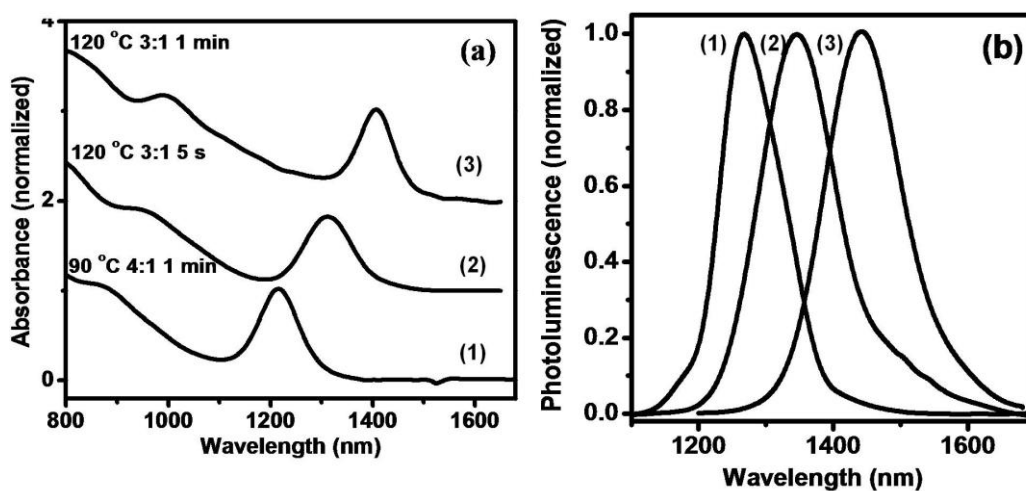


Figure R.1 Absorption (a) et photoluminescence (b) de points quantiques de PbS préparés dans des conditions optimales.

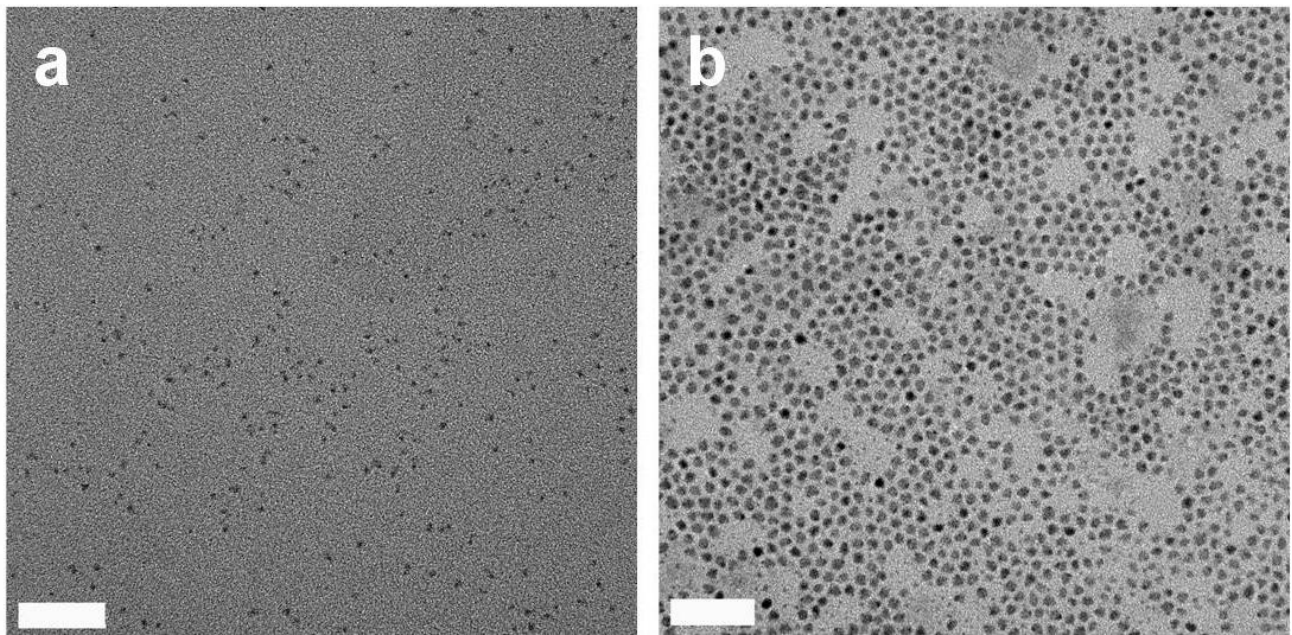


Figure R.2 Images TEM de points quantiques de PbS synthésés à 90°C avec le PbCl_2/S de 3:1 et le temps de réaction de (a) 1 minute et (b) 120 min. L'échelle indiquée est de 50 nm.

L'ensemble de ces travaux ont été présentés dans deux publications:

[68] **H. Zhao**, M. Chaker, and D. Ma. Bimodal Photoluminescence during the Growth of PbS Quantum Dots. *Journal of Physical Chemistry C*, 113:6497–6504, 2009.

[69] **H. Zhao**, T. Zhang, M. Chaker, and D. Ma. Ligand and Precursor Effects on the Synthesis and Optical Properties of PbS Quantum Dots. *Journal of Nanoscience and Nanotechnology*, 10:4897–4905, 2010.

Le rendement quantique optimal de ces points quantiques de PbS est donc de 40% dans la phase organique. Pour l'améliorer, nous avons entrepris la synthèse d'une structure cœur/coquille PbS/CdS en suivant l'approche dite d'échange de cations. Ces résultats sont présentés dans le prochain chapitre.

Chapitre 4: Synthèse et caractérisation des points quantiques de PbS/CdS dans une phase organique

Dans ce chapitre, nous reportons tout d'abord la synthèse, basée sur l'approche dite d'échange de cations [60, 88], de points quantiques de PbS/CdS avec une coquille formée d'une couche mince. En se référant aux résultats obtenus pour les points quantiques de PbSe/CdSe et de PbTe/CdTe faisant appel à la même méthode de synthèse [60, 88], on s'attend à ce que la couche mince qui forme la coquille soit composée de CdS pur. Afin de vérifier ceci, nous avons déterminé tout d'abord par TEM le diamètre total de points quantiques de PbS/CdS obtenus dans différentes conditions. Pour chacune des conditions, nous avons mesuré leur spectre d'absorption afin de calculer leur bande interdite. Enfin, le rapport Pb/Cd a été obtenu en utilisant la technique d'analyse élémentaire connue sous le nom d'ICP-OES à savoir la spectrométrie d'émission optique dans un plasma à couplage inductif. Connaissant le rapport Pb/Cd et le diamètre total de PbS/CdS, nous avons pu ainsi calculer le diamètre des points quantiques de PbS pour différentes conditions expérimentales en supposant 3 cas possibles à savoir que la coquille est formée de CdS pur (voir Figure R.3a) ou d'un alliage $\text{Cd}_x\text{Pb}_{1-x}\text{S}$ (voir figure R.3b) avec $x = 0.2$ et $x = 0.35$. Nous avons par la suite reporté sur la Figure R.3c la variation de la bande interdite en fonction du diamètre de points quantique de PbS mesuré pour du PbS sans coquille (points rouges) et calculé pour une structure cœur/coquille PbS/CdS dans les 3 cas envisagés à savoir PbS entouré de CdS pur (courbe bleue) ou PbS entouré d'alliages de $\text{Cd}_x\text{Pb}_{1-x}\text{S}$ (courbe verte pour $x=0.2$ ou courbe rose pour $x = 0.35$). Cette figure montre tout d'abord que la variation de la bande interdite en fonction du diamètre de PbS sans coquille est identique à celle rapportée dans la référence 25. De plus, c'est la courbe bleue (PbS entouré de CdS pur) qui est la plus proche de celle-ci montrant ainsi indirectement que la coquille dans notre cas est formée de CdS pur.

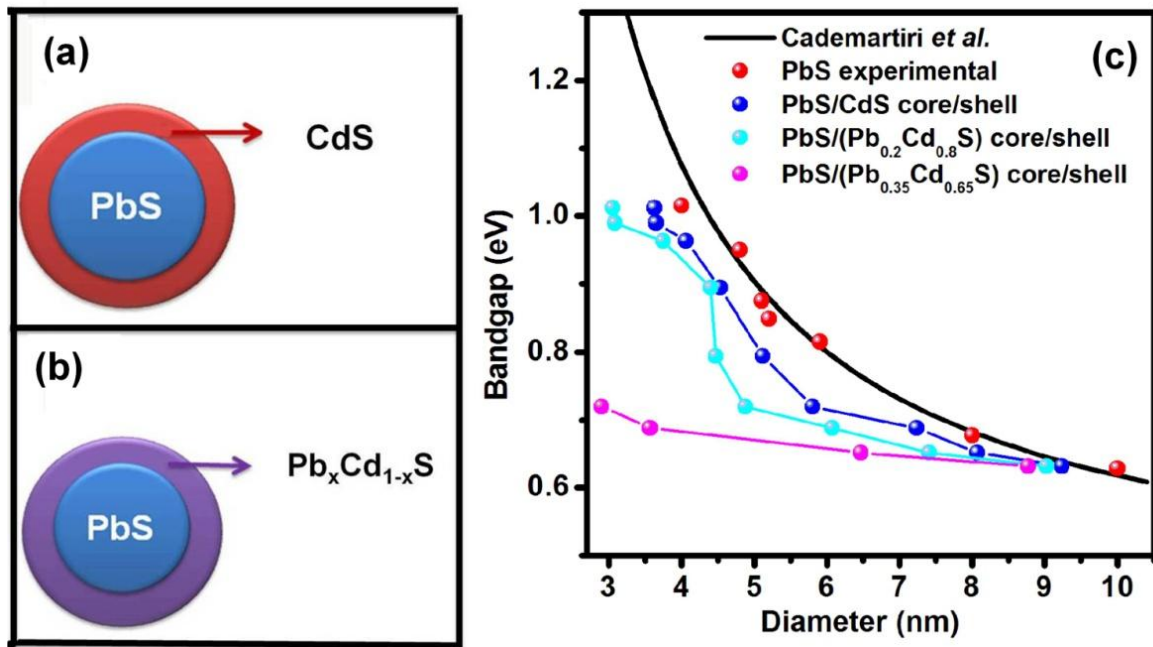


Figure R.3 Schéma de présentation d'une coquille en CdS pur (a) et d'une coquille d'un alliage (b) de points quantiques de PbS/CdS. La figure (c) montre la variation de la bande interdite des points quantiques de PbS et de PbS/CdS en fonction du diamètre du cœur (PbS). La courbe noire représente les données de la référence 25.

Pour pouvoir mieux analyser la coquille, des points quantiques de PbS/CdS, avec une couche de CdS plus épaisse que celle rapportée dans la littérature (en général inférieure à 1.5 nm), ont été également synthétisés par une approche en deux étapes d'échange de cations. En tout premier lieu, la couche de CdS est déposée à une température de 100 °C avec un excès de cadmium afin d'obtenir une coquille de faible épaisseur. Par la suite, la température est augmentée jusqu'à 200 °C permettant à l'échange de cations d'avoir lieu à une profondeur plus grande à l'intérieur du cœur. Si on commençait directement par une température élevée, la réaction d'échange de cations conduirait inévitablement à la maturation d'Ostwald des points quantiques de PbS, donnant lieu à des distributions de taille très larges. Pour éviter ceci, un simple dépôt d'une coquille mince à une température relativement basse assure tout d'abord une protection efficace des points quantiques de

PbS contre la maturation d'Ostwald et permet par la suite d'obtenir une coquille plus épaisse et une distribution de taille étroite.

Grâce à la synthèse d'une coquille relativement épaisse, la structure cœur/coquille a non seulement pu être directement observée par TEM, mais de plus les caractéristiques d'absorption et d'émission de CdS, ont également pu être mises en évidence (Figure R.4). De plus, la diffraction des rayons X et les résultats EDX démontrent également la présence d'une couche cristalline de CdS dans nos échantillons ayant une coquille épaisse. Le pic d'absorption du premier exciton des structures PbS/CdS peut être varié de 830 à 1960 nm et le pic d'émission peut être ajusté de 850 à plus de 1600 nm (limité par notre détecteur dans le domaine du proche infrarouge) en faisant varier la taille des points quantiques du PbS et l'épaisseur de la coquille. L'ensemble de ces résultats atteste clairement que la coquille se compose de CdS pur.

Le fait le plus important est que la structure cœur/coquille de PbS/CdS montre un rendement quantique sensiblement plus élevé que les points quantiques formés uniquement de PbS. Le rendement quantique a pu être augmenté ainsi de 40 % à 67% pour des points quantiques de PbS de 4.5 nm de diamètre avec une coquille de CdS dont l'épaisseur est de 0.7 nm. Ces structures ont également une meilleure photostabilité et une excellente stabilité thermique à comparer à ceux n'ayant pas de coquille, ce qui les rend potentiellement plus utiles pour une variété d'applications.

Ces travaux ont fait l'objet d'une publication à savoir:

[70] **H. Zhao**, M. Chaker, N. Wu, D. Ma. Towards Controlled Synthesis and Better Understanding of Highly Luminescent PbS/CdS Core/shell Quantum Dots. *Journal of Materials Chemistry*, 21:8898–8904, 2011.

Les points quantiques PbS or PbS/CdS synthésés jusqu'à présent sont insolubles dans l'eau. Dans les deux prochains chapitres, en utilisant l'approche originale basée sur l'utilisation des

polymères amphiphiles, nous avons étudié le transfert de ces points quantiques de la phase organique à l'eau.

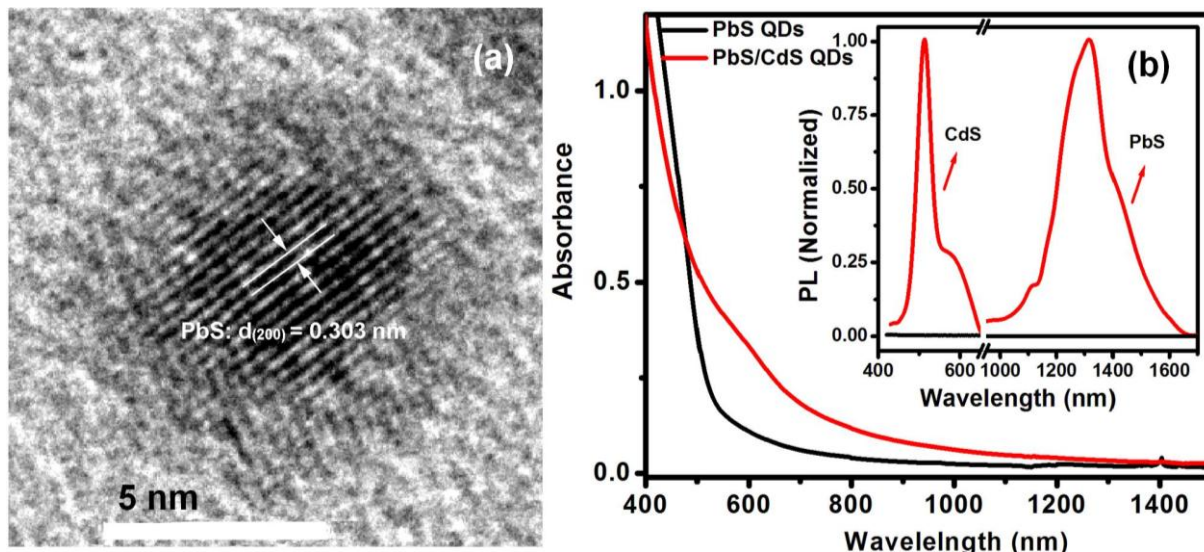


Figure R.4 (a) Image HRTEM d'une coquille épaisse pour des points quantiques de PbS/CdS, indiquant clairement le cœur et la coquille. (b) Spectres d'absorption de PbS et de PbS/CdS dans le toluène. L'encadré dans la figure(b) présente la photoluminescence des points quantiques de PbS/CdS montrant les émissions caractéristiques du CdS et du PbS

Chapitre 5: Synthèse et caractérisation de points quantiques de PbS dans l'eau

Pour les applications biomédicales, les points quantiques de PbS devraient être solubles dans l'eau tout en ayant un excellent rendement quantique. Des points quantiques de PbS de 5.4 nm de diamètre recouverts d'oléylamine solubles dans l'eau ont été obtenus par le transfert dans l'eau de points quantiques monodispersés dans le chloroforme via des polymères amphiphiles. Le processus de transfert dans l'eau conduit immédiatement à une distribution de taille double (5.6 ± 0.9 nm et 2.7 ± 0.4 nm) comme le montrent les mesures TEM et avec une disparition très rapide de la photoluminescence (Figure R.5), due à des séries d'échappées accrues par la présence de polymères amphiphiles et de l'eau. Ceci favorise la maturation d'Ostwald. Cependant, la photoluminescence des points quantiques de PbS, peut être retrouvée en entreposant les échantillons dans l'obscurité

pendant 3 mois (Figure R.5). Les mesures TEM montrent que ces points quantiques ont également une distribution de taille double (6 ± 0.4 nm et 1.9 ± 0.3 nm) après 3 mois d'entreposage. En se basant sur la référence [86] où est rapportée la corrélation entre le pic d'émission et la taille des points quantiques de PbS, on peut attribuer l'émission observée centrée à 1297 nm dans la Figure R.5 aux points quantiques de petite dimension.

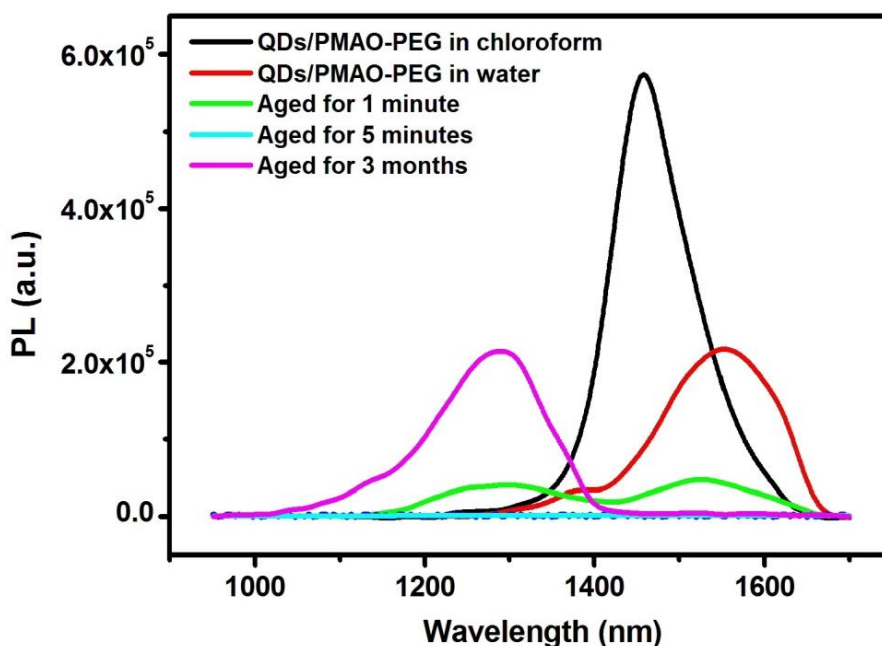


Figure R.5 Photoluminescence de polymère amphiphile encapsulant des points quantiques de PbS dans le chloroforme, après le transfert dans l'eau et après avoir été dans de l'eau à 4°C pendant 1 minute, 5 minutes et 3 mois.

Pour mieux comprendre l'évolution des spectres de photoluminescence de la figure R.5, nous avons réalisé une étude XPS des points quantiques après leur transfert dans l'eau. Nous avons tout d'abord séparé les points quantiques dans une centrifugeuse à savoir ceux de petite taille (de l'ordre de 2 nm) et ceux de grande taille (environ 6 nm). Ceci a été fait d'une part pour un échantillon obtenu quelques heures après le transfert dans l'eau et d'autre part pour celui qui fut entreposé dans l'obscurité pendant 3 mois. En examinant la figure R.6, nous observons que pour chaque échantillon et chaque taille de point quantique, il y a deux pics qui peuvent être déconvolués chacun en deux

pics à savoir celui des atomes de Pb liés au S (trait rouge) et celui des atomes de Pb non liés (trait bleu) qui correspondent aux liaisons pendantes à la surface du point quantique de PbS. Nous notons que pour les points quantiques de petite taille, le pourcentage d'atomes non liés décroît de 21% à 9% après 3 mois d'entreposage alors que pour ceux de grande taille, on observe que ce pourcentage croît de 7% à 11%. La décroissance importante des liaisons pendantes pour les points quantiques de faible taille est une indication qu'il y a eu une réorganisation de la surface se traduisant par le rétablissement de la photoluminescence. Par contre, il semble que ce pourcentage augmente pour les points quantiques de grande taille. Ce qui pourrait expliquer le fait qu'on n'observe pas le rétablissement de la photoluminescence dans ce cas.

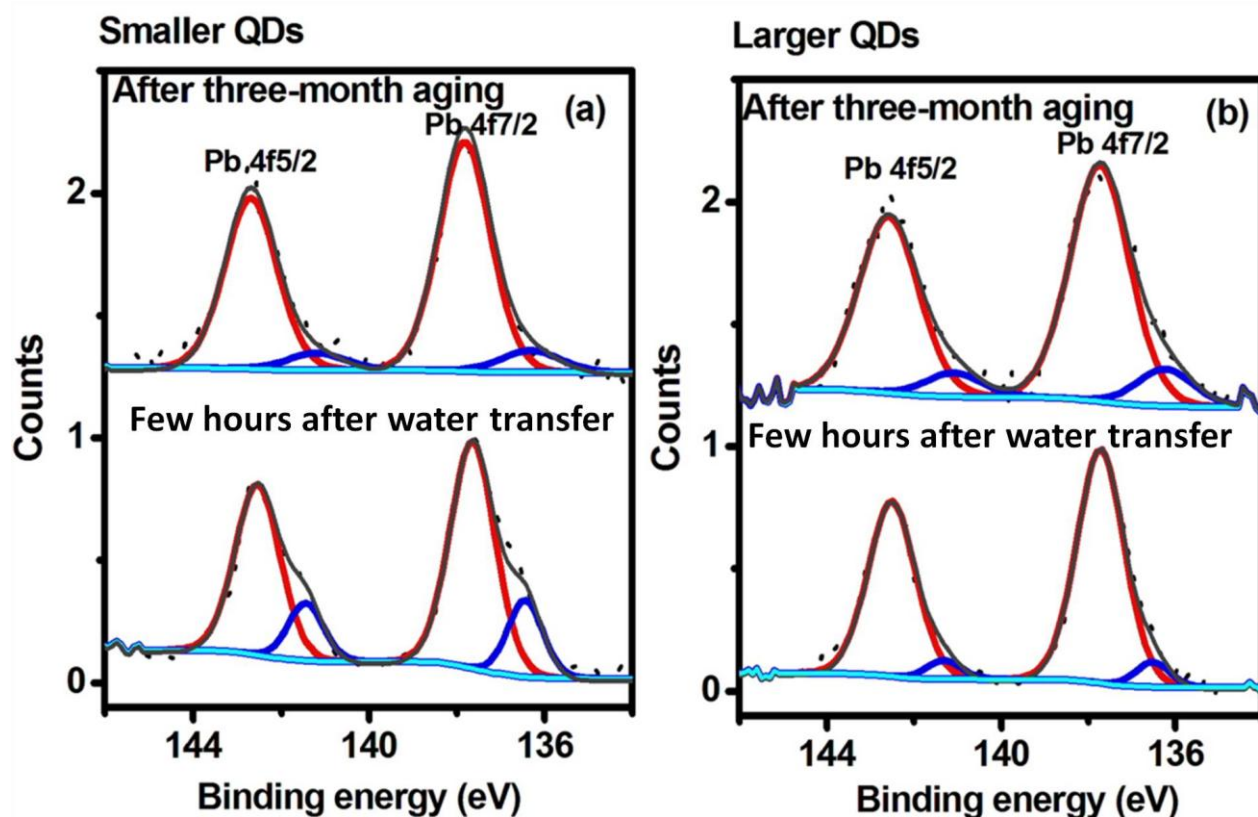


Figure R.6 Spectres XPS Pb 4f de petits (a) et grands (b) points quantiques de PbS encapsulés de polymère amphiphile quelques heures après le transfert dans l'eau et après avoir été stockés dans de l'eau à 4 °C pendant 3 mois. Les points représentent les données expérimentales. Les lignes rouges (Pb liés à S) et bleues (Pb non liés) représentent la déconvolution du signal représenté par le trait noir.

La photoluminescence ainsi rétablie est très stable dans l'eau. Nous n'avons observé aucun changement sur une période plus d'une année. Le rendement quantique de ces points quantiques est de 10%. Cependant ce procédé n'est pas très applicable dans une réalité industrielle et de plus le rendement quantique est relativement faible.

Afin d'étudier l'influence du ligand sur les propriétés des points quantiques de PbS, nous avons réalisé la synthèse en utilisant trois types de ligands (oléylamine, acide oléique ou acide oléique/trioctylphosphine) dans un solvant organique et transférés dans l'eau via le polymère amphiphile. La structure et les propriétés optiques des points quantiques de PbS encapsulés dans le polymère amphiphile après le transfert de l'eau dépendent très fortement du type du ligand. Il se trouve que le procédé d'encapsulation de polymère dans le chloroforme n'affecte ni la taille moyenne des points quantiques de PbS, ni leur distribution quel que soit le ligand utilisé (Figure R.7a-c). Néanmoins, la situation est très différente suite au transfert dans l'eau. Comme nous l'avons précisé précédemment, la distribution de la taille des points quantiques de PbS-oléylamine varie d'une simple à une double distribution de la taille après le transfert dans l'eau (Figure R.7d). En revanche, les points quantiques de PbS-acide oléique ou de PbS-acide oléique/trioctylphosphine gardent une taille unique après leur transfert dans l'eau (Figure R.7b versus R.7e et R.7c versus R.7f).

Les spectres de photoluminescence de points quantiques de PbS avant et après le transfert dans l'eau via le polymère amphiphile sont présentés dans la Figure R.8. L'élargissement considérable et le décalage vers le rouge (64 nm) du spectre de photoluminescence des points quantiques de PbS-oléylamine après le transfert dans l'eau (Figure R.8, en bas) sont le résultat de la distribution double de leur taille et de la passivation de leur surface. Le spectre de photoluminescence de points quantiques de PbS-acide oléique/trioctylphosphine montre quant à lui un décalage significatif vers le bleu de 28 nm après le transfert dans l'eau (Figure R.8, en haut) pour

lequel nous n'avons d'explication. Parmi les trois échantillons, les points quantiques PbS-acide oléique semblent être les plus stables. On observe une variation de 5 nm vers le bleu en ce qui concerne la position de leur pic et une très faible réduction de la largeur de leur spectre de photoluminescence après le transfert dans l'eau (Figure R.8, milieu).

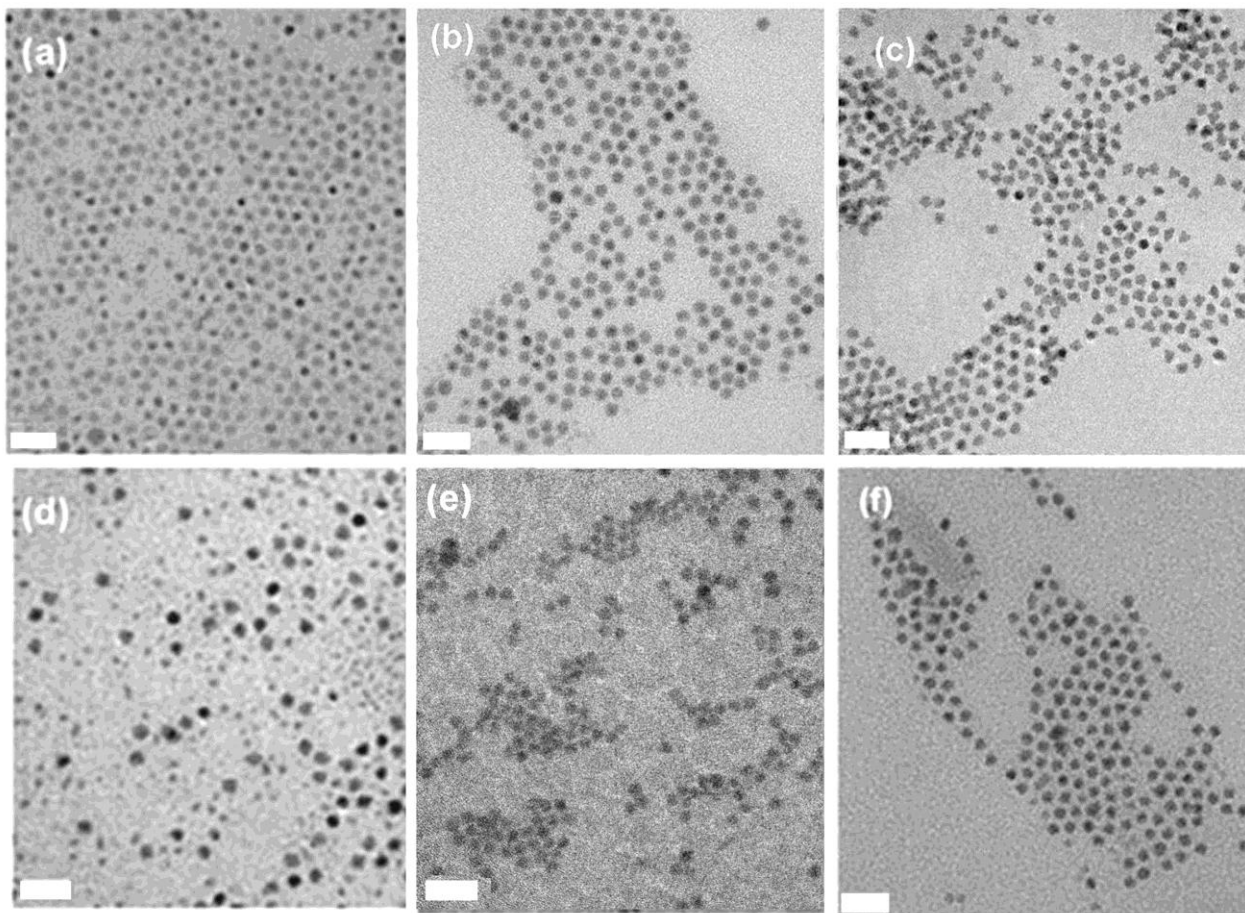


Figure R.7 Images TEM des points quantiques de PbS-oléamine (a, d), de PbS-acide oléique (b, e) et de PbS-acide oléique/trioctylphosphine (c, f) dans le chloroforme (a, b, c) et après l'encapsulation par le polymère et le transfert en l'eau (d, e, f) via le polymère amphiphile. L'échelle indiquée est de 20 nm.

En prenant en considération tous ces résultats, les points quantiques de PbS entourés par l'acide oléique/trioctylphosphine montrent le meilleur rendement quantique à savoir 20% avec une bonne photostabilité

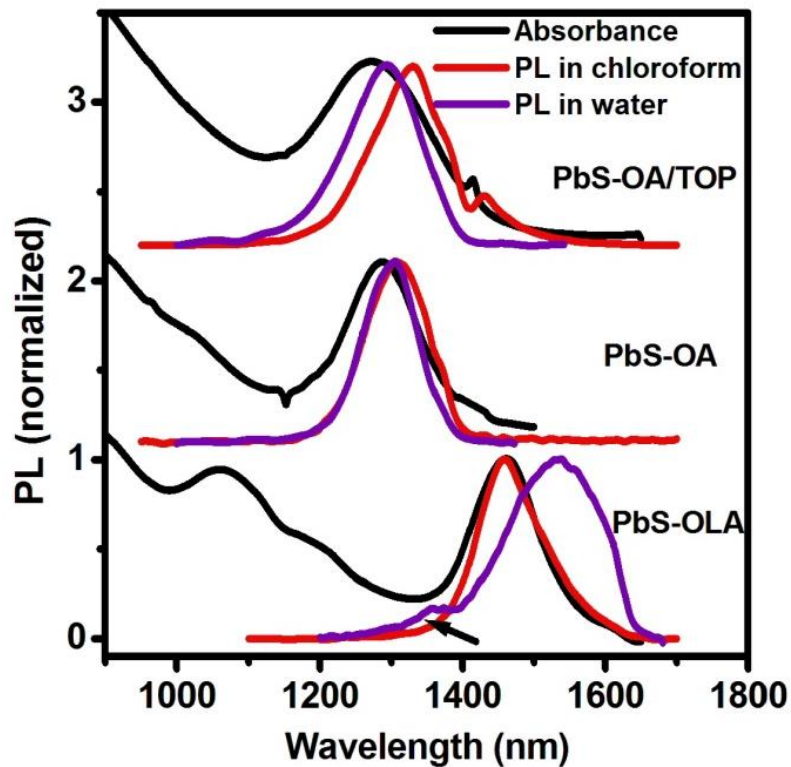


Figure R.8 Spectres d'absorption et de photoluminescence de points quantiques de PbS entourés par des ligands différents (oléylamine, acide oléique et acide oléique/trioctylphosphine) encapsulés dans du polymère amphiphile dans le chloroforme avant le transfert dans l'eau et les spectres de photoluminescence de points quantiques après le transfert dans l'eau.

L'ensemble de ces travaux ont été présentés dans deux publications:

[71] **H. Zhao**, M. Chaker, and D. Ma. Self-selective Recovery of Photoluminescence in Amphiphilic Polymer Encapsulated PbS Quantum Dots. *Physical Chemistry Chemical Physics*, 12:14754–14761, 2010.

[72] **H. Zhao**, D. Wang, M. Chaker, and D. Ma. Photoluminescence Effect of Different Types of Surface Ligands on the Structure and Optical Property of Water-soluble PbS Quantum Dots Encapsulated by Amphiphilic Polymers. *Journal of Physical Chemistry C*, 115:1620–1626, 2011.

Chapitre 6: Synthèse et caractérisation de points quantiques de PbS/CdS dans l'eau

Afin d'améliorer le rendement quantique des points quantiques PbS solubles dans l'eau, nous avons exploré l'utilisation de la structure cœur/coquille. Dans ce but, des points quantiques de PbS/CdS ont été synthétisés avec succès. Comme le montre la figure R.9, Il a été constaté que pour des points quantiques dont le diamètre du cœur est de 4.5 nm le rendement quantique des points quantiques de PbS/CdS dans l'eau augmente d'abord avec l'augmentation de l'épaisseur de la coquille jusqu'à ~ 0.7 nm avec un rendement quantique maximum de 33%, puis diminue à 1.7% lorsque l'épaisseur de la coquille atteint 2.3 nm.

Par la suite, nous avons synthétisé une série de points quantiques de PbS/CdS avec une taille du coeur variant de 2.6 nm à 5 nm avec une épaisseur de la coquille de CdS constante égale à 0.7 nm (Figure R.10a). Nous avons trouvé que tous les échantillons donnent un meilleur rendement quantique dans l'eau quel que soit la taille du coeur.

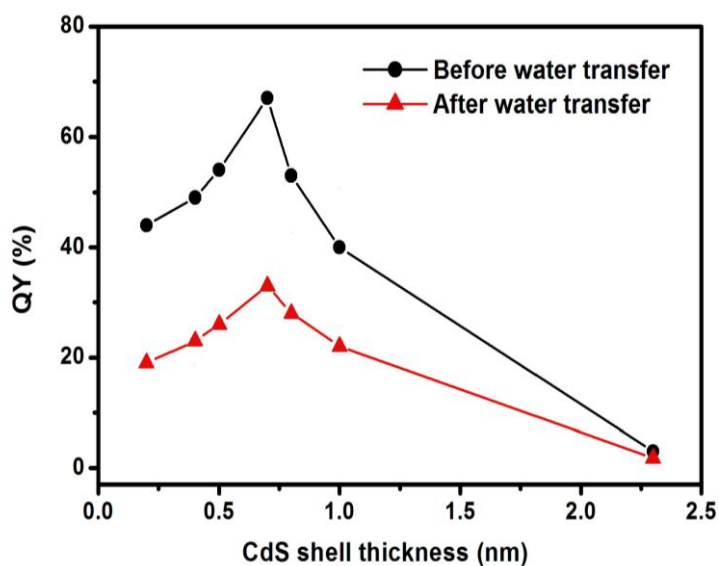


Figure R9 Le rendement quantique des points quantiques PbS/CdS avant et après le transfert dans l'eau en fonction de l'épaisseur de la coquille.

Comme le montre la Figure R.10a, nous avons produit les points quantiques de PbS/CdS solubles dans l'eau dont la position du pic de photoluminescence varie de 830 nm à 1400 nm avec une largeur à mi-hauteur des pics aussi bas que 65 meV. Les points quantiques de PbS/CdS dans l'eau montrent des rendements quantiques qui sont dans la gamme de 26 à 33% et une distribution de taille très étroite comme confirmée par l'observation TEM (Figure R.10b).

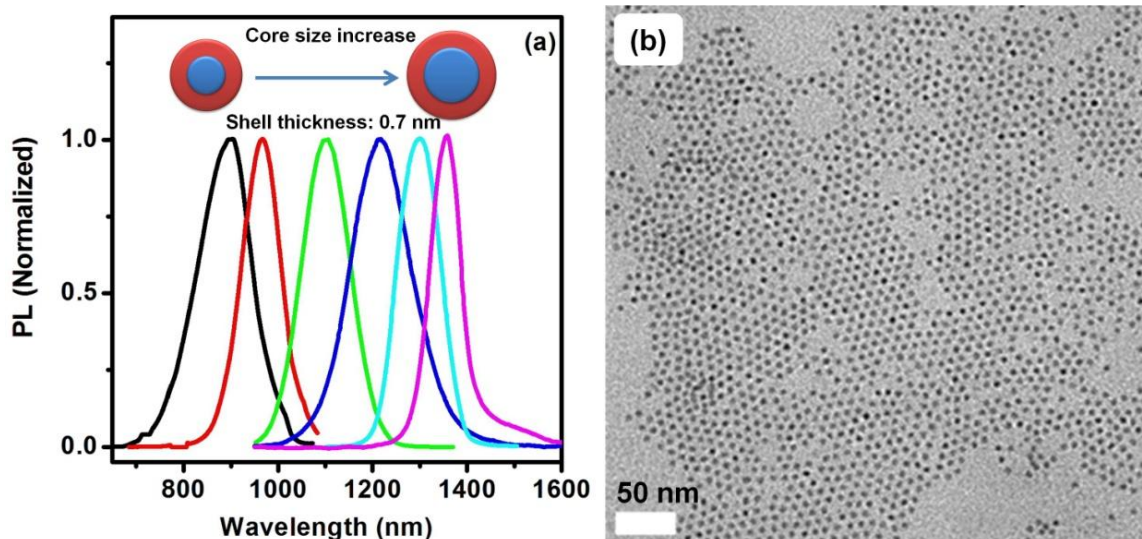


Figure R10 (a) Spectres de photoluminescence de points quantiques de PbS/CdS solubles dans l'eau avec une taille contrôlable et une épaisseur constante de la coquille CdS de 0.7 nm. (b) L'image typique du TEM de points quantiques de PbS/CdS solubles dans l'eau.

L'ensemble de ces travaux ont fait l'objet de deux publications:

[73] **H. Zhao**, D. Wang, T. Zhang, M. Chaker, and D. Ma. Two-step Synthesis of High-quality Water-soluble Near-infrared Emitting Quantum Dots via Amphiphilic Polymers. *Chemical Communications*, 46:5301–5303, 2010.

[74] **H. Zhao**, M. Chaker, and D. Ma. Effect of CdS Shell Thickness on the Optical Properties of Water-soluble Amphiphilic Polymer Encapsulated PbS/CdS Quantum Dots. *Journal of Materials Chemistry*, 21:17483–17491, 2011.